

**DESIGN AND CHARACTERIZATION OF A DOUBLE PASS LONG  
PERIOD FIBER GRATING CONFIGURATION AND ITS SENSING  
APPLICATIONS**

By

**LOH MEY CHERN**

A master dissertation submitted to the Department of Electrical and Electronic  
Engineering,  
Lee Kong Chian Faculty of Engineering and Science,  
Universiti Tunku Abdul Rahman,  
in partial fulfillment of the requirements for the degree of  
Master of Engineering Science  
September 2016

## **ABSTRACT**

### **DESIGN AND CHARACTERIZATION OF A DOUBLE PASS LONG PERIOD FIBER GRATING CONFIGURATION AND ITS SENSING APPLICATIONS**

**Loh Mey Chern**

LPFG has demonstrated its sensitivity to the surrounding refractive index and since its introduction many research work had been conducted on enhancing the sensitivity. This project is exploring whether the measurement of sensitivity of the LPFG can be based on minimum transmission of the attenuation band or notch instead of wavelength shifts and whether the sensitivity of the LPFG can be improved without any physical modification. The project proposed the use of an electric arc-induced LPFG in a double-pass configuration to increase the transmission attenuation of the resonance wavelength and subsequently improve its sensitivity. It is hypothesized that the longer travelling path in the double-pass configuration will provide better coupling between the core and cladding modes thus giving better transmission attenuation of the notch and sensitivity. This is hypothesized based on the

minimum transmission power of the attenuation bands or notches expressed by:

$$T_m = \cos^2(\kappa_{1m-01}^{clad-core}(z)L) \times 2$$

where  $\kappa_{1m-01}^{clad-core}(z)$  the coupling coefficient for the  $m^{\text{th}}$  mode of cladding, whereas L is the length of the LPFG. The transmittance of the LPFGs varies following the term  $\cos^2(\kappa_{1m-01}^{clad-core}(z)L)$  when the phase-matching condition is satisfied at  $\Delta\beta=0$ . SMF28 fiber was used to fabricate the electric arc-induced LPFGs. The double-pass LPFG configuration was optically characterized and explored as chemical and biological sensors. The double-pass configuration was also applied on a polyelectrolyte coated LPFG to observe whether the sensitivity can be further enhanced. The results of the double-pass configuration were compared to the single-pass configuration. From the study, the sensitivity of the arc-induced LPFG was able to be determined by the transmission attenuation instead of wavelength shift of the transmission notch and that the transmission attenuation sensitivity of the arc-induced LPFG sensor was increased by almost double when in double-pass configuration compared to the single-pass configuration. This supports the hypothesis and proves that the sensitivity of the arc-induced LPFG sensor based on the attenuation band's minimum transmission power variation can be increased using the double-pass configuration without any physical modification to the gratings.

## **ACKNOWLEDGEMENTS**

I would like to thank my supervisor Prof. Dr. Faidz bin Abdul Rahman, my co-supervisor Dr Teh Peh Chiong and Prof. Hideki Kuramitz from University of Toyama for their directions, assistance, and guidance. In particular, Prof. Dr. Faidz bin Abdul Rahman's numerous recommendations and suggestions have been invaluable for the project.

I also wish to thank Mr. Yong Yung Thung @ Daniel, who has taught and guided me on his fabrication system. Special thanks to Mr. Ooh Keng Fei for his assistance and guidance regarding FESEM.

Last but not least, I offer my deepest regards, blessings and thanks to all of those who supported me in any respect during the completion of the project.

## APPROVAL SHEET

This dissertation entitled "DESIGN AND CHARACTERIZATION OF A DOUBLE PASS LONG PERIOD FIBER GRATING CONFIGURATION AND ITS SENSING APPLICATIONS" was prepared by LOH MEY CHERN and submitted as partial fulfillment of the requirements for the degree of Master of Engineering Science at Universiti Tunku Abdul Rahman.

Approved by:

\_\_\_\_\_  
(Prof. Dr. FAIDZ ABD RAHMAN )

Date:.....

Professor/Supervisor

Department of Electrical and Electronic Engineering

Lee Kong Chian Faculty of Engineering and Science

Universiti Tunku Abdul Rahman

\_\_\_\_\_  
(Prof. Dr. TEH PEH CHIONG)

Date:.....

Asst. Professor/Co-supervisor

Department of Electronic Engineering

Faculty of Engineering and Green Technology

Universiti Tunku Abdul Rahman

**LEE KONG CHIAN FACULTY OF ENGINEERING AND SCIENCE**

**UNIVERSITI TUNKU ABDUL RAHMAN**

Date: \_\_\_\_\_

**SUBMISSION OF DISSERTATION**

It is hereby certified that **LOH MEY CHERN** (ID No: **11UEM06219**) has completed this dissertation entitled “DESIGN AND CHARACTERIZATION OF A DOUBLE PASS LONG PERIOD FIBER GRATING CONFIGURATION AND ITS SENSING APPLICATIONS” under the supervision of Prof. Dr. FAIDZ ABD RAHMAN (Supervisor) from the Department of Electrical and Electronic Engineering, Lee Kong Chian Faculty of Engineering and Science, and Dr. TEH PEH CHIONG (Co-Supervisor) from the Department of Electronic Engineering, Faculty of Engineering and Green Technology.

I understand that University will upload softcopy of my dissertation in pdf format into UTAR Institutional Repository, which may be made accessible to UTAR community and public.

Yours truly,

\_\_\_\_\_  
(LOH MEY CHERN)

## DECLARATION

I, Loh Mey Chern hereby declare that the dissertation is based on my original work except for quotations and citations which have been duly acknowledged. I also declare that it has not been previously or concurrently submitted for any other degree at UTAR or other institutions.

\_\_\_\_\_  
(LOH MEY CHERN)

Date \_\_\_\_\_

## TABLE OF CONTENTS

	<b>Page</b>
<b>ABSTRACT</b>	<b>ii</b>
<b>ACKNOWLEDGEMENTS</b>	<b>iv</b>
<b>APPROVAL SHEET</b>	<b>v</b>
<b>PERMISSION SHEET</b>	<b>vi</b>
<b>LIST OF TABLES</b>	<b>viii</b>
<b>LIST OF FIGURES</b>	<b>xii</b>
<b>LIST OF SYMBOLS/ABBREVIATIONS</b>	<b>xxiii</b>
<b>CHAPTER</b>	
<b>1.0 INTRODUCTION</b>	<b>1</b>
1.1 Long Period Fiber Grating	1
1.2 Research Motivation	6
1.3 Objectives	7
1.4 Dissertation Organization	8
<b>2.0 LITERATURE REVIEW</b>	<b>9</b>
2.1 Introduction to Long Period Fiber Grating	9
2.2 Electric Arc-induced Fabrication Techniques	19



<b>5.0 CONCLUSION</b>	<b>90</b>
5.1 Concluding Remarks	90
5.2 Future Work	91
<b>PUBLICATIONS</b>	<b>92</b>
<b>REFERENCES</b>	<b>93</b>

## LIST OF TABLES

Table		Page
3.1	Grating period length of LPFGs in this dissertation	39
3.2	Volume of water and 95% ethanol needed to prepare ethanol solutions in various concentrations	42
3.3	Weight of sucrose crystals and volume of water needed to prepare sucrose solutions in various concentrations	43

## LIST OF FIGURES

<b>Figures</b>		<b>Page</b>
2.1	Transmission spectrum of a band-rejection filter	10
2.2	Transmission spectrum over a broad wavelength range shows the various $LP_{0m}$ cladding modes to which the fundamental guided mode couples	11
2.3	Phase matching considerations for long period gratings	12
2.4	Pictorial description (not to scale) of mode coupling in LPFGs and spectral dependence on surface refractive index	14

2.5	A simple arc-induced long period fiber gratings fabrication setup	21
2.6	Gratings formed on fiber fabricated using electric arcing	22
2.7	Long period fiber gratings (SMF-28) produced with the fabrication setup using arcing technique	23
2.8	Experimentally determined response of the attenuation band in the spectrum of the LPG to the change in concentration of ethylene glycol and refractive index	25
2.9	Schematic of deposition on the LPFG with polyelectrolyte PSS and PDDA	25
2.10	Transmission spectral changes of LPFG with different self-assembly bilayers	26

2.11	Transmission spectra of LPFG to different concentrations of solutions of sodium nitrite (a) without polyelectrolyte films, and (b) with self-assembling polyelectrolyte films of 130 bilayers to concentrations of solutions of sodium nitrite over the range of 0.001-0.2 mol/L (M)	28
2.12	Transmission spectra of LPFG corresponding to temperatures of 0°C, 20°C, 40°C, 60°C, 80°C and 100°C from left to right	29
2.13	Scheme of the chemical removing process of half of the polymeric coating	30
2.14	Transmission spectra of partially-coated LPFG in various (a) relative humidity and (b) temperature	31

2.15	(a) Transmission spectra of colloidal Au-modified long-period fiber grating in aqueous solution containing increasing concentration of sucrose. (b) Plot of peak wavelength vs. refractive index of the sucrose solution. (c) Plot of transmission loss vs. refractive index of the sucrose solution	34
2.16	Transmission spectra of DNP-functionalized self-assembled colloid monolayer gold on LPFG in a buffer solution containing increasing concentration of anti-DNP	35
3.1	Setup of high-voltage electric arc-induced LPFG fabrication method	37
3.2	Image of taper fabricated for arc-induced LPFG	38

3.3	(a) Single pass configuration and (b) Double pass configuration	40
3.4	Illustration of arc-induced LPFG coated with a layer of PDDA and PSS	44
3.5	FESEM images of optical fiber surface (a) without PE coating at magnification of 1,600x, (b) after it was submerged in PDDA for 5 minutes at magnification of 1,600x, (c) after it was submerged in PDDA for 10 minutes at magnification of 20,000x and (d) after it was submerged in PDDA for 15 minutes at magnification of 800x.	46

3.6	FESEM image of optical fiber surface (a) after it was submerged in PDDA for 10 minutes and then in PSS for 5 minutes at magnification of 20,000x, (b) after it was submerged in PDDA for 10 minutes and then in PSS for 10 minutes at magnification of 20,000x and (c) after it was submerged in PDDA for 10 minutes and then in PSS for 15 minutes at magnification of 2,700x	48
3.7	FESEM image of gold nanoparticle synthesized via Frens method with magnification of 45,000x	50
3.8	Comparison of transmission spectra of single pass LPFG before and after avidin immobilization for fibers (a) E and (b) F	51
4.1	Transmission spectrum of single pass LPFG in various refractive indices for fibers (a) A and (b) B	53

4.2	Comparison of transmission spectra of a LPFG in various refractive indices for (a) single pass configuration, and (b) double pass configuration	55
4.3	Resonant wavelength vs refractive index of Cargille oil of two different electric arc-induced LPFGs (a) fiber A and (b) fiber B	58
4.4	Transmission attenuation of resonant wavelength vs refractive index of Cargille oil of (a) fiber A and (b) fiber B	61
4.5	Normalized transmission attenuation of the bare arc-induced LPFG vs refractive index of Cargille oil for (a) fiber A and (b) fiber B	64

4.6	Resonant transmission attenuation of the bare arc-induced LPFG vs ethanol concentration of (a) fiber A and (b) fiber B	67
4.7	Normalized transmission attenuation of bare arc-induced LPFG vs concentrations of ethanol for (a) fiber A and (b) fiber B	69
4.8	Transmission attenuation of the bare arc-induced LPFG vs concentrations of sucrose of (a) fiber C and (b) fiber D	71
4.9	Transmission power of single-pass LPFG in water before and after coatings for (a) fiber C and (b) fiber D	73

4.10	Wavelength shift of transmission notch of single-pass LPFG in sucrose with reference to 0 % sucrose for respective layers for (a) fiber C and (b) fiber D	75
4.11	Comparison of normalized transmission attenuation for both single-pass and double-pass configurations after 60 coatings in sucrose for (a) fiber C and (b) fiber D	78
4.12	Transmission of bare LPFG in single pass and double pass configuration for (a) fiber E and (b) fiber F	81

(a) Transmission of avidin-immobilized LPFG in PBS (reference) and avidin-biotin interaction (60 min) in the single pass configuration for fiber E, (b) Transmission of avidin-immobilized LPFG in PBS (reference) and avidin-biotin interaction (60 min) in the double pass configuration for fiber E, (c) transmission of avidin-immobilized LPFG in PBS (reference) and avidin-biotin interaction (60 min) in the single pass configuration for fiber F and (d) Transmission of avidin-immobilized LPFG in PBS (reference) and avidin-biotin interaction (60 min) in the double pass configuration for fiber F

4.14	Resonance wavelength (nm) versus time (minutes) during monitoring of the avidin–biotin interaction in both single and double pass for (a) fiber E and (b) fiber F	85
4.15	Normalized transmission attenuation of the LPFG resonance wavelength versus time during monitoring of the avidin–biotin interaction for (a) fiber E and (b) fiber F	88

## LIST OF SYMBOLS / ABBREVIATIONS

$a_{\text{core}}$	radius of the core
$b$	normalized effective index
$\beta_{01}$	Propagation constant of the fundamental mode
$\beta_{cl}^{(n)}$	Propagation constants of the cladding modes
CO <sub>2</sub>	Carbon dioxide
$\Delta$	Core-cladding index difference
dB	Decibel
DI	de-ionized
DNP	dinitrophenyl
$\epsilon_0$	permittivity of free space, , , , and
$E_r^{clad}$	radial vector components of the electric field for the cladding modes

$E_r^{core*}$  radial vector components of the electric field for the core modes

$E_\phi^{clad}$  azimuthal vector components of the electric field for the cladding modes

$E_\phi^{core*}$  azimuthal vector components of the electric field for the core modes

$E_{1m}^{cl}$  normalization constant based on a total power of 1 W carried by the mode

ESA Electrostatic self-assembly

FESEM field effect scanning electron microscope

FTS fiber-taper seeded

GNP Gold nanoparticle

$J_0$  Bessel function of order 0

$J_1$  Bessel function of order 1

$\kappa_{1m-01}^{clad-core}(z)$  coupling coefficient for the  $m^{\text{th}}$  mode of cladding

$k_0$	free space propagation constant
L	Length of LPFG
LB	Langmuir-Blodgett
LPFG	Long period fiber grating
LPG	Long period grating
LPGP	Long period grating pair
LbL	Layer-by-layer
$\Lambda$	Grating period
$\lambda$	Wavelength of the incident radiation
$\lambda_{resonant}^m$	the resonant wave in the $m^{\text{th}}$ mode
$n_{\text{core}}$	core refractive index
$n_{\text{clad}}$	cladding refractive index
$n_{eff,core}$	effective refractive index of the core mode
$n_{eff,cladding}^m$	effective refractive index of the $m^{\text{th}}$ cladding mode

OSA	optical spectrum analyzer
$\omega$	relative position of the propagation constants
PAA	poly(acrylic acid)
PAH	poly(allylamine hydrochloride)
PDDA	poly-dimethyl diallyl ammonium chloride
PE	Polyelectrolyte
PSS	poly (sodium-p-styrenesulfonate)
RI	Refractive index
$\sigma(z)$	slowly varying envelope of the grating
SRI	Surrounding refractive index
$\zeta_0$	axial eigenfield component of the cladding mode
$T_m$	Transmission power of attenuation band
$u_1$	normalized transverse wave number
$v$	azimuthal order of the cladding mode
$V$	normalized frequency
$Z_0$	free space electromagnetic impedance

# CHAPTER 1

## INTRODUCTION

### 1.1 Long Period Fiber Grating

Long period fiber gratings (LPFGs) have been known for more than 10 years (Vengsarkar et al., 1996). The LPFG displays sensitivity towards temperature and strain which may alter the period of the grating or the refractive index of the core or cladding (Gu and Xu, 2007). It also displays low insertion losses, low back reflection, simple fabrication, sensitivity to ambient refractive index without needing to etch the cladding to access the core's evanescent field and a high sensitivity to changes in physical external parameters. These characteristics made the LPFG a more attractive choice for applications such as band rejection filters and gain equalizing filters in optical communication besides its vast applicability as an optical sensor (James and Tatam, 2006; Gu and Xu, 2007).

LPFGs are versatile spectrally-selective components (Hwang et al., 2000) that are widely used in optical communications (Vengsarkar et al., 1996; James and Tatam, 2003; Li et al., 2011; Sakata et al., 2013) and sensing fields (Vengsarkar et al., 1996; James and Tatam, 2003; Li et al., 2011; Sakata et al., 2013). Low background reflection, low insertion loss, compact construction, and easy-to-form large grating period makes LPFGs an attractive fiber device for applications such as gain flattening filters (Vengsarkar et al., 1996; Hwang et al., 2000; Czaplá et al., 2010; Sakata et al., 2013) for erbium-

doped filters amplifiers (Vengsarkar et al., 1996; Hwang et al., 2000), band-rejection filters (Hwang et al., 2000; Dragomir and Nikogosyan, 2013), fiber-optic sensors (Vengsarkar et al., 1996; Hwang et al., 2000; Dragomir and Nikogosyan, 2013; Sakata et al., 2013) whereas high sensitivity to temperature and external refractive index changes are some of the advantages in LPFGs as an optical sensor (James and Tatam, 2003; Li et al., 2011) for measuring the temperature (Bhatia and Vengsarkar, 1996; Hwang et al., 2000) or the refractive index of liquids (Bhatia and Vengsarkar, 1996; Hwang et al., 2000).

LPFG has demonstrated its sensitivity to the refractive index (RI) of the surroundings of its grating. This enables the LPFG to be used as optical sensors to detect concentrations of salt solutions (Samer et al., 2008; Possetti et al., 2009), ethylene glycol (Patrick et al., 1998; Falciai et al., 2001), hydrocarbon (Falate et al., 2004; Falate et al., 2005; Falate et al., 2007; Mishra et al., 2008; Nanda et al., 2008; Possetti et al., 2009; Possetti et al., 2009) and hemoglobin protein (Chen et al., 2007). Its sensitivity to changes in the RI of the surrounding medium also inspired its use as flow sensors (Dankers et al., 2001; Kueh et al., 2002), liquid level sensors (Sarfraz et al., 2001) and the RI change when antigen bonds with antibody (DeLisa et al., 2000). Optical techniques including the LPFG have been considered promising for the development of chemical and biological sensors (Cusano et al., 2005; James et al., 2006; Gu and Xu, 2007; Korposh et al., 2010).

LPFGs are structures with periodic modulations of the refractive index along the length of a fiber where under certain phase-matching conditions, the

fundamental core mode couples to the discrete cladding modes. Spectrally selective loss can be obtained due to the wavelength dependence of the coupling from the guided mode to the cladding modes. LPFGs are favored as fibers sensors as they are electrically passive, electromagnetically immune, have high sensitivity and multiplexing capabilities (Kersey et al., 1997).

Usually, LPFGs are written by lasers with spectral range from ultraviolet (Vengsarkar et al., 1996; Bhatia et al., 1996; Guan et al., 2000; Kawano et al., 2001; Chen et al., 2003) to far infrared (Smietana et al., 2011). Other types of LPFG fabrication include etched corrugation (Lin and Wang, 2001; Lin et al., 2001; Wang et al., 2001; Ivanov and Wang, 2003; Ding and Andrews, 2008), CO<sub>2</sub> laser irradiation (Davis et al., 1998; Davis et al., 1998; Davis et al., 1999; Kakarantzas et al., 2001; Kakarantzas et al., 2002; Rao et al., 2003; Zhu et al., 2003; Wang et al., 2007; Lee et al., 2008; Wang et al., 2008; Xuan et al., 2009; Zhu et al., 2012), mechanical pressure (Savin et al., 2000; Lee et al., 2001; Cho and Lee, 2002; Su et al., 2005; Lee et al., 2006; Steinvurzel et al., 2006), ion beam implantation (Fujimaki et al., 2000; von Bibra et al., 2001) and femtosecond laser exposure (Kondo et al., 1999; Fertein et al., 2001; Dragomir et al., 2002; Dragomir and Nikogosyan, 2003; Hindle et al., 2004; Kalachev et al., 2005; Kalachev et al., 2005; Allsop et al., 2006; Liu et al., 2010; Liao et al., 2010; O'Regan and Nikogosyan, 2011). LPFGs can also be written with an electric arc (Hwang et al., 1999; Humbert et al., 2001; Humbert and Malki, 2002; Bock et al., 2007; Bock et al., 2007; Rego and Ivanov, 2007; Rego and Ivanov, 2011) which uses electric arc discharges to form the periodic grating structure. The electric arc method is

mostly favored for its simplicity, low cost, flexibility, and applicability. Some of the advantages of arc-induced gratings include resistance to thermal annealing, and does not require preprocessing which is time consuming. Electrical arcing using ignition coil in the arcing circuit is able to produce LPFG with lesser gratings, required smaller arcing current and deeper transmission notch as compared to other LPFGs fabricated using fusion splicer (Lee et al., 2013).

For a single mode fiber, only  $LP_{01}$  or  $HE_{11}$  exists in the core region; however, when mode coupling occurs in the perturbed region in an LPFG, co-propagating cladding modes ( $HE_{1m}$  with  $m = 1, 2, 3, 4, \dots$ ) will exist and propagate in the cladding but decay quickly due to scattering losses (Chung and Lee, 2001; Abrishamian et al., 2012). The notches formed by LPFGs are indication of transmission loss due to the coupling of the core mode to the co-propagating cladding modes. The LPFG sensitivity depends on the phase-matching condition which is affected by the difference between refractive index of the cladding and that of the surrounding medium (Vengsarkar et al., 1996). The core effective index and the cladding effective indices of various cladding modes can be determined using the three-layer fiber geometry (Chung and Lee, 2001; Rego et al., 2005; Abrishamian et al., 2012). This approach directly provides the core and cladding effective indices by means of locating the intersection points in the graphical representation of the dispersion relation (Chung and Lee, 2001; Rego et al., 2005; Abrishamian et al., 2012).

Some studies have reported the utilization of grating-based structures for bio-sensing and chemical sensing. To name a few, some work on LPFGs conducted by Shu et al. (2002) demonstrates the intrinsic sensitivity of the LPFG to the surrounding refractive index (SRI) and that the SRI sensitivity can be tailored by modifying the grating dispersion characteristics (Shu et al., 2002). Shu et al. (2001) have also demonstrated a chemical concentration sensor utilizing a LPFG/ FBG hybrid structure. Chen et al. (2004) demonstrated a chemical sensor utilizing a D-fiber LPFG with etched cladding. Pilla et al. (2011) used a dip-coating method to develop a platform for label-free biosensing. In 2016, Quero et al. (2016) demonstrated the detection of human Thyroglobulin using reflection-type LPG.

Since the introduction of the LPFG more than 10 years ago, many researchers worked on sensitizing the LPFG. Numerous methods were used to sensitize the LPFG transmission characteristics such as the turning points of the dispersion mode of the LPFG (Shu et al., 2002), fiber tapering (Allsop et al., 2006), coating the surface of the LPFG utilizing Langmuir-Blodgett (LB) (Rees et al., 2002), electrostatic self-assembly (ESA) (Villar et al., 2005) or also known as layer-by-layer (LbL) coating of polyelectrolytes (Cusano et al., 2005), dip coating (Gu and Xu, 2007), etching of the cladding (Iadicicco et al., 2007, Mysliwicz et al., 2013) and using doped fibers for LPFG fabrication (Chaubey et al., 2014). All the current methods involved modification of the physical structure of the LPFG and that the sensitivity measurements were based on wavelength shifts.

## 1.2 Research Motivation

The purpose of this research is to determine the possibility of using the minimum transmission power variation of the attenuation band or notch of the arc-induced LPFG as the parameter for measuring sensitivity instead of wavelength shifting of the transmission notch and the possibility of enhancing the sensitivity of the LPFG without physical modification of the fiber.

Based on the research questions, it was hypothesized that the use of double pass configuration is able to increase the transmission loss of the arc-induced LPFG at resonance wavelength thus improving the sensitivity of the LPFG when used as an optical sensor. This is based on the minimum transmission power of the attenuation band or notch expressed by

$$T_m = \cos^2(\kappa_{1m-01}^{clad-core}(z)L) \quad 1.1$$

where  $\kappa_{1m-01}^{clad-core}(z)$  the coupling coefficient for the  $m^{\text{th}}$  mode of cladding, whereas  $L$  is the length of the LPFG. The transmittance of the LPFG varies following the term  $\cos^2(\kappa_{1m-01}^{clad-core}(z)L)$  when the phase-matching condition is satisfied at  $\Delta\beta = 0$ . Due to the longer path in which the light passes through the grating region in the double pass configuration, there will be better coupling between the core and cladding modes thus giving better transmission

attenuation and sensitivity toward changes to the surrounding environment. In the hypothesis it is assumed the minimum transmission power of the attenuation bands in double pass configuration will be doubled to that of the single pass configuration based on the expression:

$$T_m = \cos^2(\kappa_{1m-0}^{clad-core}(z)L) \times 2 \quad 1.2$$

To our knowledge, there are no known researches on double-pass arc-induced LPFG configuration as optical sensors.

### 1.3 Objectives

To answer the research questions and to support the hypothesis, the objectives of this project are:

- to develop a double pass configuration to improve the electric arc-induced LPFG attenuation band's minimum transmission power sensitivity without physical modification on the fiber
- to characterize the double pass electric arc-induced LPFG configuration and
- to apply the developed double pass configuration as chemical and biosensor.

## **1.4 Dissertation Organization**

In this dissertation, Chapter 2 contains the literature review for this project. It covers the background theory and applications of LPFG that support the project's research motivation. Chapter 3 describes the methodology adopted to achieve the research objectives and answer the project research questions. Chapter 4 contains the results and discussions of the experiments conducted in the project. Finally, Chapter 5 concludes the dissertation.

## CHAPTER 2

### LITERATURE REVIEW

#### 2.1 Introduction to Long Period Fiber Grating

In 1986, the first known research on fabrication of LPFG-based device for mode conversion was reported by J.N. Blake, B.Y. Kim and H.J. Shaw (1986). Poole et al (1994) then fabricated LPFG-based device for mode conversion using a two-step process in 1994. It was achieved by periodically ablating the fiber surface with a CO<sub>2</sub> laser and then annealing the fiber with an electric arc. However, Vengsarkar et al. first demonstrated the long period grating (LPG) which was induced by UV laser radiation in 1996 (Vengsarkar et al., 1996). In the paper by Vengsarkar et al. (1996), the authors managed to produce a transmission spectrum of a strong grating with a maximum loss of 32 dB as shown in Figure 2.1.

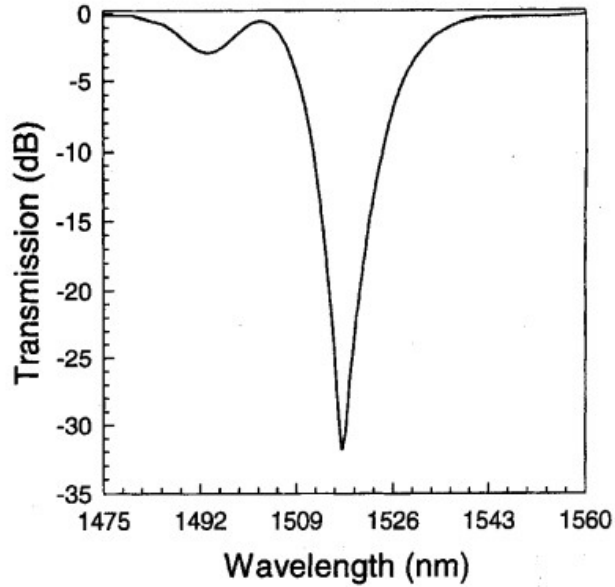


**Figure 2.1: Transmission spectrum of a band-rejection filter (Vengsarkar et al., 1996)**

A typical spectrum for a FLEXCOR fiber with different cladding modes is shown in Figure 2.2 as reported by Vengsarkar et al. (1996). It was reported that the cladding mode properties are affected by the absorptive nature of conventional polymer used for re-coating of splices. Vengsarkar et al. (1996) suggests the use of low-index polymer to maintain the guiding properties of the cladding. This will cause a shift to shorter wavelengths since the application of the coating raises the effective index of the cladding modes.

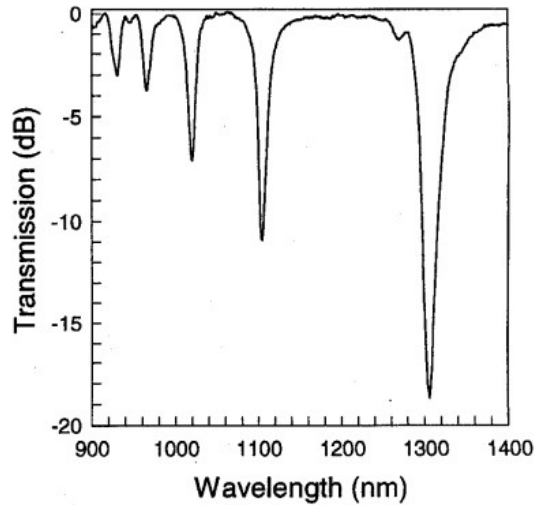


**Figure 2.2: Transmission spectrum over a broad wavelength range shows the various  $LP_{0m}$  cladding modes to which the fundamental guided mode couples (Vengsarkar et al., 1996)**

To match the grating vector to the differential propagation constants, the  $\beta$ -axis needs to be stretched as shown in Figure 2.3 where  $\beta_{01}$  is the propagation constant of the fundamental mode,  $\beta_{cl}^{(n)}$  denotes the propagation constants of the cladding modes where the superscript represents the order of the mode,  $\omega$  is the relative position of the propagation constants and  $\Lambda$  is the grating period. Vengsarkar et al. (1996) proved that the relative amplitudes of the wavelength shifts are consistent with the relative mode confinement.

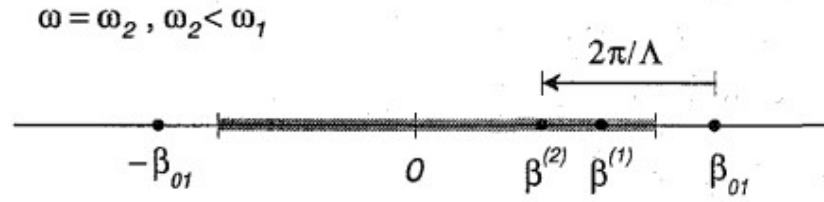


**Figure 2.3: Phase matching considerations for long period gratings**  
(Vengsarkar et al., 1996)

The grating period of a LPFG is usually a few hundred micrometres (Vengsarkar et al., 1996; Tan et al., 2015). This is due to the phase matching condition between the guided mode and the forward propagating cladding modes which is represented by

$$\beta_{01} - \beta_{cl}^{(n)} = \frac{2\pi}{\Lambda} \quad 2.1$$

In the case of long period fiber grating, the phase matching vector is short resulting in a long grating periodicity required to couple the fundamental mode to the  $n^{\text{th}}$ -cladding mode (Vengsarkar et al., 1996).

To put it simply, an LPFG is an optical fiber that has been modified structurally with periodic modulations of the refractive index along its length where under certain phase-matching conditions, the fundamental core mode couples to the discrete cladding modes. The wavelength dependence of the coupling from the guided mode to the cladding mode enables spectrally selective loss. Figure 2.4 describes mode coupling in LPFGs and its spectral

dependence on surface refractive index. In other words, gratings that couple light in an optical fiber from a guided core mode to a cladding mode (modes guided by the cladding-air boundary) propagating in the same direction as the core mode or to another guided core mode are called LPFGs (Thyagarajan, 2006). Fiber parameters and period of the grating determines the specific cladding mode to which a core mode gets coupled. The grating period, length and index modulation control the magnitude of the loss peak, spectral width, and position of the loss peak. LPFGs can be used to induce specific loss at a specific wavelength as there is no reflected wave unlike fiber Bragg gratings (FBGs). LPFGs mainly find applications as gain flattening filters in erbium-doped fiber amplifiers (EDFAs), band rejection filters, WDM isolation filters, polarization filtering components, and sensors.

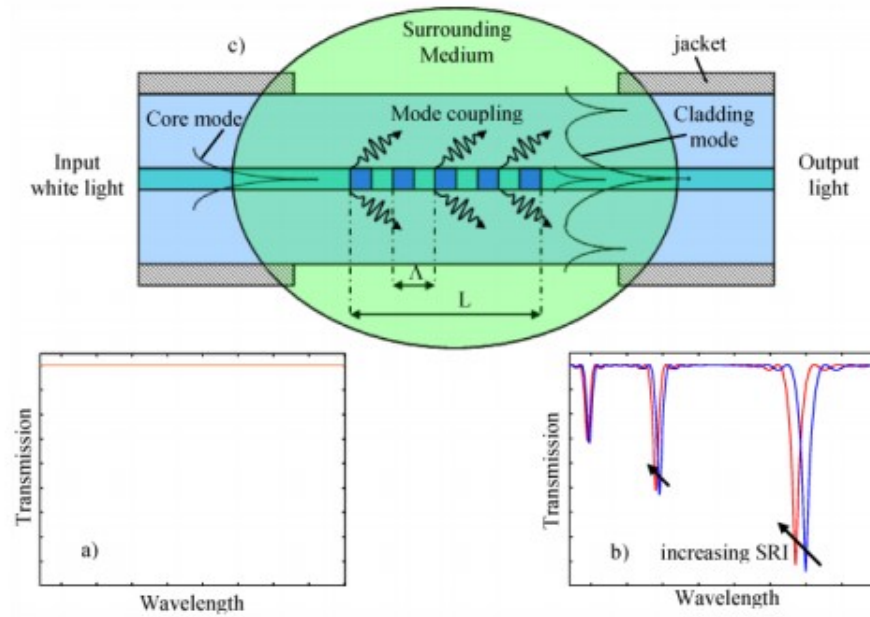


**Figure 2.4: Pictorial description (not to scale) of mode coupling in LPFGs and spectral dependence on surface refractive index (Pilla et al., 2009)**

For a single mode fiber, only  $LP_{01}$  or  $HE_{11}$  exists in the core region; however, when mode coupling occurs in the perturbed region in an LPFG, co-propagating cladding modes ( $HE_{1m}$  with  $m = 1, 2, 3, 4, \dots$ ) will exist and propagate in the cladding but decay quickly due to scattering losses (Chung and Lee, 2001; Abrishamian et al., 2012). The notches formed by LPFGs are indications of transmission loss due to the coupling of the core mode to the co-propagating cladding modes. The LPFG sensitivity depends on the phase-matching condition which is affected by the difference between refractive index of the cladding and that of the surrounding medium (Vengsarkar et al., 1996). The core effective index and the cladding effective indices of various cladding modes can be determined using the three-layer fiber geometry (Chung and Lee, 2001; Durr et al., 2005; Abrishamian et al., 2012). This

approach directly provides the core and cladding effective indices by means of locating the intersection points in the graphical representation of the dispersion relation (Chung and Lee, 2001; Durr et al., 2005; Abrishamian et al., 2012).

The grating of an LPFG has a typical period of between 100  $\mu\text{m}$  and 1 mm formed in an optical fiber in order to achieve light coupling between the fundamental core mode and the forward propagating cladding mode (Vengsarkar et al., 1996; Erdogan, 1997; James and Tatam, 2003; Czapla et al., 2010; Zhu et al., 2012). The transmission spectrum of the LPFG is characterized by a series of attenuation bands and the transmission characteristics of the LPFG formed in a single-mode fiber can be analyzed using the coupled-mode theory (Erdogan, 1997; Czapla et al., 2010). The position and intensity of the spectrum of the attenuation bands depends on temperature, strain, bend and surrounding refractive index (Czapla et al., 2010). The LPFG promotes coupling between the propagating core mode and co-propagating cladding modes in the perturbed region. The light coupled to the cladding modes decays quickly due to scattering losses, thus leaving lossy bands in the guided-core mode observed at the output of the LPFG (Singh, 2015). This causes the transmission spectrum of the long period fiber grating to have a series of attenuation bands at distinct peak resonant wavelength which satisfies the phase matching condition given by (Vengsarkar, 1996),

$$\lambda_{resonant}^m = (n_{eff,core} - n_{eff,cladding}^m)\Lambda \quad 2.2$$

where,

$\lambda_{resonant}^m$  = the resonant wave in the  $m^{\text{th}}$  mode

$n_{eff,core}$  = the effective refractive index of the core mode

$n_{eff,cladding}^m$  = the effective refractive index of the  $m^{\text{th}}$  cladding mode

$\Lambda$  = the grating period

In a weakly guided approximation, the normalized core-cladding index difference ( $\Delta$ ) is very low (Erdogan, 1997):

$$\Delta = \frac{n_{core} - n_{cladding}}{n_{core}} < 1. \quad 2.3$$

The above assumption allows the simpler solution of the characteristic equations, which approximates the exact solution (Etten and Plaats, 1991). Erdogan (1997) made use of the three-layer fiber geometry having exact vector field representations for the calculation of cladding modes where the effect of the core is not ignored when calculating the cladding effective refractive indices. This method does not ignore the effect of the core when calculating the cladding effective refractive indices.

As mentioned earlier, the core effective index and the cladding effective indices of various cladding modes can be determined using the three-layer fiber geometry which will provide the core and cladding effective indices by means of locating the intersection points in the graphical representation of the dispersion relation (Abrishamian et al., 2012). When the light is traveling within the cladding, it experiences a high loss which provides attenuation bands at resonant wavelength in the transmission spectrum. The minimum transmission power of the attenuation bands is expressed by (Rego et al., 2006):

$$T_m = \cos^2(\kappa_{1m-01}^{clad-core}(z)L) \quad 2.4$$

where  $\kappa_{1m-01}^{clad-core}(z)$  the coupling coefficient for the  $m^{\text{th}}$  mode of cladding, whereas  $L$  is the length of the LPFG. The coupling coefficient is determined by the overlap integral of the core mode  $LP_{01}$  (or  $HE_{11}$ ) and cladding modes  $HE_{1m}$  (Chung and Lee, 2001)

$$\kappa_{1m-01}^{clad-core}(z) = \frac{\omega \epsilon_0 n_{core}^2 \sigma(z)}{2} \int_0^{2\pi} d\phi \times \int_0^{a_1} r dr (E_r^{clad} E_r^{core*} + E_\phi^{clad} E_\phi^{core*}) \quad 2.5$$

where  $\omega$  is the angular frequency,  $\epsilon_0$  is the permittivity of free space,  $n_{core}$  is core refractive index,  $\sigma(z)$  is the slowly varying envelope of the grating,  $E_r^{clad}$  and  $E_r^{core*}$  are radial vector components of the electric field for the cladding and core modes, and,  $E_\phi^{clad}$  and  $E_\phi^{core*}$  are azimuthal vector

components of the electric field for the cladding and core modes, respectively. Inserting the field components, taking the azimuthal number for the cladding modes to be 1, and performing the integral along the radial direction will result in (Chung and Lee, 2001; Abrishamian et al., 2012)

$$\kappa_{1m-01}^{cl}(z) = \sigma(z)k_0 \left( \frac{\pi b}{Z_0 n_{clad} \sqrt{1+2b\Delta}} \right)^{\frac{1}{2}} \times \frac{n_{core}^2 u_1}{u_1^2 - \frac{v^2(1-b)}{a_{core}^2}} \times \left( 1 + \frac{\sigma_2 \zeta_0}{n_{core}^2} \right) \times$$

$$E_{1m}^{cl} \left[ u_1 J_1(u_1 a_{core}) \times \frac{J_0 V \sqrt{1-b}}{J_1(V \sqrt{1-b})} - \frac{v \sqrt{1-b}}{a_{core}} J_0(u_1 a_{core}) \right] \quad 2.6$$

where  $n_{clad}$  is the cladding refractive index,  $\sigma(z)$  is the slowly varying envelope of the grating,  $k_0$  is free space propagation constant,  $b$  is normalized effective index,  $Z_0$  is the free space electromagnetic impedance,  $u_1$  is the normalized transverse wave number,  $a_{core}$  is the radius of the core,  $v$  is the azimuthal order of the cladding mode,  $\sigma_2 = j(vn_{eff,clad}Z_0)$ ,  $\zeta_0$  is the axial eigenfield component of the cladding mode,  $E_{1m}^{cl}$  is the normalization constant based on a total power of 1 W carried by the mode,  $J_0$  and  $J_1$  are Bessel functions of order 0 and 1, respectively, and  $V$  is the normalized frequency.

The periodic index of the LPFG couples the core mode to the dissipating cladding modes and at resonant wavelengths, mode coupling takes place effectively (Hwang et al., 2000). At resonant wavelengths, the LPFG have loss peaks due to rapid attenuation of coupled cladding modes by the fiber jacket. The resonance wavelength of the LPFG depends on the grating period and coupling strength or the index modulation amplitude of the grating due to increment of average core index (Hwang et al., 2000).

An LPFG is more sensitive to ambient perturbation than fiber Bragg grating (FBG) in which mode coupling takes place only between forward and backward core modes and have been used for measurement of refractive index, temperature, bending and torsion (Zhu et al., 2012). It is important to enhance sensing sensitivity and overcome the cross-influence between measured parameters of the LPFG (Zhu et al., 2012).

## **2.2 Electric Arc-induced Fabrication Techniques**

As described in Chapter 1, an LPFG can be fabricated in various ways. Some of the fabricating methods include magnetic-force-induced LPFG (Sakata et al., 2013), mechanically induced (Poole et al., 1994; Cullen et al., 1997; Akiyama et al., 1998; Hwang et al., 2000; Savin et al., 2000; Jiang et al., 2002), ultraviolet laser exposure (Bhatia and Vengsarkar, 1996; Vengsarkar et al., 1996; Chen et al., 1999; Guan et al., 2000; Chen et al., 2001; Kawano et al., 2001) and CO<sub>2</sub> laser irradiation (Enomoto et al., 1998; Davis et al., 1999; Kakarantzas et al., 2001; Zhu et al., 2003; Rao et al., 2004; Wang et al., 2007; Lee et al., 2008; Xuan et al., 2009; Zhu et al., 2012; Wang et al., 2013), exposure to electric arc (Kosinski and Vengsarkar, 1998; Hwang et al., 2000; Humbert et al., 2001; Humbert and Malki, 2002; Bock et al., 2007; Rego and Ivanov, 2007; Rego and Ivanov, 2011), femtosecond lasers (Kondo et al., 1999; Fertein et al., 2001; Dragomir et al., 2002; Dragomir et al., 2002; Hindle et al., 2004; Kalachev et al., 2005; Kalachev et al., 2005; Smelser et al., 2005; Allsop et al., 2006; Liu et al., 2010; Liao et al., 2010; Li et al., 2011; O'Regan

and Nikogosyan, 2011), etched corrugation (Lin et al., 2001), diffusion of the core dopant (Dianov et al., 1998), etched corrugation (Lin et al., 2001; Wang et al., 2001; Ivanov and Wang, 2003; Ding and Andrews, 2008) and ion beam implantation (Fujimaki et al., 2000; von Bibra et al., 2001).

Although, LPFGs are usually written using lasers with spectral range from ultraviolet to far-infrared (Smietana et al., 2011), it is difficult to control the filter parameters and it requires complicated and time-consuming processes. The electric arc method was first demonstrated by Poole et al. (1994) and is favored for its simplicity, applicability to various types of fibers and easy control of the filter parameters such as bandwidth and centre wavelength (Hwang et al., 1994). The LPFG can be written with an electric arc (Dianov et al., 1997; Godbout et al., 1998; Palai et al., 2001; Humbert and Malki, 2002; Rego et al., 2002; Benoune et al., 2004; Durr et al., 2005; Iredale et al., 2006; Bock et al., 2007; Statkiewicz-Barabach et al., 2008; Kim et al., 2009; Caldas et al., 2010; Iadicicco et al., 2011; Abrishamian et al., 2012; Smietana et al., 2013; Yin et al., 2014) which uses electric arc discharges. Some of the advantages of arc-induced gratings include resistance to thermal annealing, and does not require preprocessing which is time consuming.

Majority of the electric arc induced LPFGs are fabricated using fusion splicers (Palai et al., 2001; Rego et al., 2005; Allsop et al., 2006). However, an LPFG with similar characteristics can also be fabricated using an electric arc-induced system based on ignition coil as described in Lee et al., (2013). In a

paper written by Lee et al. (2013), a detail illustration on both fabrication techniques using fusion splicers and ignition coil were discussed. The LPFG fabrication method utilizing ignition coil by Lee et al. (2013) was used in this research.

Lee et al. (2013) developed a simple electric arc induced LPFG fabrication using a light source, an ignition coil with an arcing circuit, a pair of electrodes mounted on a motorized stage and controlled by a computer, a pair of fiber clamps with and without sliders, a tension meter with weights and an optical spectrum analyzer as shown in Figure 2.5. Constant force was applied to the fiber to create a constant axial tension throughout the fabrication process.

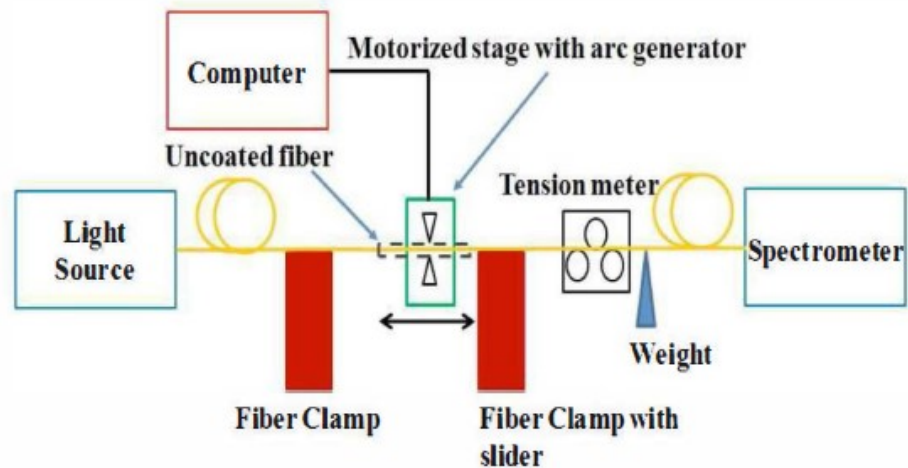


**Figure 2.5: A simple arc-induced long period fiber gratings fabrication setup (Lee et al., 2013)**

The grating periods for SMF28 were set at  $630\mu\text{m}$  with tension of  $28\text{cN}$  and exposure to electric arcs for 4 seconds per grating with the arcing current set to 9 mA. The fiber clamp with slider allows deformation of the cladding with the help of a constant axial tension during the fabrication process. The motorized stage is needed to move the electrodes to the next point for the formation of subsequent gratings on the fiber. The taper structure formation reported by Lee et al. (2013) depends on the axial tension and arcing discharge time. An image of the gratings formed by the electric arcing is shown in Figure 2.6.

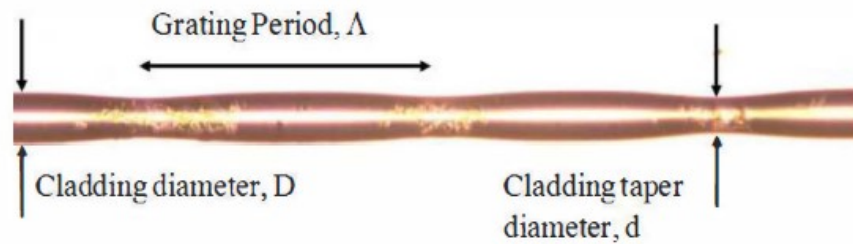


**Figure 2.6: Gratings formed on fiber fabricated using electric arcing (Lee et al., 2013)**

During the grating fabrication process (Lee et al., 2013), the fiber clamp with slider allows the deformation of the cladding with the help of a constant axial tension. As a result, tapers form at the arcing point. When the grating formation is complete, the motorised stage moves the electrodes to the next point for the formation of the next grating on the fiber. The notch formed by the transmission of the LPFG fabricated using electric arcing technique by Lee et al. (2013) is shown in Figure 2.7. The LPFG fabricated using the

ignition coil method will be referred to as arc-induced LPFG throughout the rest of the dissertation.

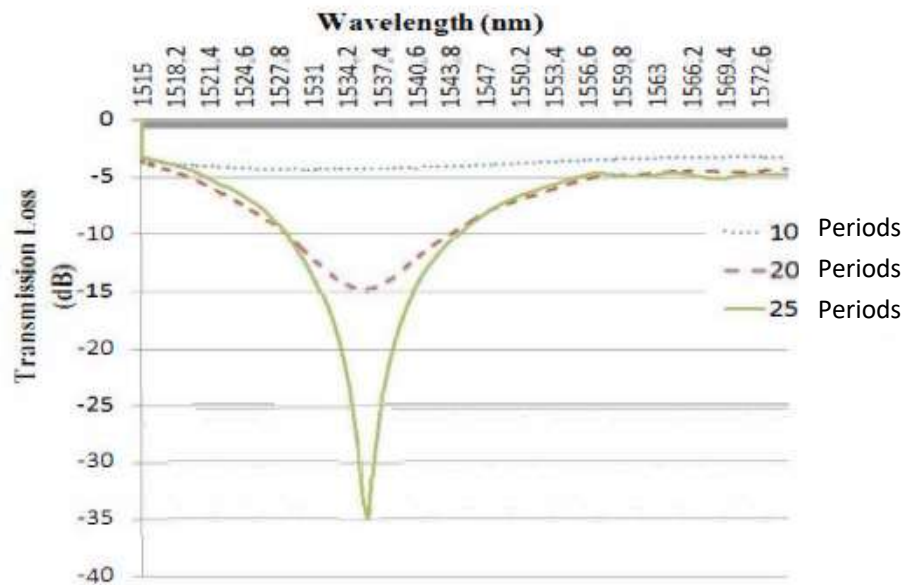


**Figure 2.7: Long period fiber gratings (SMF-28) produced with the fabrication setup using electric arcing technique (Lee et al., 2013)**

### 2.3 Increasing Sensitivity of Arc-induced LPFG

Methods to increase the sensitivity of an LPFG includes fiber tapering (Allsop et al., 2006), etching of the LPFG cladding (Iadicicco et al., 2007; Martinez-Rios et al., 2010), and coating the surface of the LPFG utilizing Langmuir–Blodgett (LB) (Rees et al., 2002), electrostatic self-assembly (ESA) (Villar et al., 2005; Villar et al., 2005) or also known as layer-by-layer (LbL), and dip coating (Cusano et al., 2005; Gu and Xu, 2007). Coating method is

preferred as tapering and etching reduces the LPFG's mechanical integrity which requires extra care while handling the fiber.

In the study on the temperature sensitivity by Lee et al. (2013), the gradient of the arc-induced LPFG that was fabricated on the SMF-28 fiber is  $0.04 \text{ nm}/^\circ\text{C}$ . The temperature sensitivity is lower than those reported in (Rego et al., 2001), which have a temperature sensitivity of  $0.06 \text{ nm}/^\circ\text{C}$  for temperatures of up to  $200^\circ\text{C}$ . It is shown in (Lee et al., 2013) that the electric arcing using ignition coil in the arcing circuit is able to produce LPFG with less gratings, required smaller arcing current and deeper transmission notch as compared to other LPFGs fabricated using fusion splicer.

Deposition of thin film overlays of higher index materials than the cladding was investigated by I.M. Ishaq et al. (2005), M. Smietana et al. (2008), and A. Cusano et al. (2005). Their results, both experimentally and theoretically, showed that the deposition of the thin film overlays modified the LPFG's sensitivity toward the surrounding index. Figure 2.8 shows the results presented by Ishaq et al., (2005) where the wavelength shift of the attenuation band is greater when the fiber is coated with a thin overlay. This proves that deposition of thin film overlay increases the LPFG's sensitivity toward its surrounding refractive index.

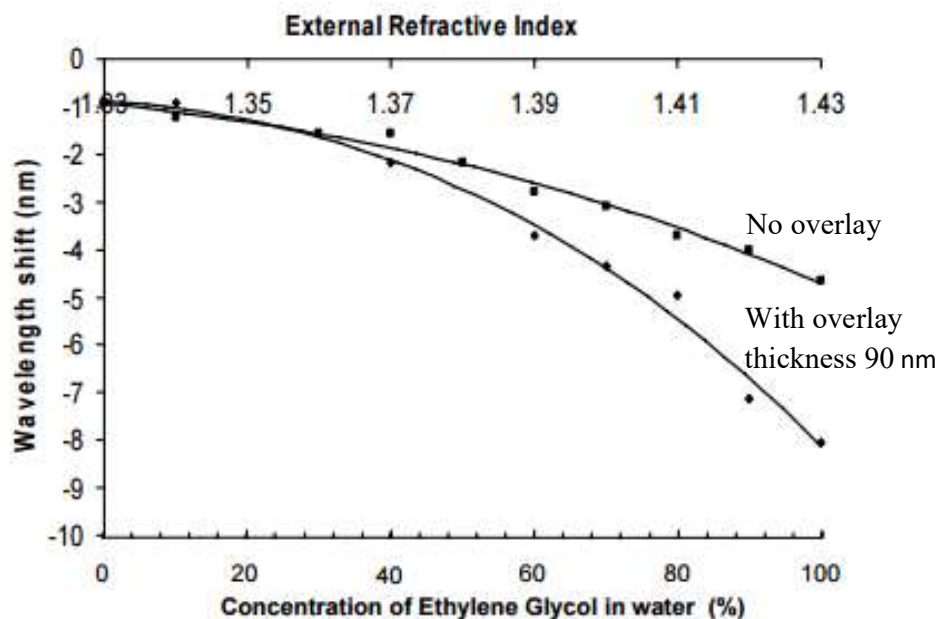


**Figure 2.8: Experimentally determined response of the attenuation band in the spectrum of the LPG to the change in concentration of ethylene glycol and refractive index (Ishaq et al., 2005)**

Q. Li et al., alternately deposited poly (sodium-p-styrenesulfonate) (PSS) and poly-dimethyl diallyl ammonium chloride (PDDA) onto the surface of LPFGs that were written in a hydrogen-loaded Corning SMF-128 fiber using a KrF excimer laser and an amplitude mask to form polyelectrolyte films by electrostatic self-assembly. Figure 2.9 shows a schematic of PDDA and PSS deposition on the LPFG. The LPFG assembled films were then immersed into different concentrations of sodium nitrite aqueous solution. It was experimentally proven by Q. Li et al. (2009) that LPFGs with assembled films have better resolution for sodium nitrite solutions in the range of 0.001-0.2 mol/ L.

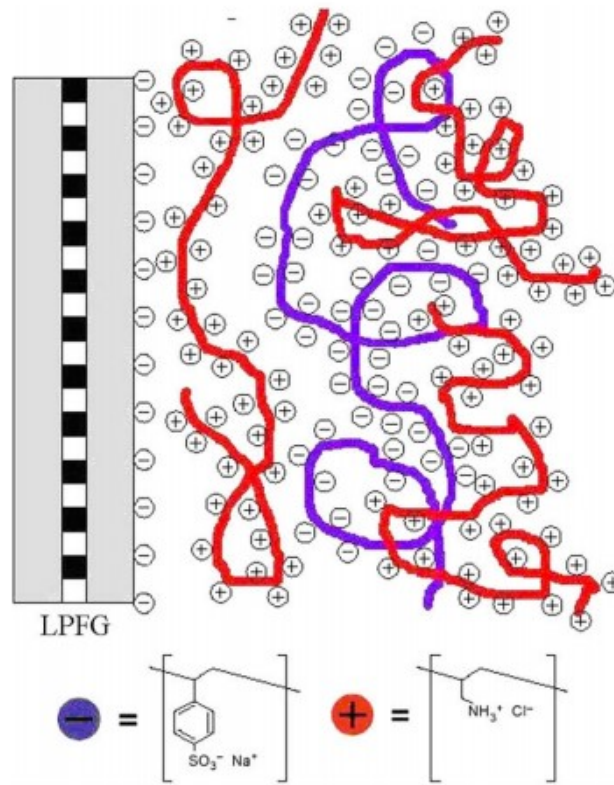


**Figure 2.9: Schematic of deposition on the LPFG with polyelectrolyte PSS and PDDA (Li et al., 2009)**

The spectral shape of the LPFG by Li et al. (2009) has little change and the center wavelength of the attenuation band shifts to the left (blue shift) as the assembly layers increase as shown in Figure 2.10. The large wavelength shift between 125 and 130 bilayers is due to the refractive index of the overcoat approaching the index of the fiber. The blue shift occurred due to the dependence of the centre wavelength of attenuation on the difference of the effective refractive index between the core and cladding. As the self-assembly layers increase, the effective refractive index of the cladding increases which

decreases the difference between the effective refractive indices of the core and cladding to satisfy the phase matching condition.

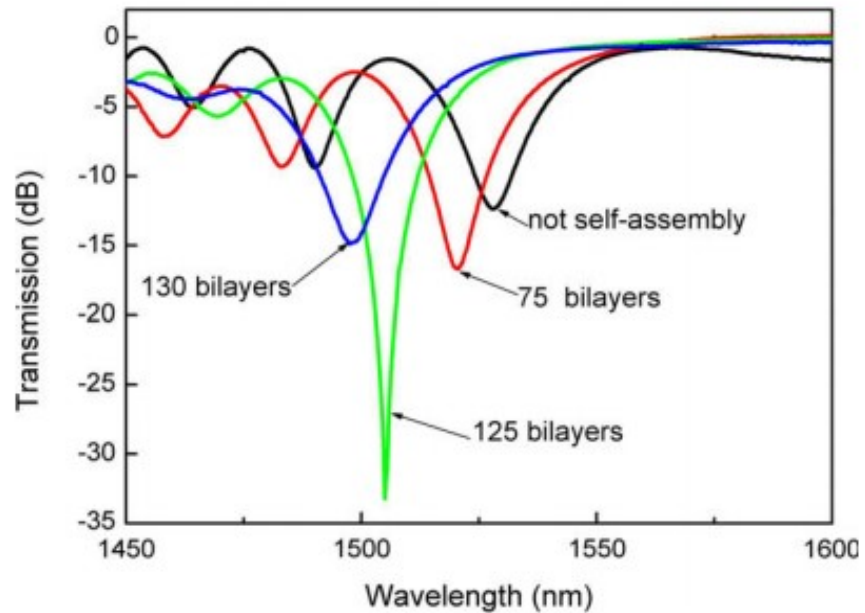


**Figure 2.10: Transmission spectral changes of LPFG with different self-assembly bilayers (Li et al., 2009)**

Figure 2.11(a) shows the transmission spectra of uncoated LPFG in sodium nitrite solutions by Li et al. (2009). It can be observed that the transmission spectra of sodium nitrite solutions in Figure 2.11(a) overlap each other which makes it difficult to distinguish the various concentrations of sodium nitrite solutions. Li et al. (2009) used LPFG with 130 bilayers of self-assembled polyelectrolyte films in various sodium nitrite solutions and the transmission spectra is shown in Figure 2.11(b). From Figure 2.11(b), it can be seen that the centre wavelength of attenuation band gradually shifts to the right (red shift) as the concentration of sodium nitrite increases. The red shift

provides a better distinction of the various concentrations of sodium nitrite solutions. Li et al. (2009) concluded that LPFGs with 130 bilayers of self-assembled polyelectrolyte films have better resolution to concentrations of sodium nitrite solutions and is a promising tool in real-time and on-line monitoring of sodium nitrite.

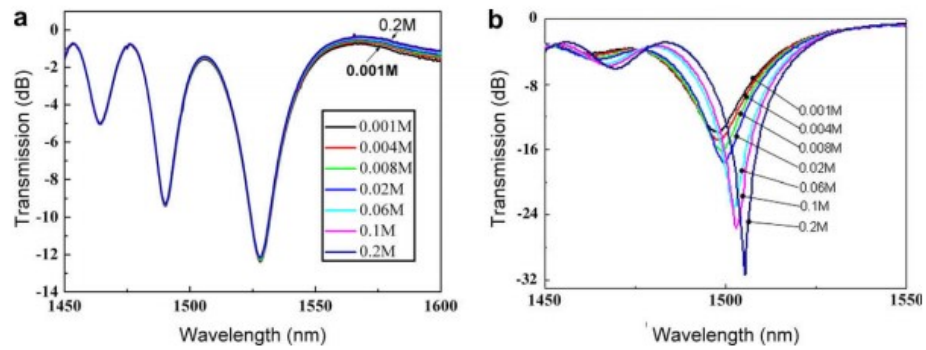


**Figure 2.11: Transmission spectra of LPFG to different concentrations of solutions of sodium nitrite (a) without polyelectrolyte films, and (b) with self-assembling polyelectrolyte films of 130 bilayers to concentrations of solutions of sodium nitrite over the range of 0.001-0.2 mol/ L (M) (Li et al., 2009)**

## 2.4 Some Applications of LPFG

Applications for LPFG are commonly found in optical communications and sensing areas. LPFGs have been researched as temperature sensors, strain sensors and refractive index sensors. Singh et al. (2014) proved that LPFGs are able to detect temperature changes between 0°C and 100°C. Figure 2.12 illustrates the sensitivity of an LPFG towards

temperature. Urrutia et al. (2015) measured humidity and temperature with partially coated LPFG. The LPFG was coated with poly(allylamine hydrochloride) (PAH) and poly(acrylic acid) (PAA) and half of the polymeric coating was removed as illustrated in Figure 2.13. Figure 2.14(a) shows the transmission spectra of the partially-coated LPFG as the relative humidity (RH) changes and Figure 2.14(b) is the transmission spectra of the partially-coated LPFG as the temperature changes.

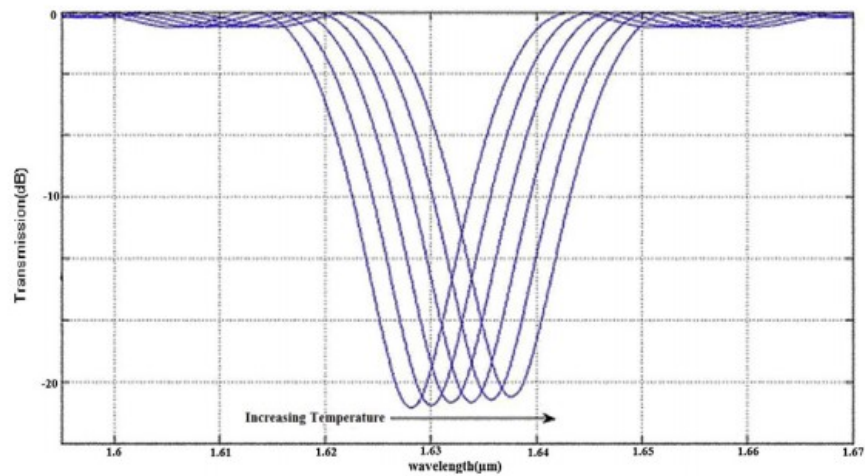


**Figure 2.12: Transmission spectra of LPFG corresponding to temperatures of 0°C, 20°C, 40°C, 60°C, 80°C and 100°C from left to right (Bhatia, 1999)**

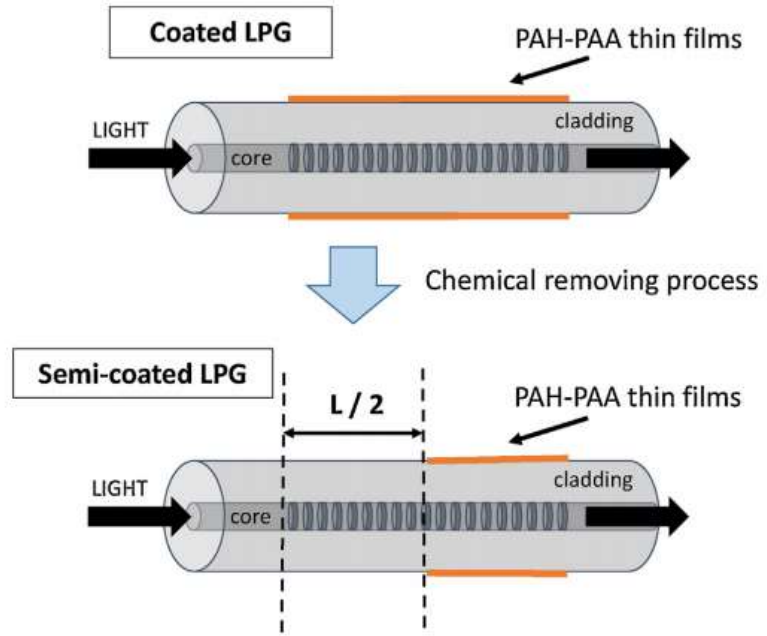
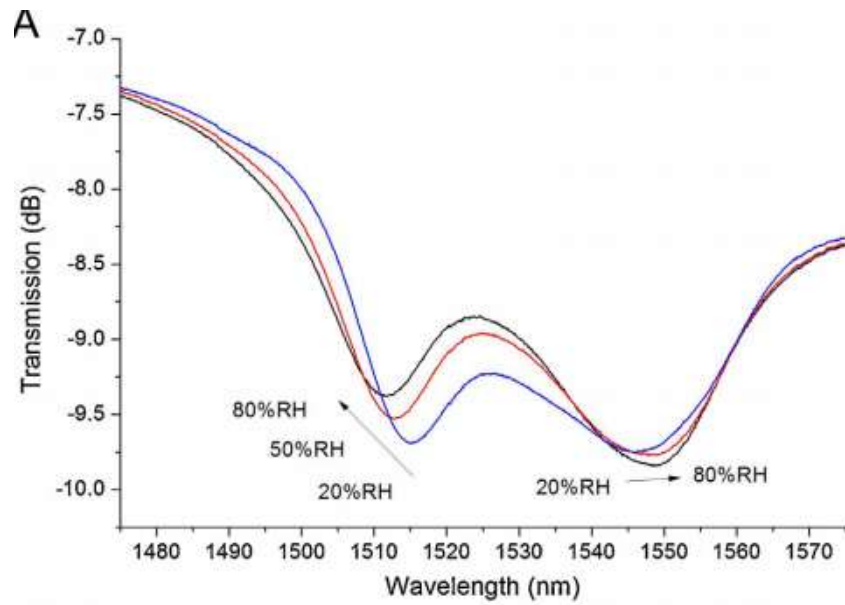
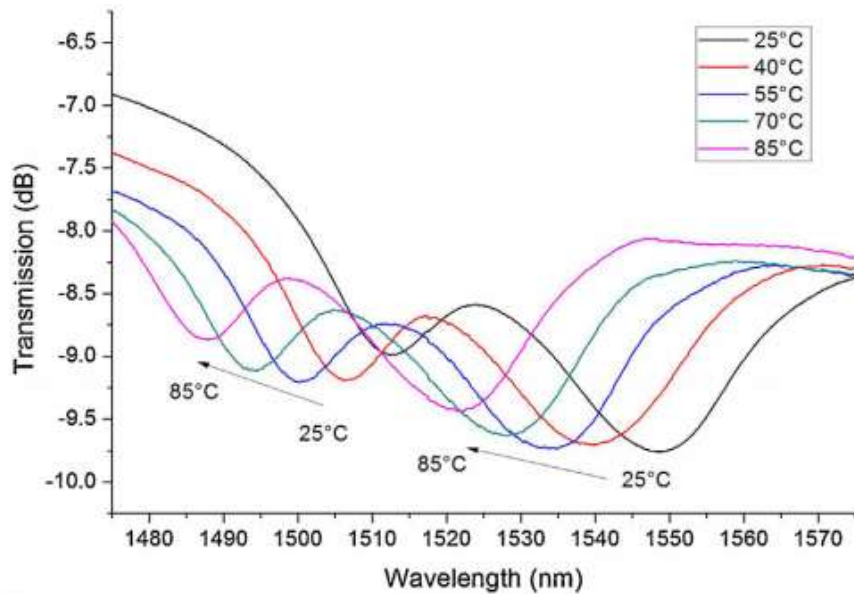


**Figure 2.13: Scheme of the chemical removing process of half of the polymeric coating (Urrutia et al., 2015)**



(a)



(b)

**Figure 2.14: Transmission spectra of partially-coated LPFG in various (a) relative humidity and (b) temperature (Urrutia et al., 2015)**

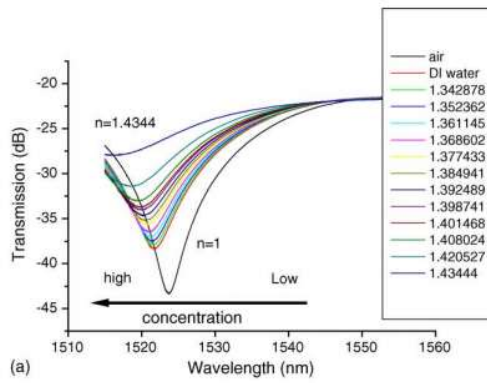
One of the unique features of LPFGs is its high sensitivity to changes in the external refractive index. This is due to the response of the LPFG that is

highly dependent on the order of the coupled cladding mode due to the refractive index changes (Bhatia, 1999; Ding et al., 2005; Yin et al., 2012). When the external refractive index increases, the sensitivity increases as well. It will however reach saturation and the mode becomes unguided (Allsop et al., 2003).

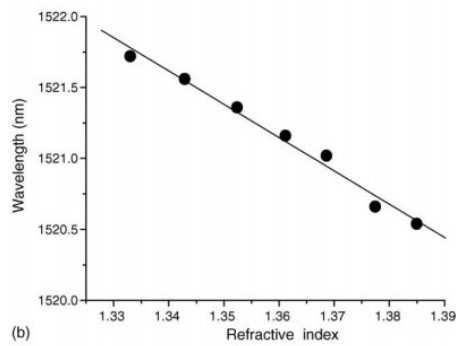
Ding et al. (2005) reported the use of fiber-taper seeded (FTS) long period grating pair (LPGP) as a refractive index sensor. The LPGPs were packaged into a shallow aluminum box and the responses to changes in the refractive index of the external medium were measured by an OSA. Ding et al. (2005) used sucrose solutions with different concentrations to create the changes in the refractive index and measurements were carried out in an environment with a constant temperature to avoid cross-sensitivity between the refractive index and temperature. Garg et al. (2013) designed a long period fiber grating based temperature-compensated sensor for bio-chemical sensing applications by splitting the LPFG transmission spectrum at its phase-matching turn-around point. Various concentrations of sucrose in distilled water were used as samples of different refractive indices to enable observation of the refractive index sensitivity due to the surrounding medium with no changes in temperature and strain (Garg et al., 2013).

Tang et al. (2005) designed a fiber-optic biochemical sensing method with a colloidal gold-modified long period fiber grating to sense antibodies. Self-assembled colloid monolayer of gold on the grating surface of the LPFG was used to detect changes in the surrounding refractive index and the result is

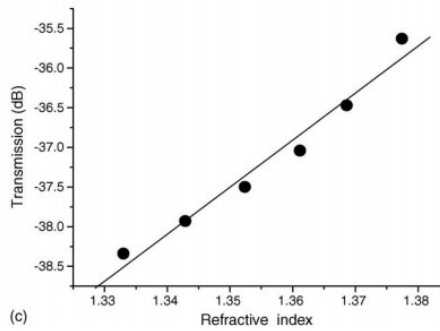
shown in Figure 2.15 (Tang et al., 2005). Figure 2.15(a) and Figure 2.15(b) shows a blue shift in the resonance wavelength which fulfils the phase matching condition. Figure 2.15(c) shows an increase in transmission loss as the refractive index increases. Tang et al. (2005) demonstrated monitoring of chemical solution concentration.



(a)



(b)



(c)

**Figure 2.15: (a) Transmission spectra of colloidal Au-modified long-period fiber grating in aqueous solution containing increasing concentration of sucrose. (b) Plot of peak wavelength vs. refractive index of the sucrose solution. (c) Plot of transmission loss vs. refractive index of the sucrose solution (Tang et al., 2005)**

To investigate the applications of the self-assembled colloid monolayer gold on the grating surface of the LPFG for biomolecular binding, Tang et al. (2005) immobilized dinitrophenyl (DNP) antigen on to the surface of the self-assembled colloid monolayer gold LPFG sensor. The sensor was then used to sense anti-DNP and the concentration-dependent response of DNP-functionalized self-assembled colloid monolayer gold on LPFG was investigated to determine the sensitivity of the sensor towards DNP-anti-DNP binding. The transmission spectra of the sensor towards various concentrations of anti-DNP in buffer solution are shown in Figure 2.16. Tang et al. (2005) were successful in designing a label-free detection of biomolecular binding at the surface of gold nanoparticles with a detection limit of  $9.5 \times 10^{-10}$  M of anti-DNP when the colloidal surface was modified with DNP.

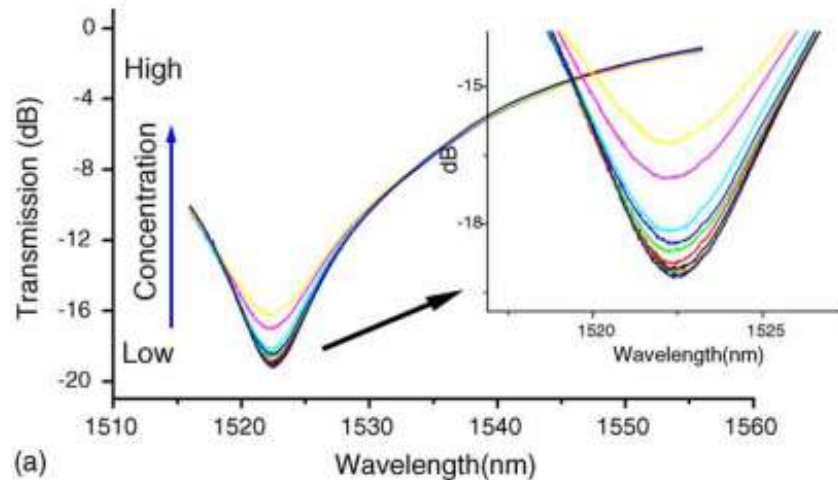


**Figure 2.16: Transmission spectra of DNP-functionalized self-assembled colloid monolayer gold on LPFG in a buffer solution containing increasing concentration of anti-DNP (Tang et al., 2005)**

## CHAPTER 3

### METHODOLOGY

#### 3.1 Introduction

The fabrication of LPFG using an electric arc induced method and its application as sensors are presented in this chapter. Section 3.2 will discuss on the fabrication method adopted in this research, while for Section 3.3, the focus will be on the characterization of the LPFG and the introduction of the double pass configuration to enhance the sensitivity of the LPFG.

Section 3.3 describes some application of the developed double pass configuration as sensors to detect ethanol, sucrose and biotin. To observe whether the sensitivity of the double pass LPFG could be further sensitized, the LPFG was coated with polyelectrolyte materials to enhance its sensitivity towards various concentrations of sucrose.

#### 3.2 Fabrication of Arc-induced LPFG

SMF28 fiber was used to fabricate the LPFGs where the fiber polymer coating was stripped off before the gratings were formed using the high-voltage electric arcing method which consists of an ignition coil (Bosch 30KW 12V), an arcing circuit, a tension meter, weights, a pair of electrodes

(Sumitomo ER10), computer-controlled motorized stage and a pair of fiber clamps with and without sliders.

The setup for the electric arc-induced LPFG fabrication method is shown in Figure 3.1. During fabrication, a constant force is applied to the fiber to create a constant axial tension. The fiber clamp with slider allows the deformation of the cladding with the help of the constant axial tension as the fiber clamp without slider holds the other end of the fiber in position. This results in a taper forming at the arcing point. Once the grating formation is complete, the motorized stage will move the electrodes to the next point to form the subsequent gratings on the fiber. The structure of the tapers depends on axial tension and arcing discharge time (Lee et al., 2013).

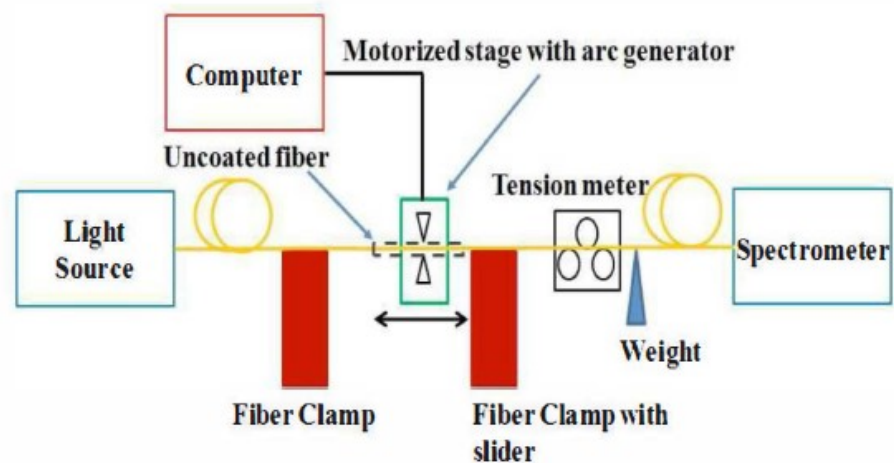


**Figure 3.1: Setup of high-voltage electric arc-induced LPFG fabrication method (Lee et al., 2013).**

Figure 3.2 shows an image of a taper formed using the high-voltage electric arcing method.

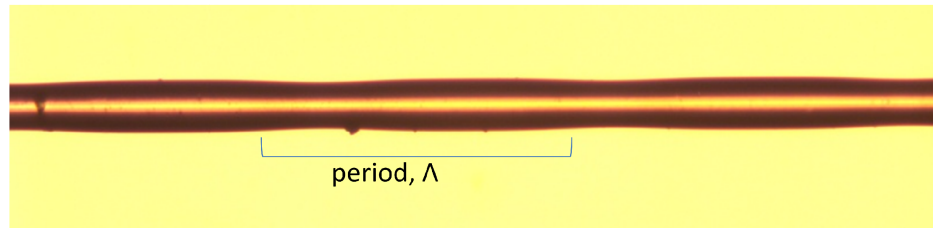


**Figure 3.2: Image of taper fabricated for arc-induced LPFG.**

Electric arc-induced LPFGs with grating period within the range of  $610\mu\text{m}$  to  $680\mu\text{m}$  and grating length between 16 mm and 28 mm were used for this project. A broadband light source (Alnair Labs, LNA-220C-40-SM Low Noise Optical Amplifier) was used throughout the experiments while the output transmission spectra were observed using an optical spectrum analyzer (OSA) (Yokogawa, AQ6370C 600-1700nm Optical Spectrum Analyzer). A constant force of 15 cN was applied to the LPFG to create a constant axial tension throughout the experimental process. The LPFGs used in this dissertation are presented in Table 3.1.

**Table 3.1: Grating period length of LPFGs used in this dissertation**

Fiber	Grating period length ( $\mu\text{m}$ )
A	630
B	640
C	675
D	630
E	650
F	650

### **3.3 Characterization of arc-induced LPFG**

Figures 3.3(a) and (b) illustrate the experimental setups for the single pass and double pass configurations, respectively. In the single-pass configuration, the broadband light signal enters the first circulator through port 1, passes through the LPFG, exits the second circulator at port 2, and finally monitored through the OSA. The setup is similar for the double-pass configuration only up to the point where the light enters the second circulator at port 2, following which the signal is then re-circulated back to the LPFG, i.e. by connecting port 3 to port 1. The signal that double-passed through the LPFG will re-enter the first circulator and exits through port 3 to the OSA. The light passes through the LPFG once in the single pass configuration but passes through the LPFG twice, once from the first circulator through the LPFG to the second circulator and the second time from the second circulator

through the LPFG again to the first circulator before entering the OSA, in the double pass configuration.

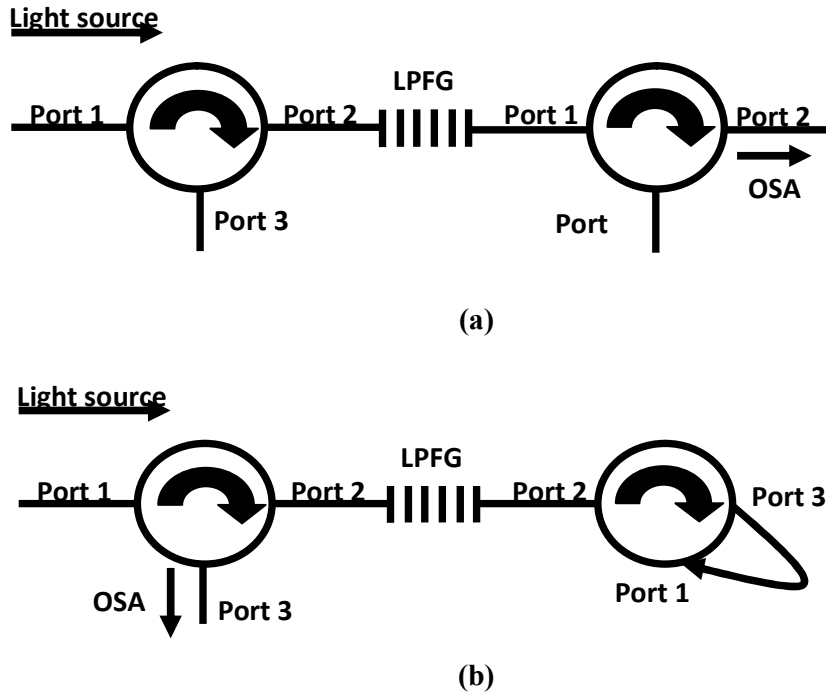


**Figure 3.3: (a) Single pass configuration and (b) Double pass configuration**

To characterize the arc-induced LPFG, using the set-ups shown in Figure 3.3, the LPFG was immersed in refractive index (RI) matching liquid (Cargille Refractive Index Liquids) with refractive indices of 1.4000, 1.4100, 1.4200, 1.4300, 1.4400, 1.4500, 1.4600, 1.4700, 1.4800, 1.4900 and 1.5000. The transmission spectra were recorded for both the single pass and double

pass configurations of the same fiber. The LPFG was cleaned with isopropyl alcohol before immersing in different RI matching liquids. The experiment was repeated with a different LPFG to observe the spectral response and sensitivity of the LPFGs in both single and double pass configurations. The environment of the lab when the experiments were conducted averaged at 18°C and 75% humidity. This applies to all other experiments mentioned in this dissertation as well.

### **3.4 Applications of Double Pass LPFG Configuration**

This section describes the application of the double pass arc-induced LPFG as a chemical and biosensor. Sucrose, ethanol and biotin were used to test the sensitization of the double pass LPFG as compared to the single pass LPFG configuration.

#### **3.4.1 Sensing of Ethanol Concentration**

The experimental set-ups to test the arc-induced LPFG for various ethanol (GmbH, 95% ethanol) concentrations are similar to the set-ups described in Section 3.3. Ethanol solution was prepared according to Table 3.1. The LPFG was immersed in 10 % ethanol and the process was repeated for 20 %, 30 %, 40 %, 50 %, 60 %, 70 %, 80 %, 90 % and 95 % ethanol. The transmission of the arc-induced LPFG was then recorded for both single and

double pass configurations. The arc-induced LPFG was cleaned with water between immersions in different ethanol concentrations. The experiment was repeated with a different LPFG to observe the spectral respond and sensitivity of the LPFGs in both single and double pass configurations.

**Table 3.2: Volume of water and 95% ethanol needed to prepare ethanol solutions in various concentrations**

Concentration (%)	Volume of ethanol (mL)	Volume of water (mL)
10	6.3	53.7
20	12.6	47.4
30	18.9	41.0
40	25.3	34.7
50	31.6	28.4
60	37.9	22.1
70	44.2	15.8
80	50.5	9.5

### 3.4.2 Sensing of Sucrose Concentration

Similar to the experiment described in Section 3.4.1, the arc-induced LPFG in both single and double pass configurations was immersed in sucrose solution (Acros Organics, AR sucrose) with concentrations of 10%, 20 %, 30 %, 40 %, 50 %, 60 %, 70 % and 80 %. The sucrose solutions were prepared

according to Table 3.2. The transmission of the arc-induced LPFG was then recorded for both single and double pass configurations. The arc-induced LPFG was cleaned with water between immersions in different sucrose concentrations. The experiment was repeated with a different LPFG to observe the spectral respond and sensitivity of the LPFGs in both single and double pass configurations.

**Table 3.3: Weight of sucrose crystals and volume of water needed to prepare sucrose solutions in various concentrations**

Concentration (wt%)	Sucrose (g)	Water (mL)
10	10	100
20	20	100
30	30	100
40	40	100
50	50	100
60	60	100
70	70	100
80	80	100

The experiment on sucrose concentration was extended by modifying the surface and dimension of the LPFG with polyelectrolyte (PE) materials. The arc-induced LPFGs were cleaned with de-ionized (DI) water before they were coated with the PE materials using the layer by layer (LbL) method. Steps in the coating process involve immersion of the LPFG in a solution of

5wt% poly (diallyldimethylammonium chloride) (PDDA) (Mw of 100,000 – 200,000, Sigma Aldrich) for 10 minutes and then rinsed with DI water before being immersed in a solution of 5wt% poly (sodium 4-styrenesulfonate) (PSS) (Mw of 70,000, Sigma Aldrich) for 10 minutes. The layer-by-layer (LbL) coating process was repeated n times for each PE to achieve (PDDA/ PSS)<sub>n</sub> layers. Figure 3.4 is an illustration of an LPFG coated with single layer of PDDA and PSS.

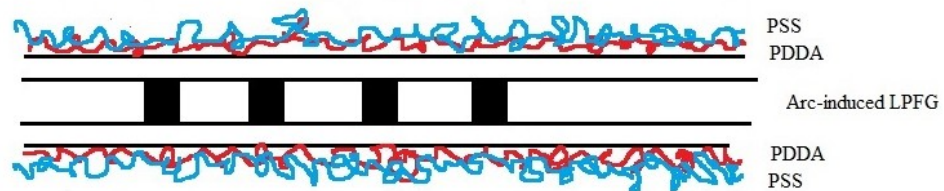


**Figure 3.4: Illustration of arc-induced LPFG coated with a layer of PDDA and PSS**

After coating the arc-induced LPFG with (PDDA/PSS)<sub>5</sub>, the LPFG was immerse in sucrose with 10 %, 20 %, 30 %, 40 %, 50 %, 60 %, 70 % and 80 % concentration respectively and the results were recorded for both single and double pass. The process was repeated for every (PDDA/PSS)<sub>5</sub> up to (PDDA/PSS)<sub>35</sub>. The transmission spectra of the arc-induced LPFG were recorded in both single pass and double pass configurations. The experiment for sensing sucrose without and with PE coatings was repeated with a different LPFG to observe the spectral respond and sensitivity of the LPFGs in both single and double pass configurations.

A field effect scanning electron microscope (FESEM) (JEOL JSM-6701F) was used to determine the existence of the PE coatings on the optical fibers. The PE coated fibers were cut to size and adhered to the sample holder with a carbon tape. The samples were then sputtered with gold/ palladium alloy and mounted onto a stage.

Samples of fibers were used to observe the surface morphology of coated and uncoated SMF28 fibers. To determine the amount of time needed for the PDDA coating to be monolayer, fibers each coated with PDDA for 5, 10 and 15 minutes were prepared. The surface of the samples was then observed using the FESEM. Figure 3.5(a) shows the field effect scanning electron microscope (FESEM) image of the fiber surface without modification as a control. The fiber that was coated with PDDA for 5 minutes shows some of the fiber's surface is coated with PDDA but there are still areas that were uncoated as seen in Figure 3.5(b). Figure 3.5(c) shows the surface of a fiber that was coated with PDDA for 10 minutes and it can be seen that there is a monolayer formed on the surface of the fiber. It is also obvious that the fiber that was coated with PDDA for 10 minutes is coated more evenly and denser than the fiber that was coated with PDDA for 5 minutes. A sample fiber that was coated with PDDA for 15 minutes is shown in Figure 3.5(d). From Figure 3.5(d), it can be seen that the PDDA coating is no longer monolayer although the entire fiber is covered with PDDA. Based on this observation, it has been determined that 10 minutes is needed for a monolayer of PDDA to be form and cover most of the surface area.

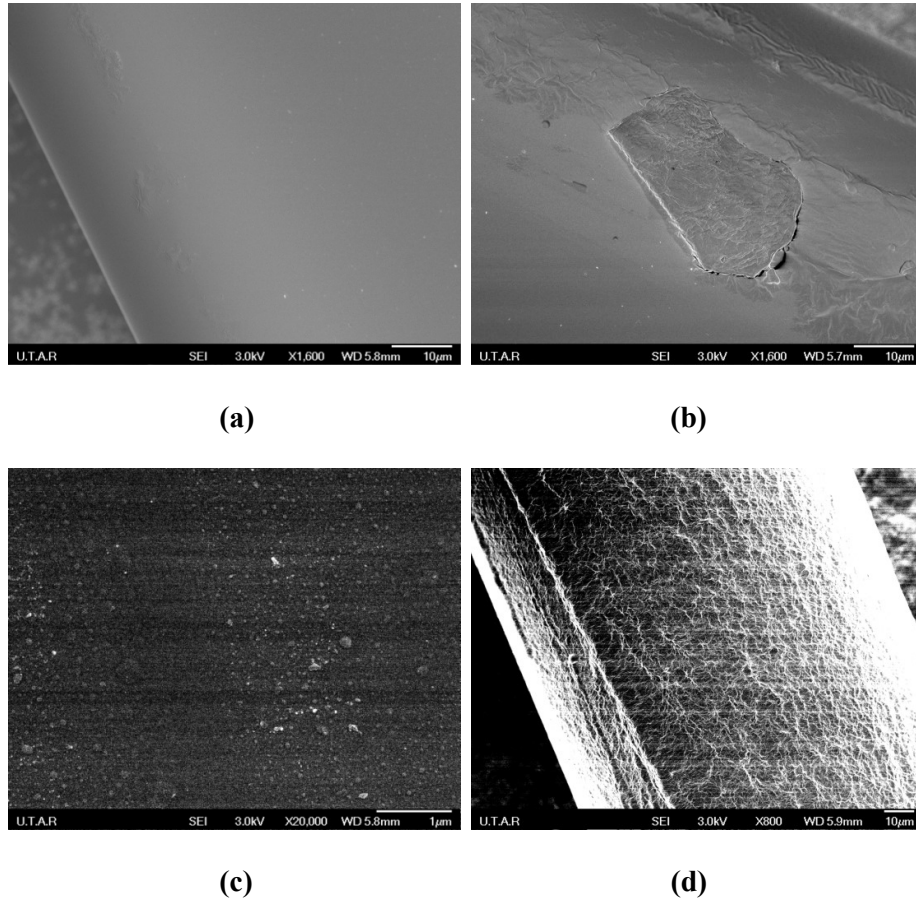
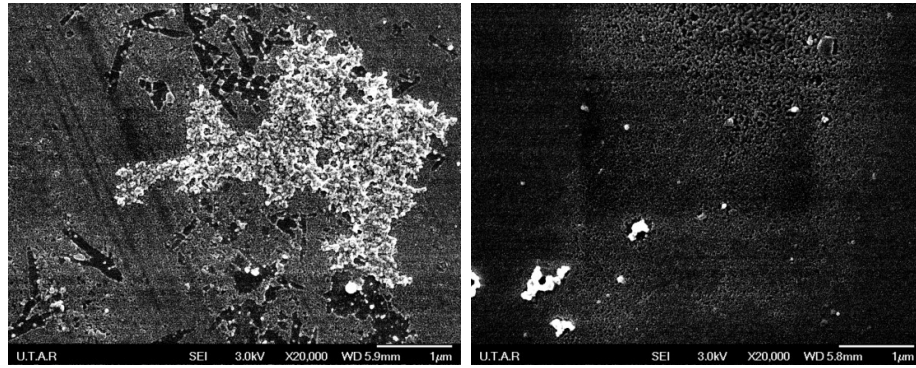


**Figure 3.5: FESEM images of optical fiber surface (a) without PE coating at magnification of 1,600x, (b) after it was submerged in PDDA for 5 minutes at magnification of 1,600x, (c) after it was submerged in PDDA for 10 minutes at magnification of 20,000x and (d) after it was submerged in PDDA for 15 minutes at magnification of 800x**

After the time needed to coat the fiber surface with a monolayer of PDDA determined, the next step is to determine the time needed to coat PDDA-coated fibers with a monolayer of PSS. Fibers that were coated with PDDA for 10 minutes were coated with PSS for duration of 5, 10 and 15 minutes, respectively. The surface morphology of the sample fibers was observed using an FESEM. Figure 3.6(a) shows the image of the surface of a

fiber coated with PDDA for 10 minutes and then in PSS for 5 minutes. It can be seen a layer of PSS has formed on a small area of the surface of the fiber. A better coating of the fiber can be seen in Figure 3.6(b) where the fiber was coated with PDDA for 10 minutes before it was coated with PSS for 10 minutes. It can be seen that the coating is more uniform compared to Figure 3.6(a). To confirm that submerging the PDDA-coated fiber in PSS for 10 minutes leads to a uniform and monolayer coat of PSS on the surface of the fiber, a sample fiber that was coated with PDDA for 10 minutes and PSS for 15 minutes was observed using the FESEM. The surface of the fiber has an irregular coating of PSS as shown in Figure 3.6(c) proving that the appropriate amount of time needed for a uniform monolayer of either PDDA or PSS is 10 minutes each.



(a)

(b)



(c)

**Figure 3.6: FESEM image of optical fiber surface (a) after it was submerged in PDDA for 10 minutes and then in PSS for 5 minutes at magnification of 20,000x, (b) after it was submerged in PDDA for 10 minutes and then in PSS for 10 minutes at magnification of 20,000x and (c) after it was submerged in PDDA for 10 minutes and then in PSS for 15 minutes at magnification of 2,700x**

### 3.4.3 Sensing of Biotin

In this section, the LPFG sensor used to monitor the avidin-biotin interaction over a period of time is described. This avidin-biotin interaction

has diverse applications in various analytical fields especially for molecular detection. The avidin family of proteins, with 4 biotin-binding sites per molecule, is capable of forming tight complexes with biotinylated compounds. Biotin is also known as vitamin H (cis-hexahydro-2-oxo-1-H-thieno-[3,4]-imidazoline-4-valeric acid) and can form an avidin-biotin complex that is very stable. The affinity of avidin-biotin complex is high and the avidin-biotin bond is the strongest known biological interaction between a ligand and a protein (dissociation constant of 10-15M).

To test the applicability of the arc-induced LPFG as a biosensor, the surface of the arc-induced LPFG was modified to detect biotin. After the LPFG fabrication, the grating region of the optical fiber was coated with gold nanoparticles (GNP) synthesized via Frens method (Shao et al., 2010). The Frens method is a chemical reduction method to synthesize GNP. The type of nanoparticles that were synthesized via this method is nanospheres. 50mL of 0.01 wt % chlorauric acid ( $\text{HAuCl}_4 \cdot 3\text{H}_2\text{O}$ ) solution (Sigma Aldrich, Mw of 339.79) was stirred and heated to boiling in a 100mL beaker. 300 $\mu\text{L}$  of 1 wt% trisodium citrate dihydrate ( $\text{Na}_3\text{C}_6\text{H}_5\text{O}_7 \cdot 2\text{H}_2\text{O}$ ) solution (R&M, Mw of 294.10) was added drop-wise to the auric solution. The colour of the solution changed from yellow to black and then to red. The GNP was left to cool before it was immobilized onto the LPFG by utilizing electrostatic self-assembly for 60 minutes. The image of GNP is shown in Figure 3.7. After coating of GNP, the optical fiber was rinsed with deionized water and left to dry in air before the immobilization of avidin.

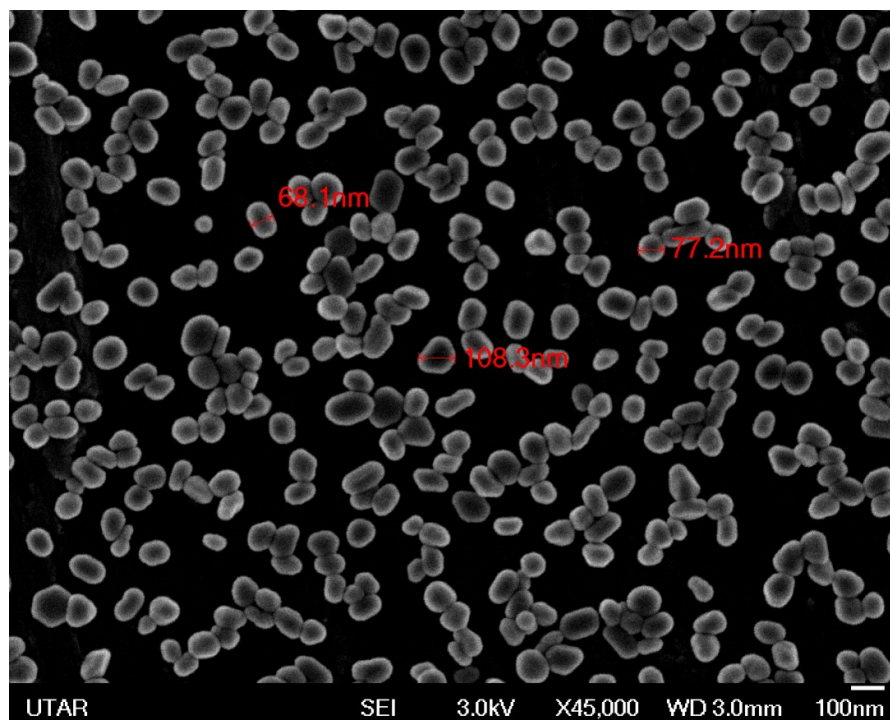
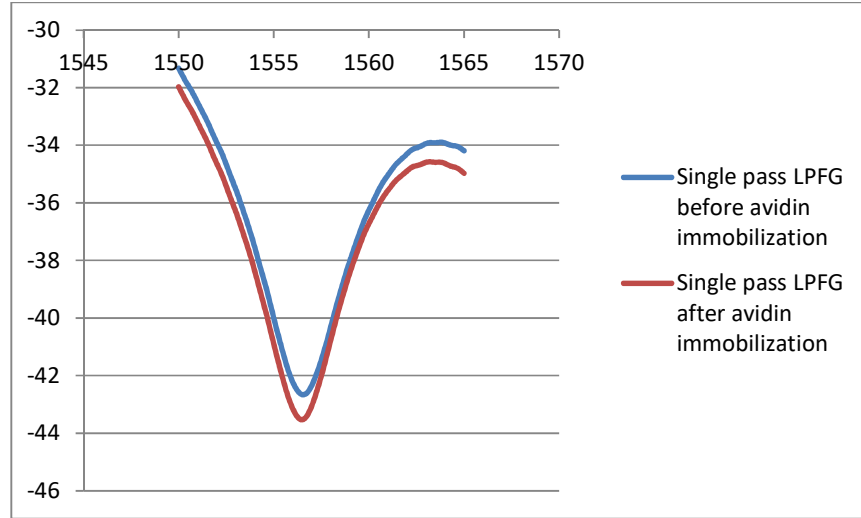


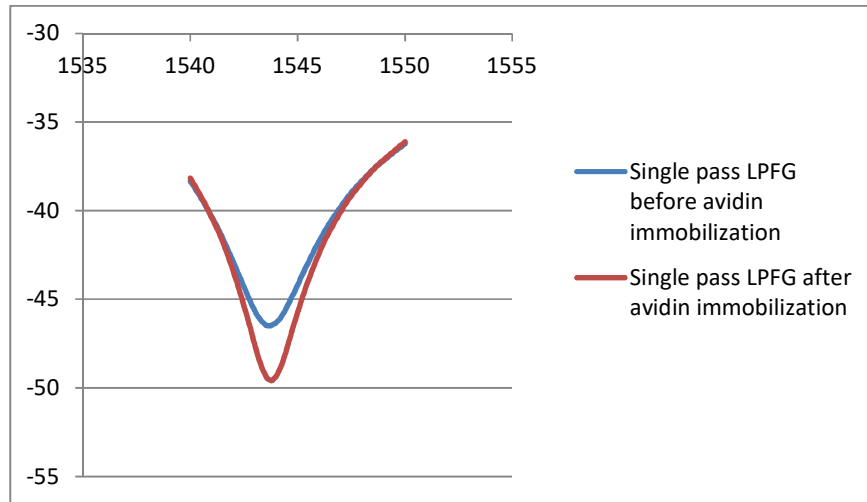
**Figure 3.7: FESEM image of gold nanoparticle synthesized via Frens method with magnification of 45,000x**

Avidin coated LPFG was prepared using the ESA method by immersing the GNP modified LPFG in a phosphate buffer solution (PBS) with pH 7.5 and containing 10 mM of avidin (Sigma Aldrich,  $\geq 98\%$ ) for 60 min. The transmission spectra were as shown in Figure 3.8. The pristine avidin-immobilized LPFG was then connected using single-pass and double-pass configurations. Results of avidin– biotin interaction were obtained when the pristine avidin-immobilized LPFG was submerged into PBS with pH 7.5 containing 10 mM of sulfo-NHS-SS-biotin (EZ-Link, Mw of 504.65) and the transmission spectra were recorded every minute for both single-pass and double-pass configurations. The experiment was repeated with a different

LPFG to observe the spectral response and sensitivity of the LPFGs in both single and double pass configurations.



(a)



(b)

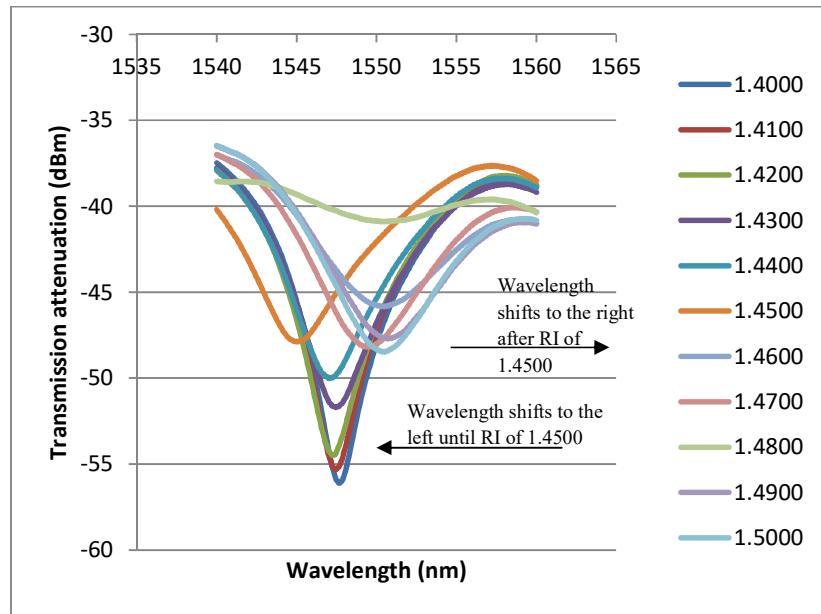
Figure 3.8: Comparison of transmission spectra of single pass LPFG before and after avidin immobilization for fibers (a) E and (b) F.

## CHAPTER 4

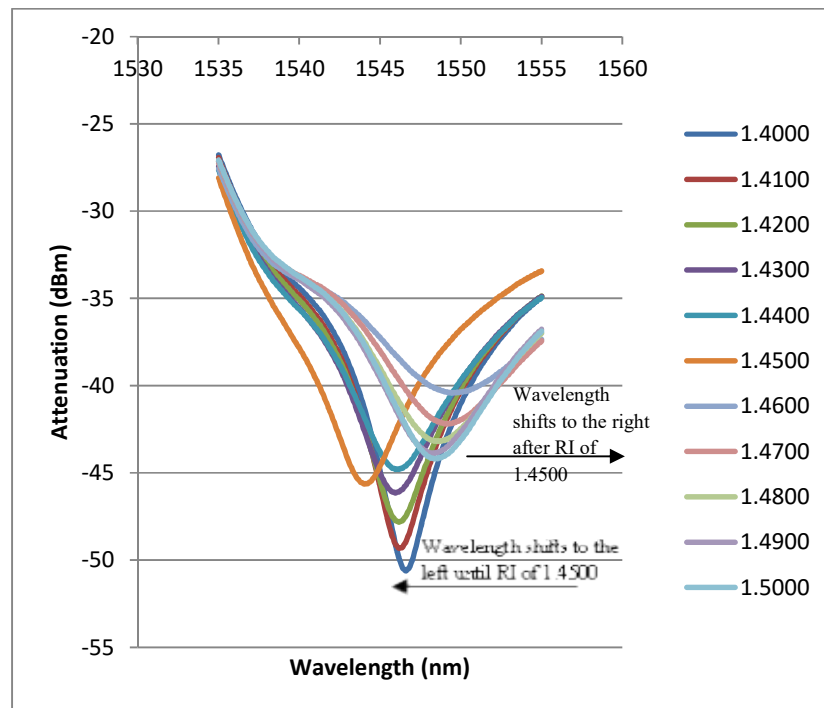
### RESULTS AND DISCUSSION

#### 4.1 Characterization of Single Pass and Double Pass LPFG

Research on the sensitivity of single pass LPFGs toward external refractive index have been done by numerous researchers. The phase-matching condition of an LPFG is affected by the difference between refractive index of the cladding and that of the surrounding medium and thus, causing the LPFG to be sensitive to external refractive index. Figure 4.1(a) and (b) are two LPFG's transmission spectra in various refractive indices. The transmission notch blue shifts from refractive index of 1.4000 up to refractive index of 1.4500 before it starts to red shift at refractive index of 1.4600. The jump between 1.4500 and 1.4600 is due to the external refractive index approaching the refractive index of the cladding. The grating length for fibers A and B are 630  $\mu\text{m}$  and 640  $\mu\text{m}$  respectively. The experiment was conducted in a laboratory with an average temperature of 18°C, average humidity of 75% and tension of both fibers was 5cN. The condition was maintained for fibers A and B when sensing ethanol as well.



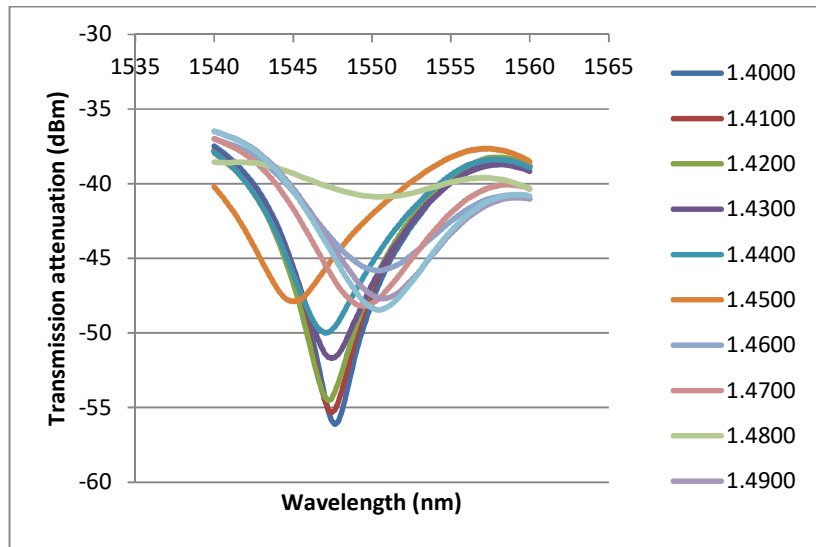
(a)



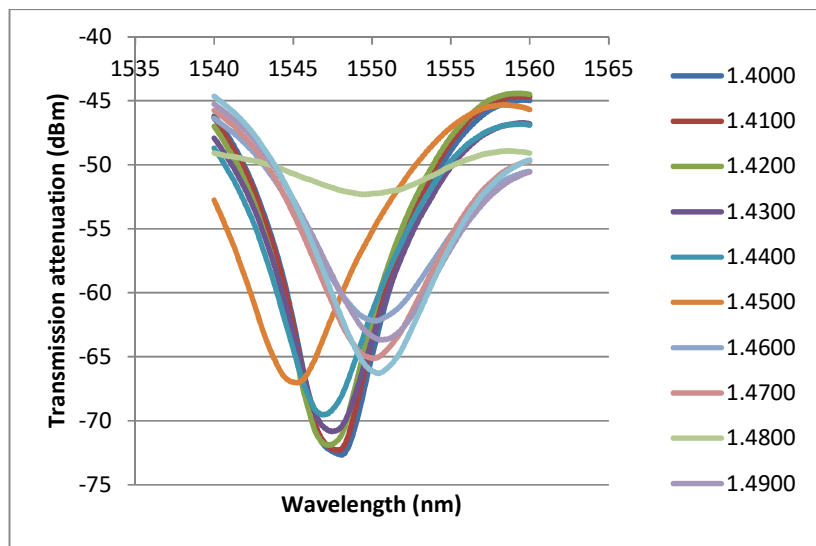
(b)

**Figure 4.1: Transmission spectrum of single pass LPFG in various refractive indices for fibers (a) A and (b) B**

The minimum transmission power of the attenuation band in double pass configuration is almost double when compared to single pass configuration. It is possible that over-coupling of the light as it passes through the LPFG a second time is a factor for not being able to achieve double attenuation when in double pass configuration compared to single pass configuration. Transmission spectra from experiments for LPFGs in single and double pass configurations for the same surrounding refractive index are given in Figure 4.2 which displays better transmission attenuation in double pass configuration compared to single pass configuration. A comparison of transmission spectra for various external refractive indices in single and double pass configuration is given in Figure 4.2 which indicates that the wavelength shifts in double pass configuration is similar to single pass configuration.



(a)



(b)

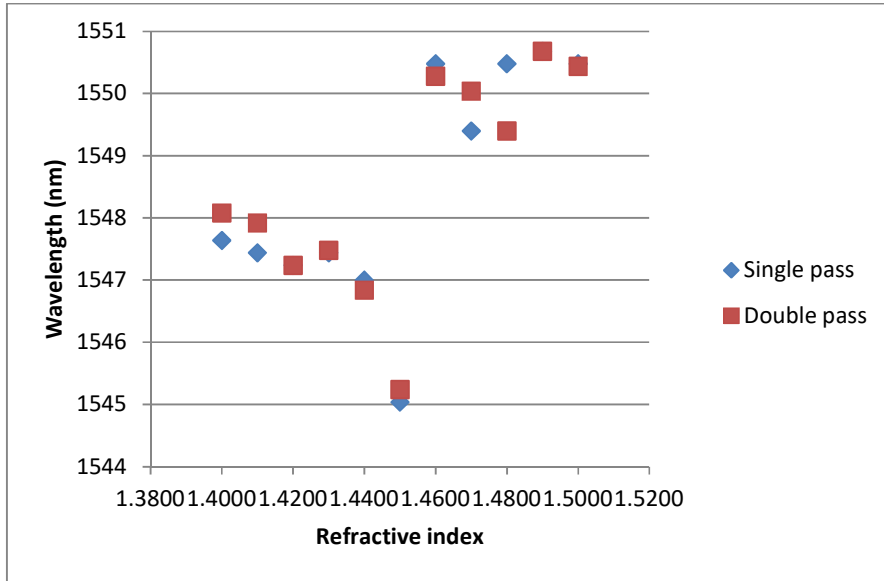
**Figure 4.2: Comparison of transmission spectra of a LPFG in various refractive indices for (a) single pass configuration, and (b) double pass configuration**

## 4.2 Sensitivity of LPFG in Single Pass and Double Pass

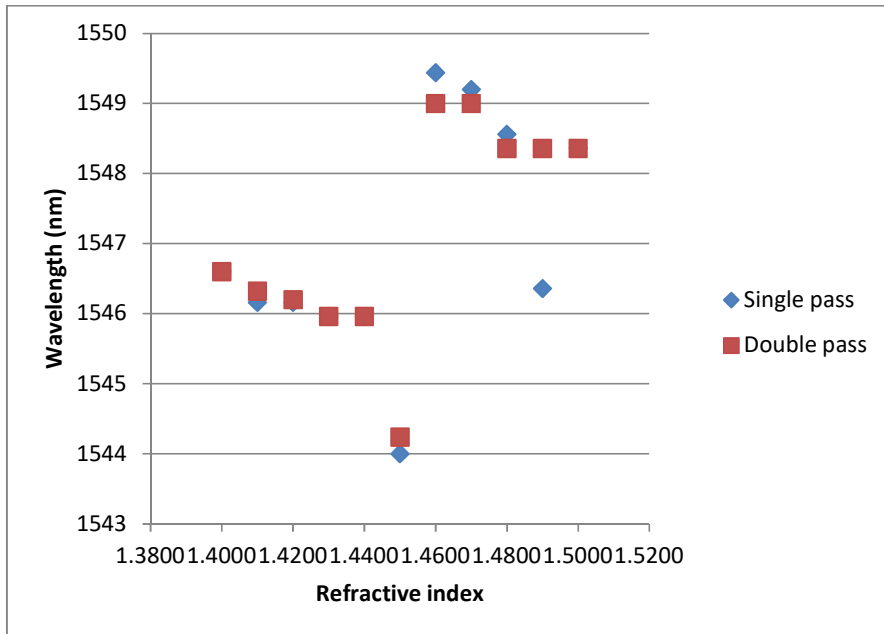
From the previous section, the double pass configuration displays higher transmission attenuation compared to the single pass configuration although the wavelength shift in double pass configuration is similar to that in single pass configuration which can be explain by phase matching condition. This section is to the findings that an electric arc-induced LPFG in double pass configuration is more sensitive towards external refractive index than single pass configurations.

In Figure 4.3, the resonant wavelength of a bare arc-induced LPFG in various refractive indices using Cargille oil is shown for two different electric arc-induced LPFG in both single and double pass configurations. It shows that both single and double pass configurations are most sensitive between refractive indices of 1.4500 and 1.4600 as it approaches the refractive index of the cladding. The wavelengths of the transmission notch for refractive indices of 1.4500 and 1.4600 are 1545.04 nm and 1550.48 nm in single pass, and, 1545.24 nm and 1550.28 nm in double pass for fiber A. The wavelength shift patterns for both single and double pass in Figure 4.3(a) are similar to each other and that there is no significant difference between the resonant wavelengths of single and double pass configurations with wavelength difference between refractive indices of 1.4500 and 1.4600 at 5.44 nm and 5.04 nm for the respective configurations. The wavelengths of the transmission notch for refractive indices of 1.4500 and 1.4600 are 1544 nm

and 1549.44 nm in single pass, and, 1544.24 nm and 1549 nm in double pass for fiber B. The wavelength difference between refractive indices of 1.4500 and 1.4600 for fiber B at the transmission notch is also at 5.44 nm and 5.04 nm as shown in Figure 4.3(b). This proves that the fiber detecting various refractive indices is supported by  $\lambda_i = \left( n_{core}(\lambda_i) - n_{clad}^i(\lambda_i) \right) \Lambda$ . Since  $n_{core}(\lambda_i)$  and  $\Lambda$  are constant, the refractive index of the Cargille oil affects the  $\lambda_i$  and thus, cause the wavelength shift as seen in Figure 4.3.



(a)

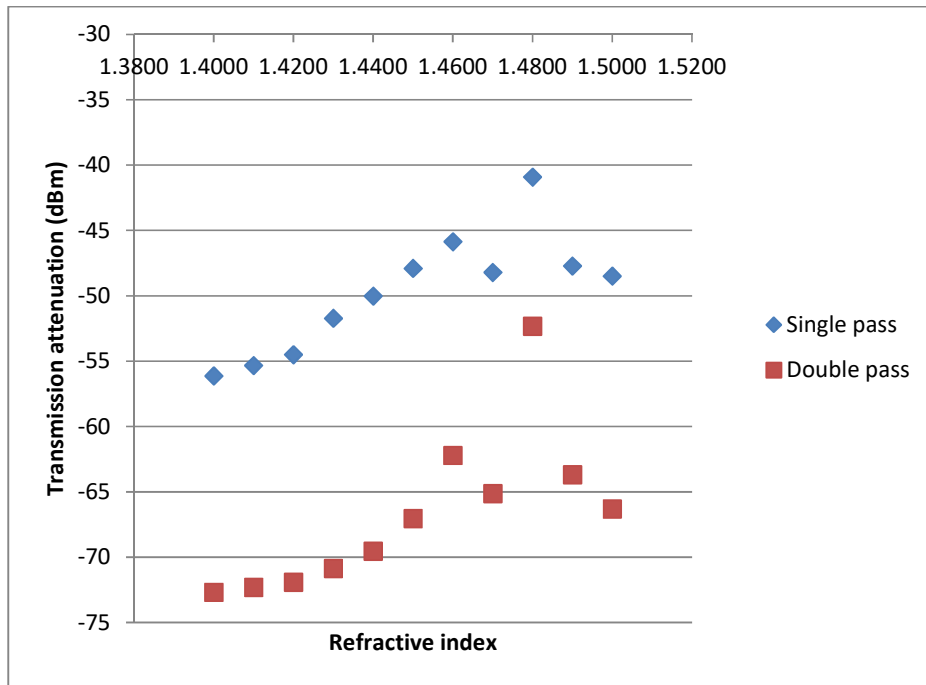


(b)

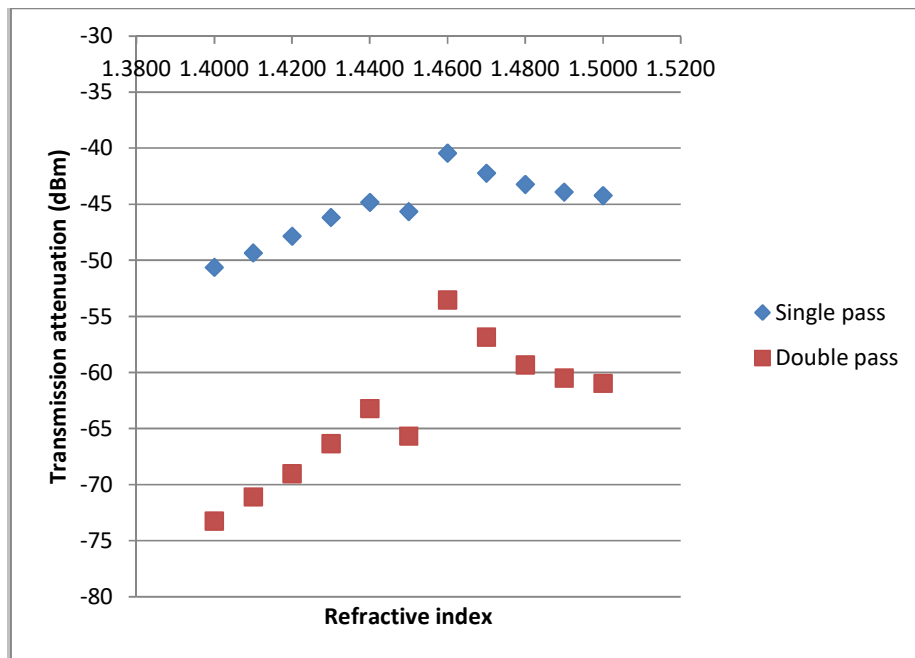
**Figure 4.3: Resonant wavelength vs refractive index of Cargille oil of two different electric arc-induced LPFGs (a) fiber A and (b) fiber B**

Figure 4.4 presents the transmission attenuation of resonant wavelengths for both single and double pass configuration of two different bare arc-induced LPFGs. The transmission attenuation for both single and double pass show similar pattern. In Figure 4.4(a), both single and double pass configurations display highest sensitivity between refractive indices 1.4700 and 1.4800. The values for attenuation at transmission notch for refractive indices of 1.4700 and 1.4800 are -48.201 dBm and -40.908 dBm in single pass, and, -65.128 dBm and -52.32 dBm in double pass for fiber A. However, single pass configuration for fiber A at the transmission notch had a transmission difference of 7.293 dB between refractive indices of 1.4700 and 1.4800 while double pass configuration shows a transmission difference of 12.808 dB. The transmission attenuation notches of the resonant wavelength peak shows that double pass configuration has almost twice the transmission attenuation compared to single pass configuration. Fiber B displays similar characteristics in Figure 4.4(b) with highest sensitivity between refractive indices of 1.4500 and 1.4600 for both single and double pass configurations. The values for attenuation at transmission notch for refractive indices of 1.4500 and 1.4600 are -45.636 dBm and -40.427 dBm in single pass, and, -65.655 dBm and -53.507 dBm in double pass for fiber B. The transmission attenuation difference of the transmission notches between refractive indices of 1.4500 and 1.4600 for single and double pass configurations were 5.209 dB and 12.148 dB respectively. Figure 4.4 shows the double pass configuration had almost two times more attenuation compared to single pass configuration which is attributed by the transmission characteristics of the LPFG influenced by the transmittance factor  $\cos^2(\kappa L) \times 2$ . This is due to the signal passing

through the arc-induced LPFG twice before entering the OSA. Since the purpose of this project is to increase the sensitivity of electric arc-induced LPFG without surface modification, this dissertation will focus on the transmission attenuation as there isn't much difference in wavelength shift between single and double pass configurations.



(a)

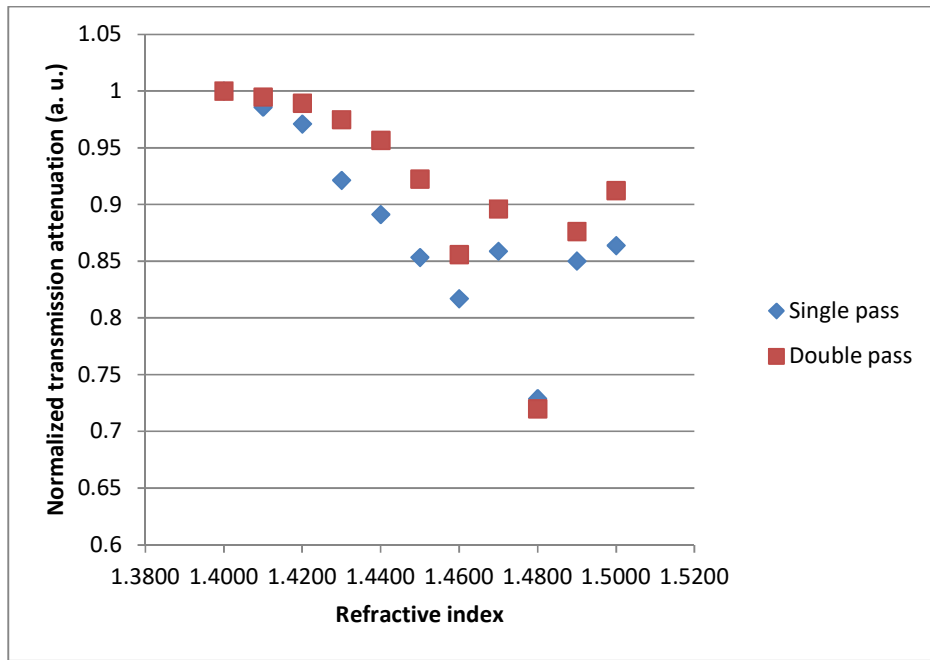


(b)

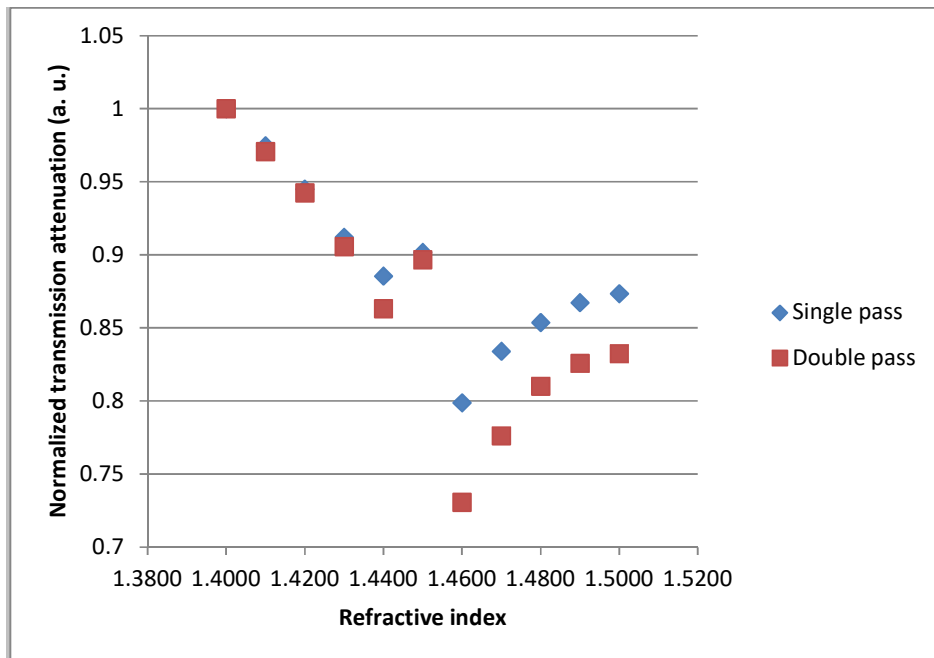
**Figure 4.4: Transmission attenuation of resonant wavelength vs refractive index of Cargille oil of (a) fiber A and (b) fiber B**

The normalized transmission attenuation of two different bare arc-induced LPFGs were presented in Figure 4.5. Normalization was done to bring the results of both single and double pass configurations to the same baseline for purpose of comparison. The normalized value is the division of the value by the value of the transmission attenuation notches in refractive index of 1.4000 for the respective configurations. In Figure 4.5(a), fiber A is most sensitive to ambient refractive indices between 1.4700 and 1.4800 in both single and double pass configurations. The values for normalized attenuation at the transmission notch for refractive indices of 1.4700 and 1.4800 are 0.858891661 a.u. and 0.72893799 a.u. in single pass, and, 0.896166442 a.u. and 0.719927347 a.u. in double pass for fiber A. The difference between the two normalized transmission attenuation values at the transmission notch for single and double pass configurations are 0.128997862 a.u. and 0.176239095 a.u. Dividing the difference between two normalized values in double pass by the difference between the two normalized values in single pass, the value in double pass is almost 1.5 times of that in single pass. Fiber B is most sensitive between ambient refractive indices of 1.4500 and 1.4600 as seen in Figure 4.5(b). The values for normalized attenuation at transmission notch for refractive indices of 1.4500 and 1.4600 are 0.901629952 a.u. and 0.798715796 a.u. in single pass, and, 0.896558787 a.u. and 0.73067049 a.u. in double pass for fiber B. The difference between the two normalized transmission attenuation values for single and double pass configurations are 0.102914156 a.u. and 0.165888297 a.u. Dividing the difference between two normalized values in double pass by the difference between the two normalized values in

single pass, the value in double pass is slightly more than 1.5 times of that in single pass.



(a)



(b)

**Figure 4.5: Normalized transmission attenuation of the bare arc-induced LPFG vs refractive index of Cargille oil for (a) fiber A and (b) fiber B**

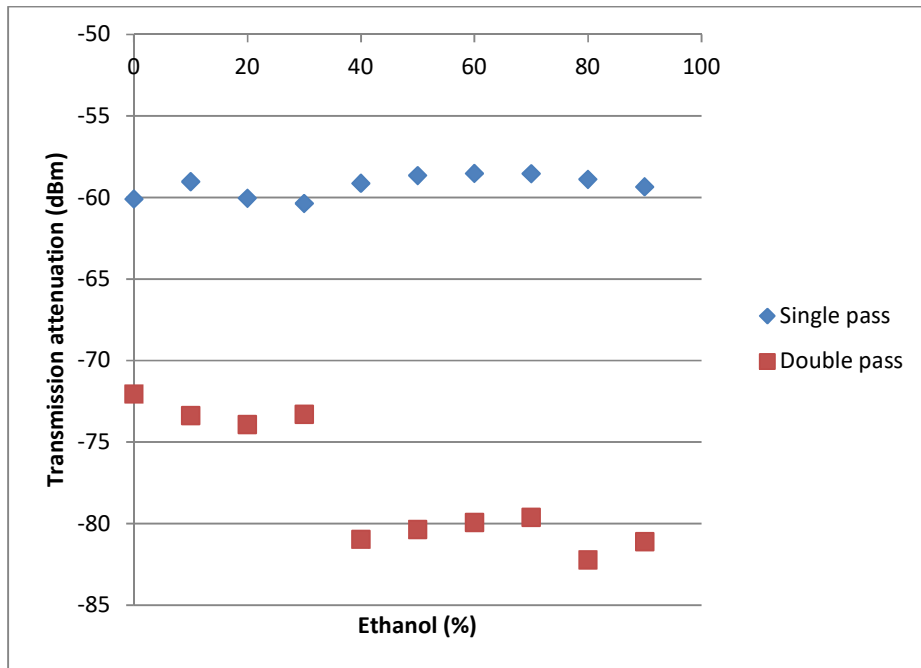
### 4.3 Applications of Double Pass LPFG Configuration

#### 4.3.1 Sensing of Ethanol Concentration

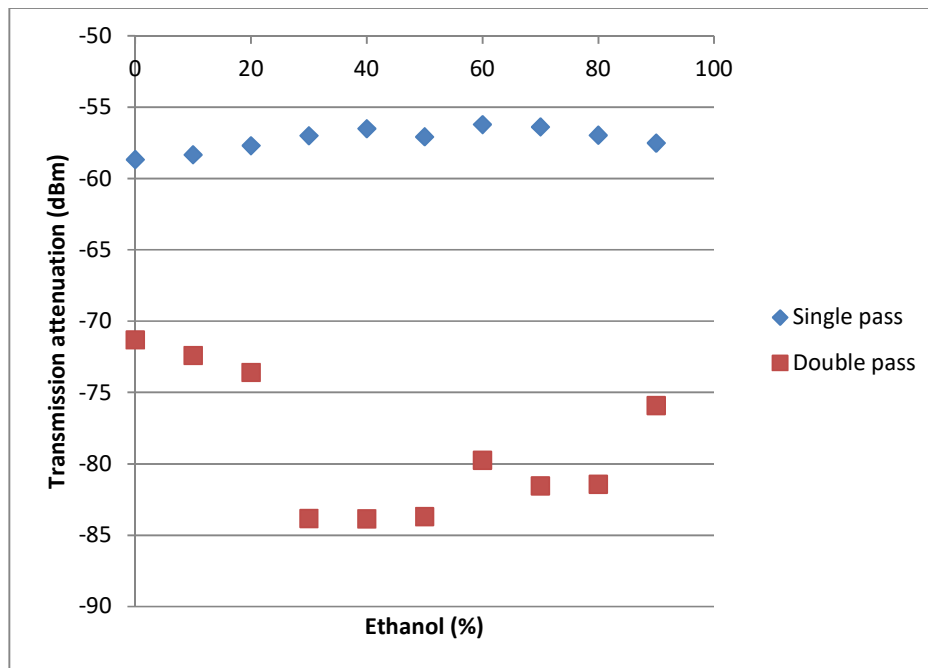
To test the applicability of the arc-induced LPFG as a chemical sensor, two different bare arc-induced LPFG were used to detect various concentrations of ethanol. Various concentrations of ethanol were used because the refractive indices of ethanol vary with concentration.

Figure 4.6(a) shows the double pass configuration had almost two times more attenuation compared to single pass configuration which is attributed to the transmission characteristics of the LPFG influenced by the transmittance factor  $\cos^2(\kappa L) \times 2$ . It can be seen from Figure 4.6(a) and Figure 4.6(b) that the transmission attenuation in single pass configuration is not as significant as in double pass configuration. This is especially true between 30% and 40% ethanol for fiber A and 20% and 30% for fiber B. The values for attenuation at transmission notch for refractive indices of 30 % and 40 % are -60.36 dBm and -59.13 dBm in single pass, and, -73.291 dBm and -80.956 dBm in double pass for fiber A and the values for attenuation at transmission notch for refractive indices of 20 % and 30 % are -57.693 dBm and -56.989 dBm in single pass, and, -73.583 dBm and -83.816 dBm in double pass for fiber B. The difference between transmission attenuation notches of fiber A for concentrations of 30% and 40% ethanol are 1.23 dB and 7.665 dB in single

and double pass where as the difference between transmission attenuation notches for fiber B in concentrations of 20% and 30% ethanol are 0.704 dB and 10.233 dB.



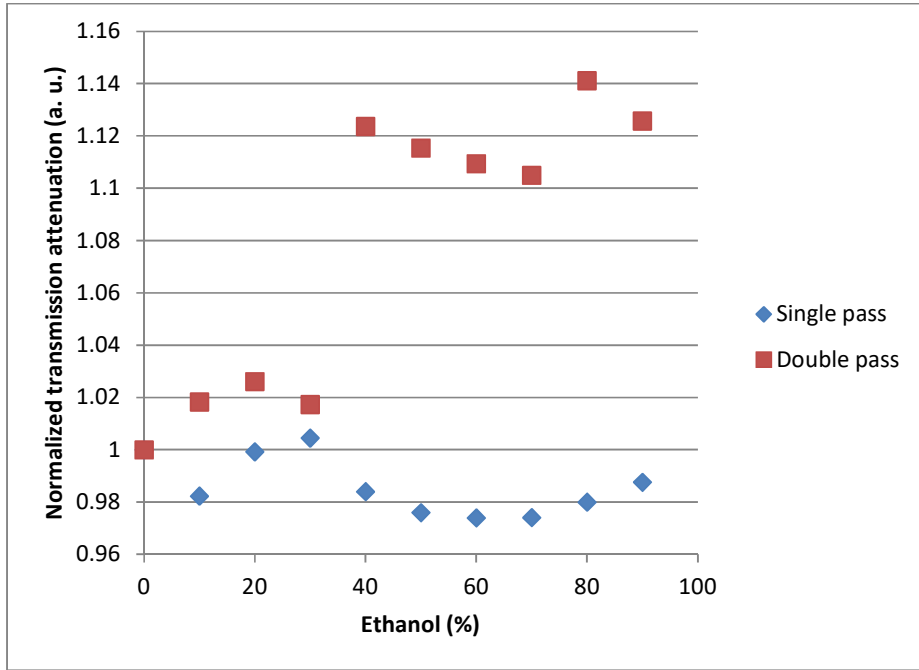
(a)



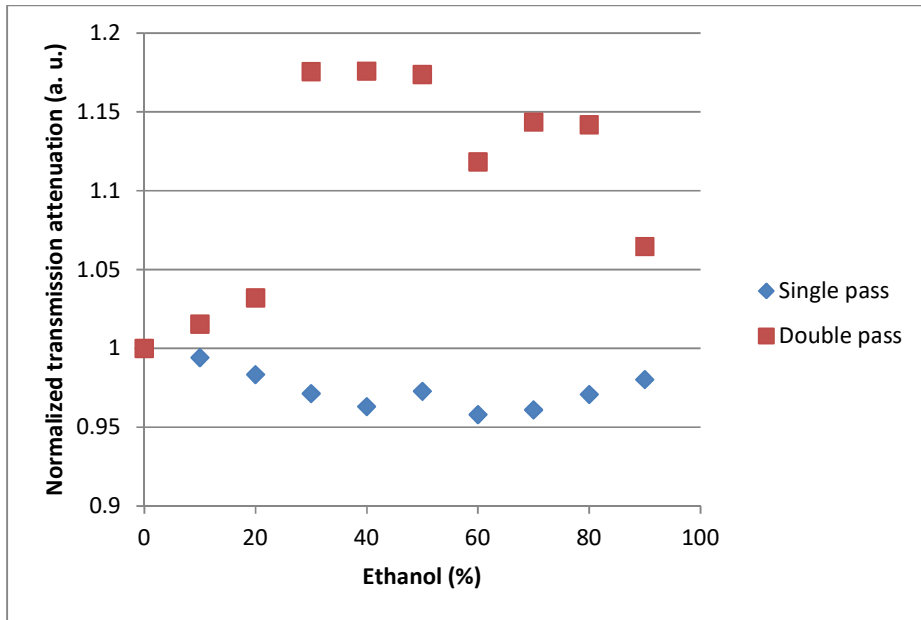
(b)

**Figure 4.6: Resonant transmission attenuation of the bare arc-induced LPFG vs ethanol concentration of (a) fiber A and (b) fiber B**

The normalized values in Figure 4.7 are derived from division of the transmission attenuation by the value of the transmission attenuation at 0 % ethanol for the respective configurations. The normalized transmission attenuation as shown in Figure 4.7(a) indicates that the transmission attenuation notches of fiber A is most sensitive between 30% and 40% ethanol for both single and double pass configurations respectively. The values for normalized attenuation at transmission notch for refractive indices of 30 % and 40 % are 1.00449326 a.u. and 0.984023964 a.u. in single pass, and, 1.017280626 a.u. and 1.123670988 a.u. in double pass for fiber A. The normalized transmission difference for fiber A between 30% and 40% ethanol are 0.020469296 a.u. and 0.106390362 a.u. in single and double pass configurations. Fiber B displays in Figure 4.7(b) that it is most sensitive between 20% and 30% ethanol in both single and double pass configurations. The values for normalized attenuation at the transmission notch for refractive indices of 20 % and 30 % are 0.98338106 a.u. and 0.971381332 a.u. in single pass, and, 1.032048585 a.u. and 1.175572947 a.u. in double pass for fiber B. The normalized wavelength difference between 20% and 30% ethanol for fiber B are 0.000103 a.u. and 0.143524 a.u. in single and double pass configurations respectively. It is clear in Figure 4.7 that the transmission attenuation of the double pass configuration is more sensitive compared to the transmission attenuation of the single pass configuration.



(a)



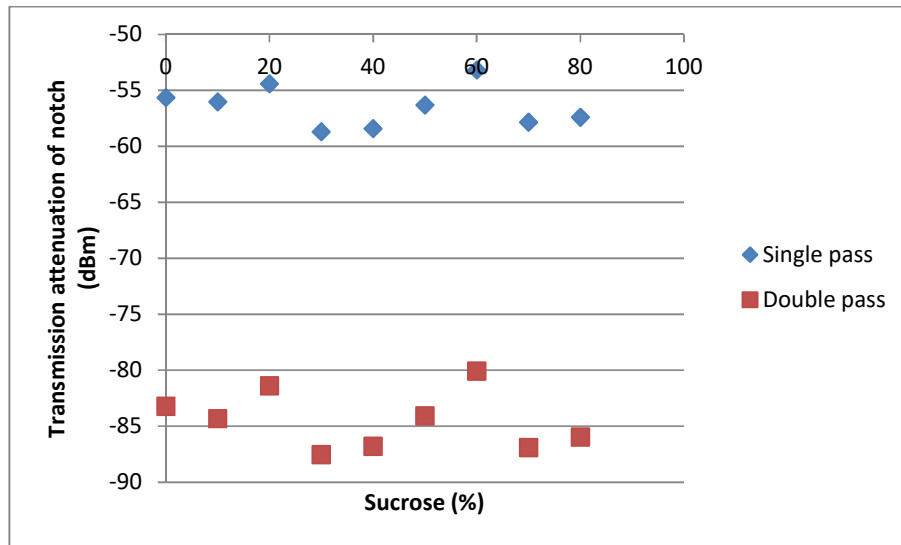
(b)

**Figure 4.7: Normalized transmission attenuation of bare arc-induced LPFG vs concentrations of ethanol for (a) fiber A and (b) fiber B**

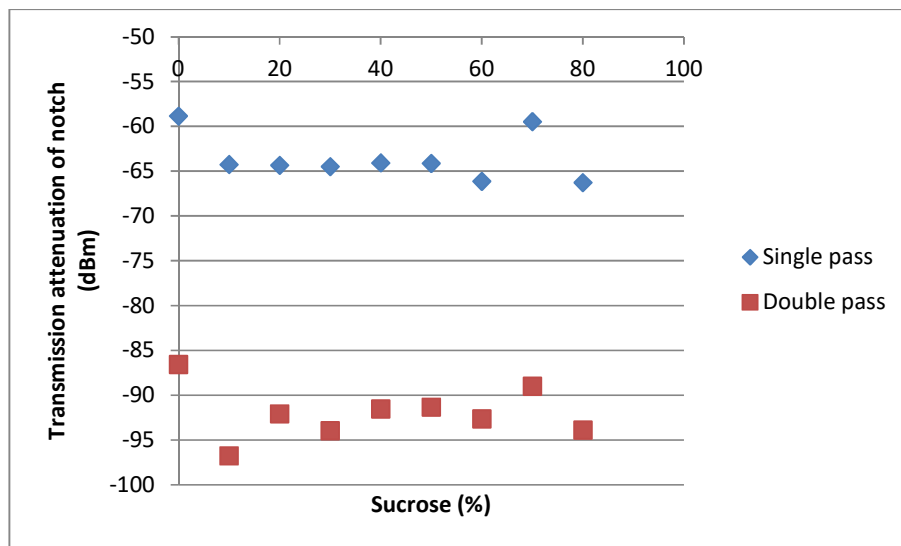
## **4.3.2 Sensing of Sucrose Concentration**

### **4.3.2.1 Sensing of Sucrose Concentrations with uncoated Electric Arc-induced Double Pass LPFG**

Another way to prove the applicability of the electric arc-induced LPFG as a chemical sensor is to detect various concentrations of sucrose. Fiber C has grating length of 675 nm and fiber D has a grating length of 630 nm. The tension for both fibers during the experiment was 5cN and the environment of the laboratory was maintained at an average of 18°C and 75% humidity. In Figure 4.8, we could observe that the trend for single and double pass of fibers C and D are similar. Although the trend is similar, the changes in the transmission attenuation were slight for both fibers in single and double pass configurations. In order to further increase the sensitivity of the double pass LPFGs, PEs were coated using the layer by layer (LbL) method.



(a)



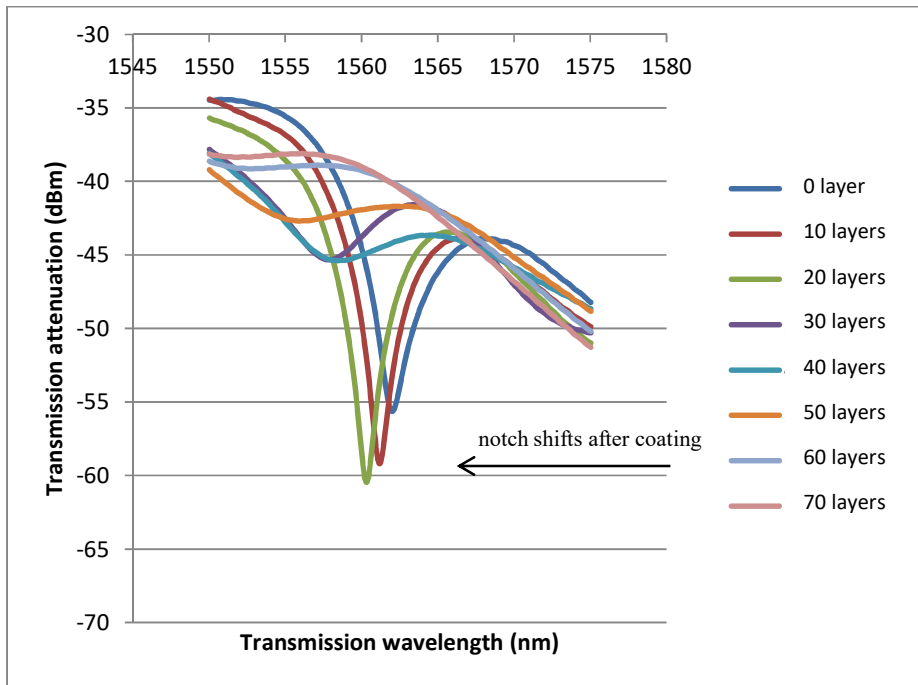
(b)

**Figure 4.8: Transmission attenuation of the bare arc-induced LPFG vs concentrations of sucrose of (a) fiber C and (b) fiber D**

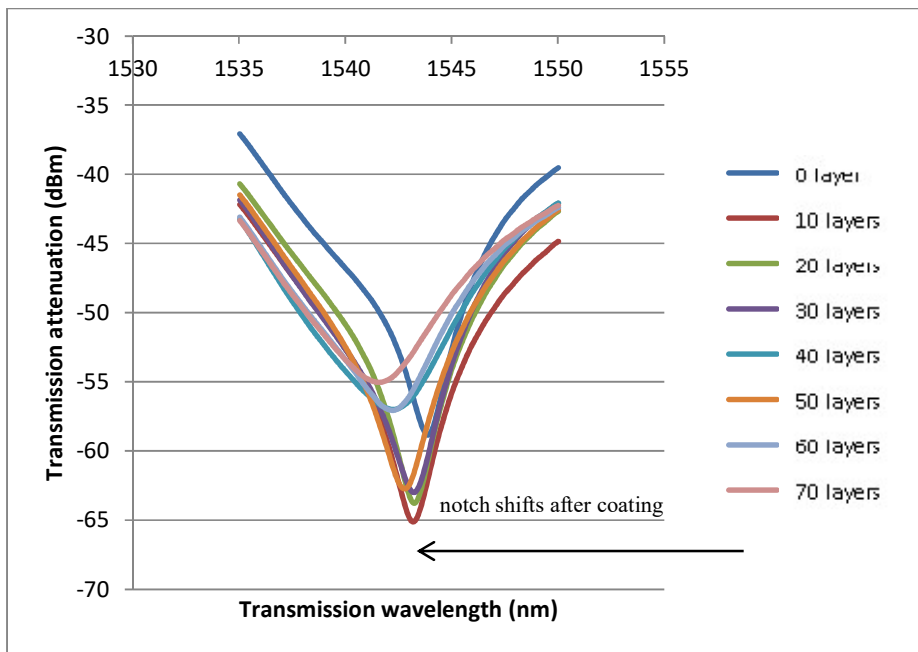
#### **4.3.2.2 Sensing of Sucrose Concentrations with coated Electric Arc-induced Double Pass LPFG**

To increase the sensitivity of the double pass LPFG sensor, the gratings were coated with PE. Figure 4.14 displays the transmission power spectra of single-pass LPFGs in water, before and after they were coated with PDDA/PSS up to 70 layers of coating (35 bilayers). The transmission notch blue shifted after every 10 layers of coating (five bilayers). The trend is similar to the observation by Q. Li, et al. (2009), where the deepest transmission notch was achieved after 125 bilayers of PDDA/PSS, which is equivalent to 250 layers of coating. In this work, the deepest notch was achieved after 20 layers of coating (10 bilayers).

The wavelength shifts of single-pass LPFG notch for fibers C and D in sucrose concentration varied between 0 % and 80 % sucrose are shown in Figure 4.9. Fibers C and D with coating of 60 and 70 layers of PDDA/PSS were sensitive between 30 and 40 % of sucrose as compared to lower number of layers. This drastic change in sensitivity is due to the effective index of the cladding modes which increases with additional PDDA/PSS layers. As the coating reaches around 60 layers of PDDA/PSS, the RI difference between the cladding and the sucrose narrows and for sucrose concentrations of between 30 and 40 %, there was a red shift in the transmission notch.



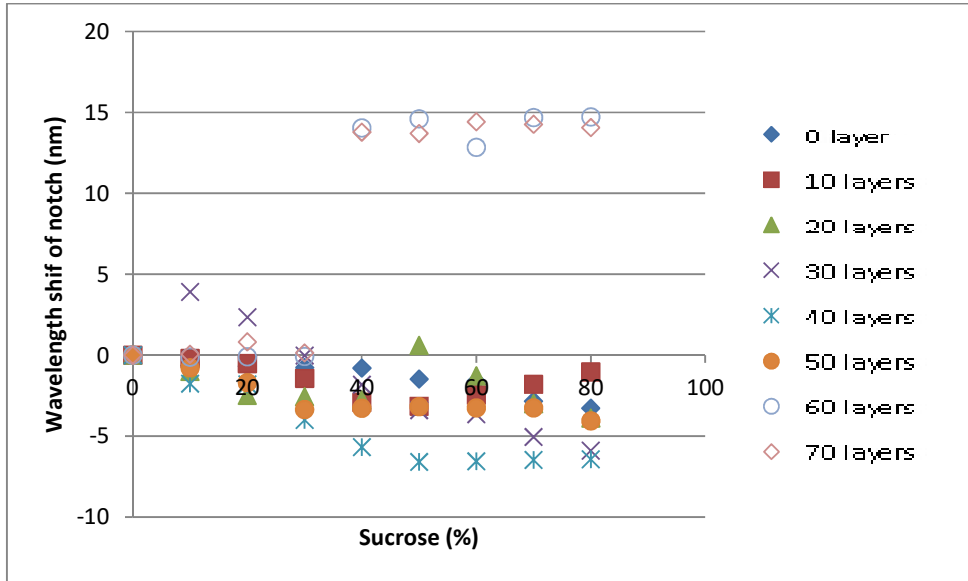
(a)



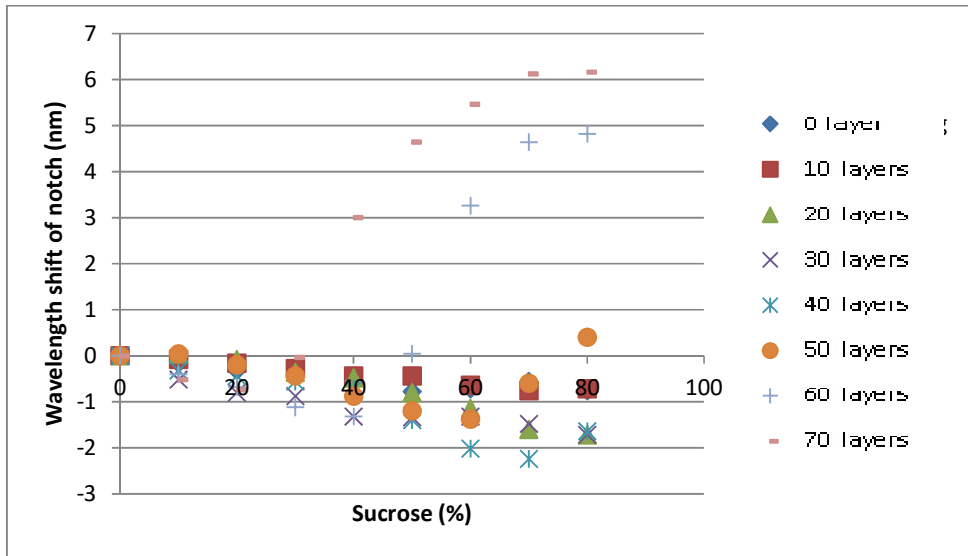
(b)

Figure 4.9: Transmission power of single-pass LPFG in water before and after coatings for (a) fiber C and (b) fiber D

Figure 4.10(a) and Figure 4.10(b) each shows the comparison in terms of wavelength shift for the single-pass and double-pass configurations for a 60 layer PDDA-/PSS-coated LPFG in various concentrations of sucrose. The wavelength shifts were more pronounced for 60 and 70 layers of coating. In terms of transmission attenuation of the notch, there is a significant difference in the transmission power between the single-pass and double-pass configurations for 60 coatings as shown in Figure 4.11(a) and (b).



(a)



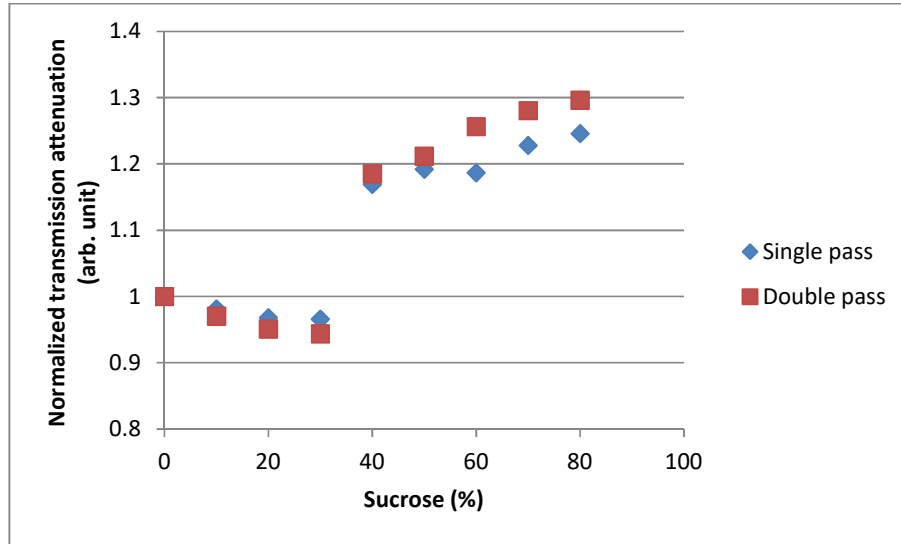
(b)

**Figure 4.10: Wavelength shift of transmission notch of single-pass LPFG in sucrose with reference to 0 % sucrose for respective layers for (a) fiber C and (b) fiber D**

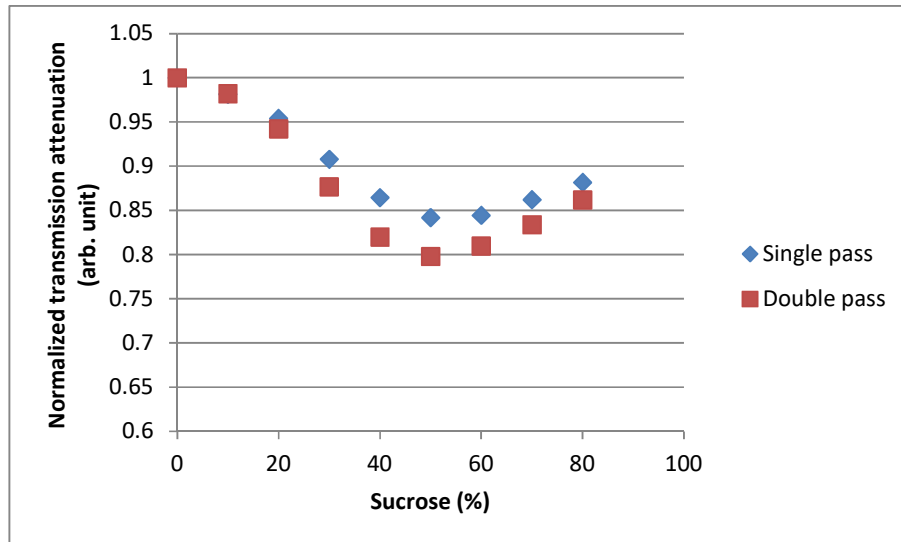
The normalized transmission attenuation in Figure 4.11(a) and Figure 4.11(b) is derived from division of the transmission attenuation value by the transmission attenuation value of 0 % sucrose for the respective configurations. In Figure 4.11(a), from 0 to 30 % sucrose concentrations, the gradient of the transmission power at the transmission notch for the single-pass configuration is 0.0452 dB/%, while for the double-pass configuration the gradient of the transmission power at the transmission notch is 0.098 dB/%, which is 2.168 times higher than the single-pass configuration. For sucrose concentrations of between 30 and 40 %, the gradient of the transmission power at the transmission notch for the single-pass configuration is  $-0.795$  dB/%, while for the double-pass configuration, the gradient is  $-1.2544$  dB/%, which is about 1.578 times of the single-pass configuration. For the single-pass configuration, the gradient of transmission power at the transmission notch between 40 and 70 % sucrose concentrations is  $-0.0668$  dB/%, whereas the gradient for double-pass configuration is  $-0.1721$  dB/%. This translates to the double-pass configuration having a gradient which is 2.576 times more than the single-pass configuration.

For fiber D, there is a significant difference in the transmission power at the transmission notch between the single-pass and double-pass configurations as shown in Figure 4.11(b). From 0 to 30 % sucrose concentrations, the gradient of the transmission power at the transmission notch for the single-pass configuration is 0.1732 dB/%, while for the double-pass configuration the gradient of the transmission power at the transmission notch is 0.3509 dB/%, which is 2.026 times higher than the single-pass

configuration. For sucrose concentrations of between 30 and 40 %, the gradient of the transmission power at the transmission notch for the single-pass configuration is 2.477 dB/%, while for double-pass configuration, the gradient is 4.876 dB/%, which is about 1.968 times of the single-pass configuration. For the single-pass configuration, the gradient of transmission power at the transmission notch between 40 and 70 % sucrose concentrations is 0.0028 dB/%, whereas the gradient for double-pass configuration is  $-0.0460$  dB/%. This translates to the double-pass configuration having a gradient which is 16.4286 times more than the single-pass configuration despite of the direction of the slope (Loh, Yong, Kuramitz, Teh and Faidz, 2015).



(a)



(b)

**Figure 4.11: Comparison of normalized transmission attenuation for both single-pass and double-pass configurations after 60 coatings in sucrose for (a) fiber C and (b) fiber D**

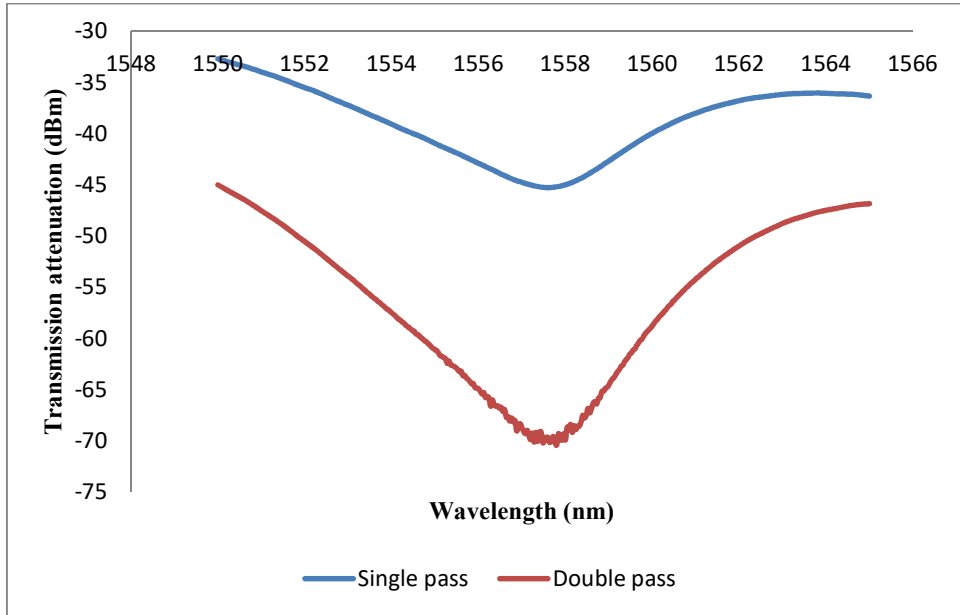
The results for fibers C and D indicate that the double-pass configuration has a sensitivity of almost double of that of the single-pass

configuration in terms of the transmission power of the resonant wavelength. The increase in the transmission loss of the resonant wavelength can be explained by the increase in the overlap of the core and cladding modes. This is attributed to the transmission characteristics of the LPFG which is influenced by the transmittance factor given in the equation for minimum transmission power.

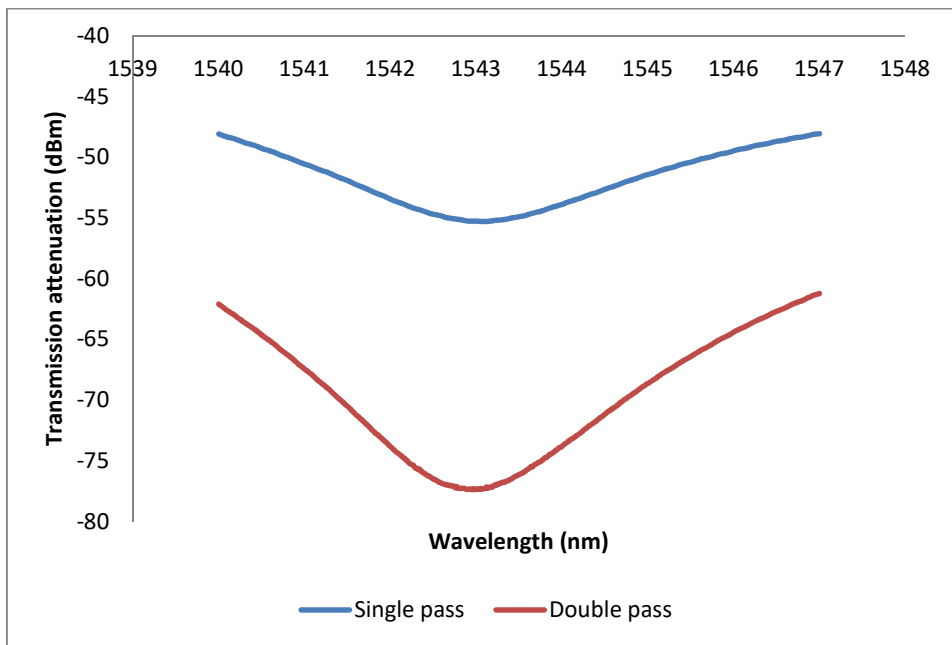
#### **4.3.3 Sensing of Biotin**

In order to prove the applicability of the electric arc-induced LPFG as a biosensor, the surface of two LPFGs were immobilized with avidin in order to detect the presence of biotin in a solution. Fibers E and F has grating length of 650  $\mu\text{m}$ . The tension for both fibers E and F were maintained at 5cN throughout the experiment. The average temperature and humidity of the laboratory was maintained at 18°C and 75% humidity. Figure 4.12 compares the transmission attenuation of the resonance wavelength for two bare arc-induced LPFGs, that is, in both single pass and double pass configurations. It is visible that the double pass configuration has higher transmission attenuation compared to the single pass configuration. The transmission attenuation of the resonance wavelength of fiber E in double pass configuration is about 20 dBm as compared to the single pass which was about 10 dBm. Coincidentally, the transmission attenuation of the resonance wavelength of fiber F in double pass configuration is about 20 dBm as compared to the single pass which was about 10 dBm. The higher attenuation for the double pass configuration is due to the higher coupling strength which

is directly influenced by the grating length. The transmittance of the double pass LPFGs varies following the term  $\cos^2(\kappa L) \times 2$  when the phase-matching condition is satisfied at  $\Delta\beta=0$ , where  $\kappa$  is the coupling coefficient and  $L$  the grating length (Young-Geun,2009). Both fibers prove that the higher attenuation for the double pass configuration is due to the higher coupling strength which is directly influenced by the grating length.



(a)



(b)

**Figure 4.12: Transmission of bare LPFG in single pass and double pass configuration for (a) fiber E and (b) fiber F**

The transmission spectra of avidin-immobilized LPFG fiber E in PBS (as reference) and in PBS containing biotin for both double pass and single pass configuration are shown in Figures 4.13(a) and (b), respectively. From Figures 4.13(a) and (b), it was observed that there was slight blue shifting of the LPFG resonance wavelength during the avidin–biotin interaction, whereas the transmission attenuation of the LPFG resonance wavelength increased as compared to the reference spectra for both configurations. The changes were more obvious for the double pass configuration as compared to the single pass.

The transmission spectra of avidin-immobilized LPFG fiber F in PBS (as reference) and in PBS containing biotin for both double pass and single pass configuration are shown in Figures 4.13(c) and (d), respectively. From Figures 4.13(c) and (d), it was observed that there was slight red shifting of the LPFG resonance wavelength during the avidin–biotin interaction, whereas the transmission attenuation of the LPFG resonance wavelength decreased as compared to the reference spectra for both configurations. The changes in fiber F were also more obvious for the double pass configuration as compared to the single pass. Red shifting occurs when the fiber is over-coupled.

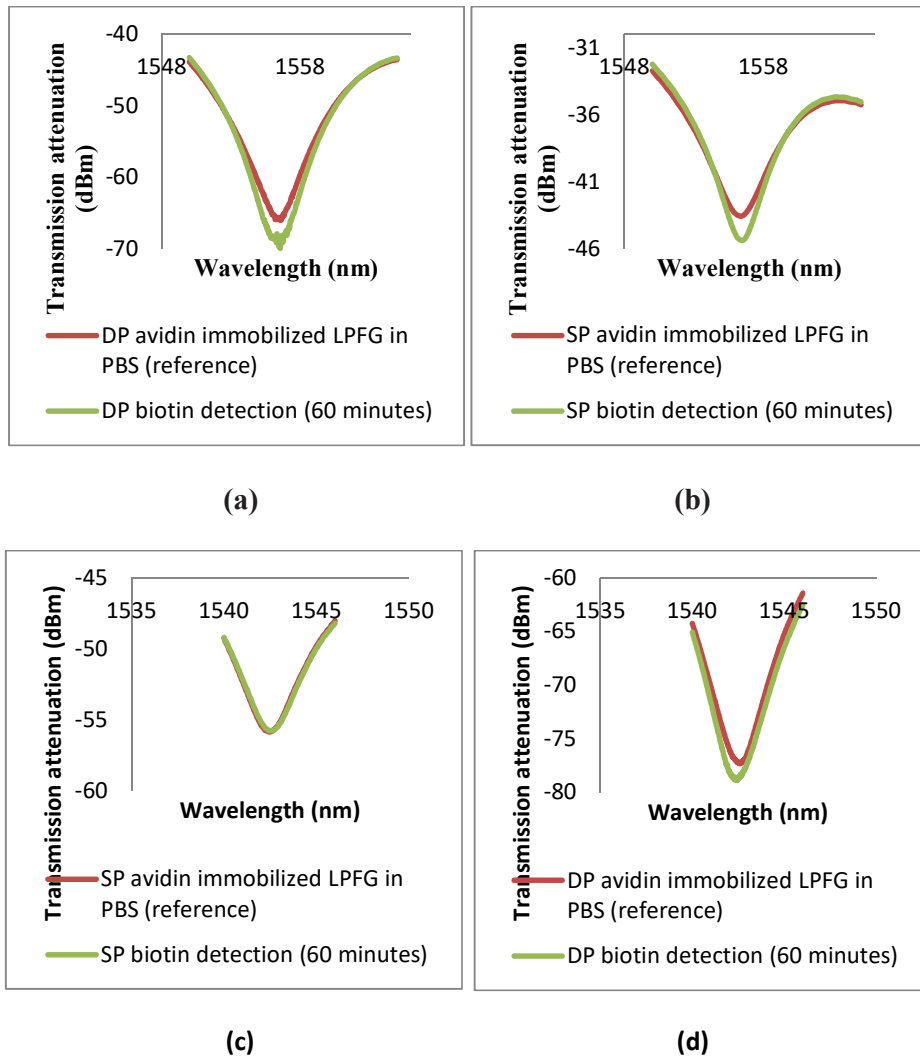
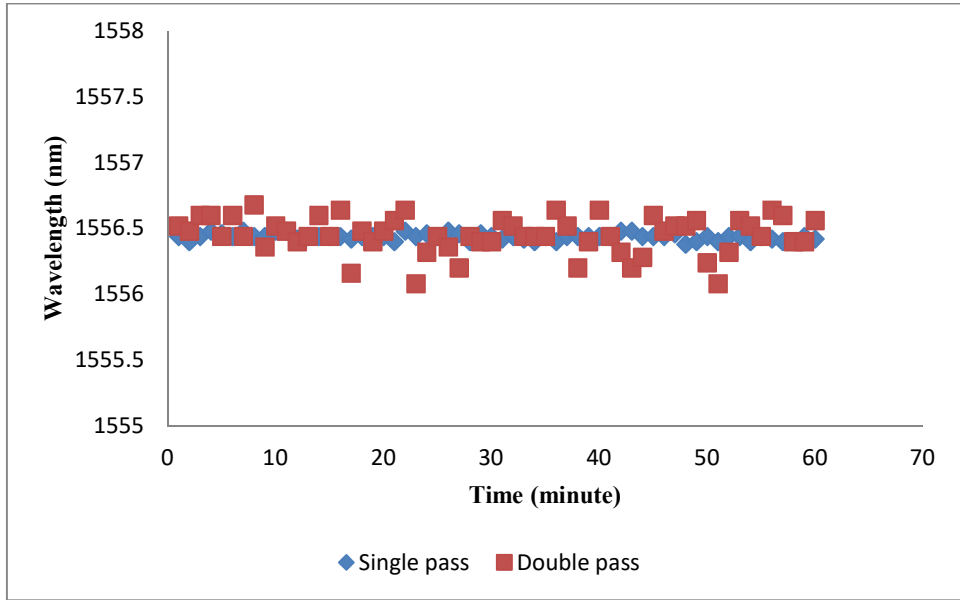
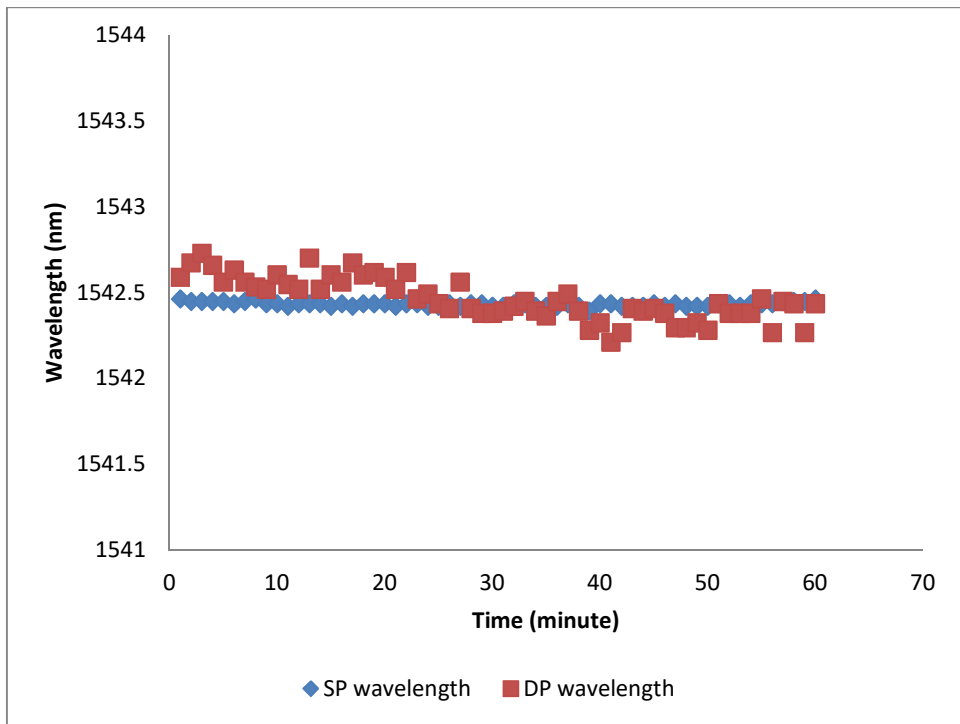


**Figure 4.13: (a) Transmission of avidin-immobilized LPFG in PBS (reference) and avidin–biotin interaction (60 min) in the single pass configuration for fiber E, (b) Transmission of avidin-immobilized LPFG in PBS (reference) and avidin–biotin interaction (60 min) in the double pass configuration for fiber E, (c) transmission of avidin-immobilized LPFG in PBS (reference) and avidin–biotin interaction (60 min) in the single pass configuration for fiber F and (d) Transmission of avidin-immobilized LPFG in PBS (reference) and avidin–biotin interaction (60 min) in the double pass configuration for fiber F**

Figure 4.14 shows the avidin-immobilized LPFG resonance wavelength during the avidin–biotin interaction in both single pass and double pass configurations over a period of 60 min for fibers E and F. There were no significant changes in the resonance wavelength of the notch over time for both single pass and double pass, although the double pass showed larger variation as compared to the single pass. This is a strong indication that there was no significant change in the optical thickness of the avidin-biotin overlay forming on the grating surface which influences the effective index of the cladding. This is supported by  $\lambda_i = \left( n_{core}(\lambda_i) - n_{clad}^i(\lambda_i) \right) \Lambda$ , where  $\lambda_i$  is the resonance wavelength,  $n_{core}(\lambda_i)$  is the effective index of the core mode,  $n_{clad}^i(\lambda_i)$  is the effective index of the  $i^{\text{th}}$  cladding mode and  $\Lambda$  is the grating period.



(a)



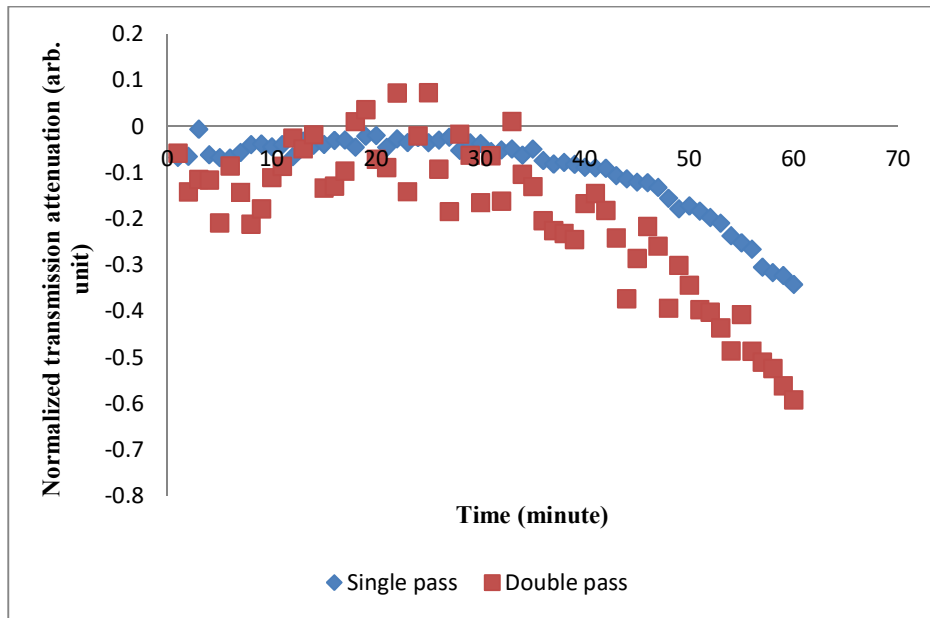
(b)

**Figure 4.14: Resonance wavelength (nm) versus time (minutes) during monitoring of the avidin–biotin interaction in both single and double pass for (a) fiber E and (b) fiber F**

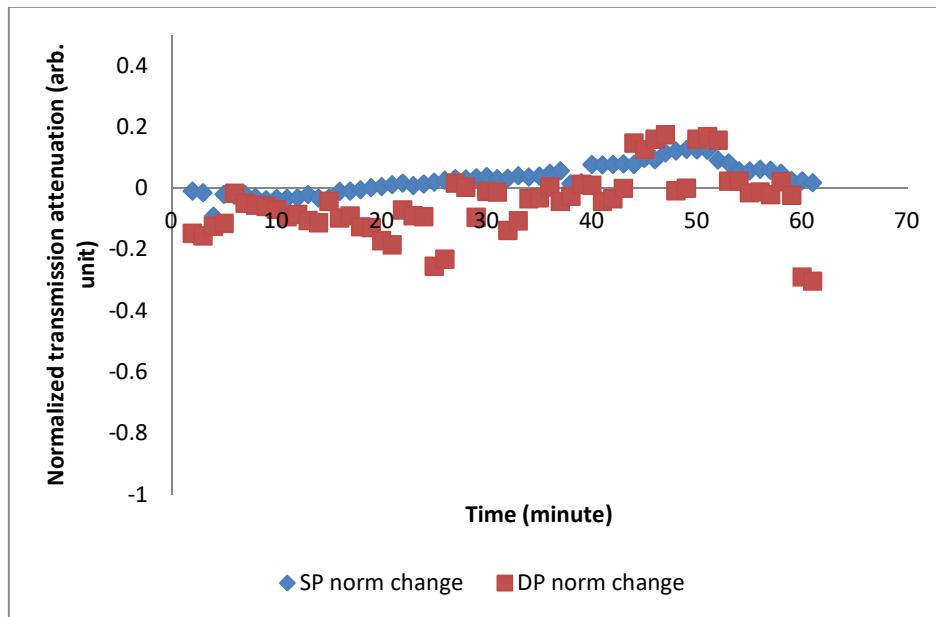
Figure 4.15 shows the normalized transmission attenuation of the LPFG resonance wavelength during the avidin–biotin interaction of both single-pass and double-pass configurations over a period of 60 min for fibers E and F. The change of transmission attenuation was more significant in double-pass configuration as compared to the single-pass configuration. From Figure 4.15(a), single-pass configuration in fiber E has a variation of the normalized transmission attenuation notches of about 0.336 a.u., whereas the double-pass configuration has a variation of the normalized transmission attenuation notches of 0.666 a.u. The normalized transmission attenuation was calculated relative to the reference spectra of respective configurations and by first converting the attenuation from dBm to mW. The gradient of the slope (beyond 30 min) of the single-pass configuration was measured to be around 20.0097 (a.u./mins.) whereas it was 20.0160 (a.u./mins.) for the double-pass configuration.

Based on Figure 4.15(b), single-pass configuration for fiber F has a variation of the normalized transmission attenuation notches of about 0.218 a.u., whereas the double-pass configuration has a variation of the normalized transmission attenuation notches of about 0.477 a.u. The normalized transmission attenuation notch was calculated relative to the reference spectra of respective configurations and by first converting the attenuation from dBm to mW. The gradient of the slope (beyond 30 min) of the single-pass configuration was measured to be around -0.0097 (a.u./mins.) whereas it was -

0.016 (a.u./mins.) for the double-pass configuration (Loh, Faidz, Kuramitz and Yong, 2014).



(a)



(b)

**Figure 4.15: Normalized transmission attenuation of the LPFG resonance wavelength versus time during monitoring of the avidin–biotin interaction for (a) fiber E and (b) fiber F**

The results indicate that the double-pass configuration for both fibers have a sensitivity of almost double as compared to the single-pass configuration, that is, in terms of the transmission attenuation of the resonance wavelength. The increase in the transmission attenuation of the resonance wavelength, for double-pass and single-pass configurations is due to the increase in the overlap of the core and cladding modes induced by the overlay film formed during the avidin–biotin interaction. However, for the double-pass configuration the attenuation showed better sensitivity to the interaction between avidin and biotin which may be attributed to the transmission characteristics of the LPFG which is influenced by the transmittance factor  $\cos^2(\kappa L) \times 2$ .

## CHAPTER 5

### CONCLUSION

#### 5.1 Concluding Remarks

From this research, it is now known that it's possible for the sensitivity of the electric arc-induced LPFG sensor to be based on transmission loss instead of wavelength shift of the transmission notch and that it is also possible to improve the sensitivity of an electric arc-induced LPFG sensor without physically modifying the fiber. A double pass configuration was successfully developed to improve the sensitivity of an electric arc-induced LPFG. The double pass electric arc-induced LPFG was also characterized and its applications were proven to be suitable for chemical and bio-sensing.

The use of double pass configuration to increase the transmission attenuation of the LPFG resonance wavelength and subsequently improve the sensitivity of the LPFG as an optical sensor was proven experimentally. Due to the longer path in which the light passes through the grating region in the double pass configuration, there was better coupling between the core and cladding modes thus giving better transmission attenuation and sensitivity toward changes to the surrounding environment as it is influenced by the transmittance factor  $\cos^2(\kappa L) \times 2$ .

## 5.2 Future Work

For future work, the applications of the double pass electric arc-induced LPFG is proposed to be further studied especially for applications in environment conservation and medical diagnostics. The double pass electric arc-induced LPFG is a promising sensor for both fields as it can be modified to be a chemical and/ or biological sensor. One application that will be beneficial for environment conservation is detection of heavy metals in soil or water. This ensures that the soil or water is not contaminated by heavy metals which will affect the health of plants, animals and humans within the vicinity.

For the field of medical diagnostics, the double pass electric arc-induced LPFG is promising for real time sensing of bacteria and viruses. This could save lives as time is crucial for medical diagnostics.

## PUBLICATIONS

Loh, M.C., Faidz, A.R., Kuramitz, H. and Yong, Y.T., 2014. Method to sensitize an arc-induced LPFG-based sensor using double-pass configuration. *Microwave and Optical Technology Letters*, 5(12), pp. 2766-2769.

Loh, M.C., Yong, Y.T., Kuramitz, H., Teh, P.C. and Faidz, A.R., 2015. Double-pass configuration to enhance the sensitivity of a polyelectrolyte-coated arc-induced long-period fiber grating. *Journal of Electromagnetic Waves and Applications*, 29(14), pp. 1908-1916.

## REFERENCES

- Abrishamian, F., Dragomir, N. and Morishita, K., 2012. Refractive index profile changes caused by arc discharge in long-period fiber gratings fabricated by a point-by-point method. *Applied Optics*, 51, pp. 8271–8276.
- Akiyama, M., Nishide, K., Shima, K., Wada, A. and Yamauchi, R., 1998. A novel long-period fiber grating using periodically released residual stress of pure-silica core fiber, in *Proceedings of Optical Fiber Communications Conference*, pp. 276–27.
- Allsop T., Webb D.J. and Bennion I., 2003. A comparison of the sensing characteristics of long period gratings written in three different types of fiber. *Optical Fiber Technology*, 9, pp. 210–223.
- Allsop, T. et al., 2006. Bending characteristics of fiber long-period gratings with cladding index modified by femtosecond laser, *Journal of Lightwave Technology*, 24(8), pp. 3147–3154.
- Allsop, T. et al., 2006a. A comparison of the spectral properties of high temperature annealed long period gratings inscribed by fs laser, UV and fusion-arc, *Proceedings of International Society for Optics and Photonics*, 6193.
- Allsop, T. et al., 2006b. Spectral characteristics of tapered LPG device as a sensing element for refractive index and temperature. *Journal of Lightwave Technology*, 24, pp. 870–878.
- Anzuetto-Sánchez, G., Martínez-Rios, A. and Castellon-Urbe, J., 2012. Tuning and wavelength switching erbium-doped fiber ring lasers by controlled bending in arc-induced long-period fiber gratings. *Optical Fiber Technology*, 18, pp. 513–517.
- Ayala, J.M.E., Chavez, R.I.M., Garcia, J.C.H. and Laguna, R.R., 2012. *Long period fiber grating produced by arc discharges*. Rijeka: InTech, pp. 295–316.
- Benoune, M. et al., 2004. LPFG implementation using electric-arc and micro-deformations. *IEEE International Conference on Industry Technology (ICIT)*, Dec 8–10 2004 Hammamet, Tunisia.
- Bey, S. K.A.K., Chung, C. L., Tong, S. and Grattan, T. V., 2008. Chloride ion optical sensing using a long period grating pair, *Sensors and Actuators, A*, 141, pp. 390–395.
- Bhatia, V. and Vengsarkar, A.M., 1996. Optical fiber long-period grating sensors. *Optics Letters*, 21(9), pp. 692–694.

- Bhatia, V., 1999. Applications of long-period gratings to single and multi-parameter sensing. *Optics Express*, 4(11), pp. 457–466.
- Blake, J. N., Kim, B. Y. and Shaw, H. J., 1986. Fiber-optic modal coupler using periodic microbending. *Optics Letters*, 11(3), pp. 177-179.
- Bock, W. J., Chen, J., Mikulic, P. and Eftimov, T., 2007. A novel fiber-optic tapered long-period grating sensor for pressure monitoring. *IEEE Transactions on Instrumentation and Measurement*, 56, pp. 1176–1180.
- Bock, W.J., Chen, J., Mikulic, P., Eftimov, T. and Korwin-Pawlowski, M., 2007. Pressure sensing using periodically tapered long-period gratings written in photonic crystal fibres, *Measurement Science and Technology*, 18(10), pp. 3098–3102.
- Caldas, P., Rego, G., Ivanov, O.V. and Santos, J.L., 2010. Characterization of the response of a dual resonance of an arc-induced long-period grating to various physical parameters. *Applied Optics*, 49, pp. 2994–2999.
- Chaubey, S., Kher, S., Kishore, J. and Oak, S.M., 2014. CO<sub>2</sub> laser-inscribed low-cost, shortest-period long-period fibre grating in B-Ge co-doped fibre for high-sensitivity strain measurement. *Pramana*, 8, pp. 373–377.
- Chen, K.P., Herman, P.R., Zhang, J. and Tam, R., 2001. Fabrication of strong long-period gratings in hydrogen-free fibers with 157-nm F<sub>2</sub>-laser radiation. *Optics Letter*, 26(11), pp. 771–773.
- Chen, X., Zhou, K., Zhang, L. and Bennion, I., 2003. Optical biochemical sensors based on long-period fibre gratings UV-inscribed in D-fibre with enhanced sensitivity by HF etching process. *Proceedings of the SPIE International Conference on Advanced Laser Technologies: Biomedical Optics (ALT '03)*, 5486, pp. 187–191.
- Chen, X., Zhou., K., Zhang, L. and I. Bennion, I., 2004. Optical Chemsensors Utilizing Long-Period Fiber Gratings UV-Inscribed in D-Fiber with Enhanced Sensitivity Through Cladding Etching. *IEEE Photonics Technology Letter*, 16(5), pp. 1352-1354.
- Chen, X., Zhou, K., Zhang, L. and Bennion, I., 2007. Dual-peak longperiod fiber gratings with enhanced refractive index sensitivity by finely tailored mode dispersion that uses the light cladding etching technique. *Applied Optics*, 46, pp. 451-455.
- S.F. Cheng, S.F. and L.K. Chau, L.K., 2003. Colloidal gold-modified optical fiber for chemical and biochemical sensing. *Analytical Chemistry*, 75, pp. 16–21.
- Cho, J.Y. and Lee, K.S., 2002. A birefringence compensation method for mechanically induced long-period fiber gratings. *Optics Communications*, 213(4-6), pp. 281–284.

- Chung, C. and Lee, H.J., 2001. Wavelength characteristics of arc-induced long-period fiber grating by core and cladding diameter modulation. In: Lasers and Electro-Optics Society (LEOS). *IEEE 14th Annual Meeting*, Nov 12–13 2001, San Diego, CA, USA.
- Cullen, T. J., Jolley, N.E., Davis, F. and Mun, J., 1997. EDFA gain flattening using periodic tapered fibre filters. Willner, A., Zervas, M. and Sasaki, S., 1997. eds. *Optical Amplifiers and Their Applications*, OSA Trends in Optics and Photonics Series (Optical Society of America, Washington, D.C., 1997), 16(paper FAW13), pp. 231.
- Cusano, P., et al., 2005. High sensitivity optical chemosensor based on coated long-period gratings for sub-ppm chemical detection in water. *Applied Physics Letter*, 87(23), pp. 234105-23105-3.
- Cusano, A., et al., 2005. Cladding mode reorganization in high-refractive-index coated long-period gratings: effects on the refractive-index sensitivity. *Optics Letter*, 30, pp. 2536–2538.
- Czapla, A., et al., 2010. An electrically tunable filter based on a long-period fiber grating with a thin liquid crystal layer. *Photonics Letters of Poland*, 2(3), pp. 116-118.
- Dankers, J.P., et al., 2001. Fiber optic flow and cure sensing for liquid composite molding. *Optics and Lasers in Engineering*, 35, pp. 91–104 (2001).
- Davis, D.D. et al., 1998. Long-period fibre grating fabrication with focused CO2 laser pulses. *Electronics Letters*, 34(3), pp. 302–303.
- Davis, D.D., Gaylord, T.K., Glytsis, E.N. and Mettler, S.C., 1998. CO2 laser-induced long-period fibre gratings: spectral characteristics, cladding modes and polarisation independence. *Electronics Letters*, 34(14), pp. 1416–1417.
- Davis, D.D., Gaylord, T.K., Glytsis, E.N. and Mettler, S.C., 1999. Very-high-temperature stable CO2-laser-induced long-period fibre gratings. *Electronics Letters*, 35(9), pp. 740–742.
- DeLisa, M.P., Zhang, Z., Shiloach, M., Pilevar, S., Davis, C.C., Sirkis, J.S. and Bentley, W.E., 2000. Evanescent Wave Long-Period Fiber Bragg Grating as an Immobilized Antibody Biosensor. *Analytical Chemistry*, 72, pp. 2895-2900.
- Dianov, E.M. et al., 1997. Thermo-induced long-period fibre gratings. In: *23rd European Conference on Optical Communication (ECOC '97)*, Sep 22–25 1997, Edinburgh.
- Dianov, E.M., Karpov, V.I., Grekov, M.V. and Kurkov, A.S., 1998. Long period gratings and mode field converters fabricated by thermodiffusion in phosphosilicate fibers. *24th European Conference of Optical Communications*, 20-24 Sept 1998, 1, pp.396-397.

- Ding, J.F., Zhang, A.P., Shao, L.Y., Yan, J.H. and He, S., 2005. Fiber-taper seeded long-period grating pair as a highly sensitive refractive-index sensor. *IEEE Photonics Technology Letters*, 17, pp. 1247–1249.
- Ding, W. and Andrews, S.R., 2008. Modal coupling in surface-corrugated long-period-grating fiber tapers. *Optics Letters*, 33(7), pp. 717–719.
- Dobb, H., Kalli, K. and Webb, D.J., 2006. Measured sensitivity of arc-induced long-period grating sensors in photonic crystal fibre. *Optics Communications*, 260, pp. 184–191.
- Dragomir, A., Nikogosyan, D.N., Ruth, A.A., Zagorul'ko, K.A. and Kryukov, P.G., 2002. Long-period fibre grating formation with 264 nm femtosecond radiation, *Electronic Letters*, 38, pp. 269-271.
- Dragomir, A. and Nikogosyan, D.N., 2013. Femtosecond UV Approach to Inscription of Long-Period Fiber Gratings. *Lasers and Electro-Optics Europe (CLEO EUROPE/IQEC)*, Conference on and International Quantum Electronics Conference.
- Dragomir, A., McInerney, J.G., Nikogosyan, D.N. and Kazansky, P.G., 2002. Two-photon absorption properties of commercial fused silica and germanosilicate glass 264 nm. *Applied Physics Letters*, 80, pp. 114-116.
- Durr, F. et al., 2005. Tomographic stress profiling of arc-induced long-period fiber gratings. *Journal of Lightwave Technology*, 23, pp. 3947–3953.
- Enomoto, T., Shigehara, M., Ishikawa, S., Danzuka, T. and Kanamori, H., 1998. Long-period fiber grating in a pure-silica-core fiber written by residual stress relaxation. *Optical Fiber Communication Conference*, Vol. 2 of 1998 OSA Technical Digest Series (Optical Society of America, Washington, D.C., 1998), paper ThG2.
- Erdogan, T., 1997. Cladding-mode resonances in short- and long-period fiber grating filters. *Journal of the Optical Society of America A*, 14(8), pp. 1760-1773.
- Etten, W.V. and Plaats, J.V.D., 1991. *Fundamentals of optical fiber communications*. New York: Prentice Hall, 1991.
- Falate, R., Kamikawachi, R.C., Muller, M. Kalinowski H.J. and Fabris, J.L., 2005. Fiber optic sensors for hydrocarbon detection. *Sensors and Actuators B*, 105, 430–436.
- Falate, R. et al., 2007. Alternative Technique For Biodiesel Quality Control Using An Optical Fiber Longperiod Grating Sensor. *Quimica Nova*, 30, pp. 1677-1680.
- Falate, R., Kamikawachi, R.C., Fabris, J.L., Müller M. and Kalinowski, H.J., 2004. Fiber Optic Hydrocarbon Sensors Based On Long Period Gratings. *Journal of Microwaves and Optoelectronics*, 3, pp. 47-55.

- Falciai, R., Mignani, A.G. and Vannini, 2001. A Long period gratings as solution concentration sensors. *Sensors and Actuators B*, 74, pp. 74–77.
- Feng, T., Jenkins, M.H., Yan, F.P. and Gaylord, T.K., 2013. Arc fusion splicing effects in large-mode-area single-mode ytterbium-doped fibers. *Applied Optics*, 52, pp. 7706–7711.
- Fertein, E. et al., 2001. Refractive-index changes of standard telecommunication fiber through exposure to femtosecond laser pulses at 810 cm. *Applied Optics*, 40(21), pp. 3506–3508.
- M. Fujimaki, M., Ohki, Y., Brebner, J.L. and Roorda, S., 2000. Fabrication of long-period optical fiber gratings by use of ion implantation. *Optics Letters*, 25(2), pp. 88–89.
- Garg, R., Tripathi, S.M., Thyagarajan, K. and Bock, W. J., 2012. Long period fiber grating based temperature-compensated high performance sensor for biochemical applications. *Sensors and Actuators B*, 176, pp. 1121–1127.
- Geng, T., Zi, D.D., Yang, W.L. and Tong, C.G., 2013. The LPFG temperature characteristic research based on electric heating method. In: *2013 International Conference on Optoelectronics and Microelectronics (ICOM)*, Sep 7–9 2013, Harbin, China.
- Godbout, N., Daxhelet, X., Maurier, A. and Lacroix, S., 1998. Long-period fiber grating by electrical discharge. In: *24th European Conference on Optical Communication (ECOC)*, Sep 20–24 1998, Madrid, Spain.
- Guan, O., Tam, H.Y., Ho, S.L., Liu, S.Y. and Dong, X.Y., 2000. Growth of long-period gratings in H<sub>2</sub>-loaded fiber after 193-nm UV inscription. *IEEE Photonics Technology Letters*, 12(6), pp. 642–644.
- Gu, Z. and Xu, Y., 2007. Design optimization of a long-period fiber grating with sol-gel coating for a gas sensor. *Measurement Science Technology*, 18(11), pp. 3530–3536.
- Hindle, F. et al., 2004. Inscription of long-period gratings in pure silica and germano-silicate fiber cores by femtosecond laser irradiation. *IEEE Photonics Technology Letters*, 16(8), pp. 1861–1863.
- Humbert, G., Malki, A., Prioleau, C. and Ketata, M., 2000. Fabrication of long period fiber grating using electric discharge in non-hydrogenated fiber. In: *Proceedings of SPIE, Photonics 2000: International Conference on Fiber Optics and Photonics*, Sep 25 2001; S. Das, Calcutta, India.
- Humbert, G., Malki, A. and Ketata, M., 2001. Long-period fiber gratings filters fabrications and characterizations using electric arc in non-hydrogenated fibers. in *Proceedings of the SPIE Active and Passive Optical Components for WDM Communication*, 4532, pp. 510–516, August 2001.

- Humbert, G. and Malki, A., 2002. Characterizations at very high temperature of electric arc-induced long-period fiber gratings. *Optics Communications*, 208(4–6), pp. 329–335, 2002.
- Humbert, G. and Malki, A., 2002. Annealing time dependence at very high temperature of electric arc-induced long-period fibre gratings. *Electronic Letters*, 38, pp. 449–450.
- Humbert, G. and Malki, A., 2003. High performance bandpass filters based on electric arc-induced  $\pi$ -shifted long-period fibre gratings. *Electronic Letters*, 39, pp. 1506–1507.
- Humbert, G., Malki, A., Février, S., Roy, P. and Pagnoux, D., 2003. Electric arc-induced long-period gratings in Ge-free air-silica microstructure fibres. *Electronic Letters*, 39, pp. 349–350.
- Humbert, G. et al., 2003. Long period grating filters fabricated with electric arc in dual concentric core fibers. *Optics Communication*, 225, pp. 47–53.
- Hwang, K., Yun, S.H. and Kim, B.Y., 1999. Long-period fiber gratings based on periodic microbends. *Optics Letters*, 24(18), pp. 1263–1265.
- Iadicicco, A., Campopiano, S., Giordano, M. and Cusano, A., 2007. Spectral behavior in thinned long period gratings: effects of fiber diameter on refractive index sensitivity. *Applied Optics*, 46, pp. 6945–6952.
- Iadicicco, A. et al., 2008. Refractive index sensitivity in thinned UV and arc induced long-period gratings: a comparative study. *International Journal of Smart Sensors*, 1 pp. 354–369.
- Iadicicco, A., Campopiano, S. and Cusano, A., 2011. Long-period gratings in hollow core fibers by pressure- assisted arc discharge technique. *IEEE Photonics Technology Letters*, 23 pp. 1567–1569.
- In, S.H., Chung, C. and Lee, H.J., 2002. The resonance wavelength-tuning characteristic of the arc-induced LPFGs by diameter modulation. *In: Optical Fiber Sensors Conference Technical Digest*, May 10 2002, Portland, OR, USA.
- Iredale, T.B., Steinvurzel, P. and Eggleton, B.J., 2006. Electric-arc-induced long-period gratings in fluid-filled photonic bandgap fibre. *Electronic Letters*, 42 pp. 739–740.
- Ishaq, I.M. et al., 2005. Modification of the refractive index response of long period gratings using thin film overlays. *Sensors and Actuators B*, 107, pp. 738–741.
- Ivanov, O.V. and Wang, L.A., 2003. Wavelength shifts of cladding-mode resonance in corrugated long-period fiber gratings under torsion. *Applied Optics*, 42(13), pp. 2264–2272.

- Ivanov, O.V. and Rego, G., 2007. Origin of coupling to antisymmetric modes in arc-induced long-period fiber gratings. *Optics Express*, 15, pp. 13936–13941.
- James, S.W. and Tatam, R.P., 2006. Fiber Optic Sensors with Nano-Structured Coatings. *Journal of Optics A, Pure and Applied Optics*, 8(7), S430.
- James, S.W. and Tatam, R.P., 2003. Optical fibre long-period grating sensors: characteristics and application. *Measurement Science and Technology*, 14, pp. 49–61.
- Jiang, Y. et al., 2002. A novel strain-induced thermally tuned long-period fiber grating fabricated on a periodic corrugated silicon fixture. *IEEE Photonics Technology Letter*, 14, pp. 941.
- Kakarantzas, G., Birks, T.A. and P. S. J. Russell, P.S.J., 2002. Structural long-period gratings in photonic crystal fibers. *Optics Letters*, 27(12), pp. 1013–1015.
- Kakarantzas, G., Dimmick, T.E. Birks, T.A., Le Roux, R. and Russell, P.S.J., 2001. Miniature all-fiber devices based on CO<sub>2</sub> laser microstructuring of tapered fibers. *Optics Letters*, 26(15), pp. 1137–1139.
- Kalachev, I., Nikogosyan, D.N. and Brambilla, G., 2005. Long-period fiber grating fabrication by high-intensity femtosecond pulses at 211 nm. *Journal of Lightwave Technology*, 23(8), pp. 2568–2578.
- Kalachev, I., Pureur, V. and Nikogosyan, D.N., 2005. Investigation of long-period fiber gratings induced by high-intensity femtosecond UV laser pulses. *Optics Communications*, 246(1–3), pp. 107–115.
- Kawano, H., Muentz, H., Sato, Y., Nishimae, J. and Sugitatsu, A., 2001. Reduction of transmission spectrum shift of long-period fiber gratings by a UV-preexposure method. *Journal of Lightwave Technology*, 19(8), pp. 1221–1227.
- D. Kersey, D. et al., 1997. Fiber grating sensors. *Journal of Lightwave Technology*, 15, pp. 1442–1463.
- Khaliq, S., James, S.W. and Tatam, R.P., 2001. Fiber-optic liquid-level sensor using a long-period grating. *Optics Letter*, 26, pp. 1224–1226.
- Kim, M.W., Lee, D.W., Hong, B. and Chung, H.Y., 2002. Performance characteristics of long-period fiber gratings made from periodic tapers induced by electric-arc discharge. *Journal of Korean Physics Society*, 40, pp. 369–373.
- Kim, S. et al., 2009. Investigation of an arc-induced long period fiber grating inscribed in a photonic crystal fiber with two large air holes. *Journal of Optics Society Korea*, 13, pp. 428–433.

- Y. Kondo, Y. et al., 1999. Fabrication of long-period fiber gratings by focused irradiation of infrared femtosecond laser pulses. *Optics Letters*, 24(10), pp. 646–648.
- Korposh, S. et al., 2010. Fiber optic long period grating sensors with a nanoassembled mesoporous film of SiO<sub>2</sub> nanoparticles. *Optics Express*, 18(12), 126062.
- Kosinski, G., Hill, S.M., Vengsarkar, A.M., Eyck, T. and Alexander, C., 2010. Methods for making longperiod fiber gratings. *European Patent Specification*.
- Kosinski, S.G. and Vengsarkar, A.M., 1998. Splicer-based long-period fiber gratings. *Optical Fiber Communication Conference*, Vol. 2 of 1998 OSA Technical Digest Series (Optical Society of America, Washington, D. C., 1998), paper ThG3.
- Kueh, S.R.M., Parnas, R.S. and Advani, S.G., 2002. A methodology for using long-period gratings and mold-filling simulations to minimize the intrusiveness of flow sensors in liquid composite molding. *Composites Science Technology*, 62, pp. 311–327.
- Lee, Y.J. et al., 2006. Highly polarization-dependent periodic coupling in mechanically induced long-period grating over air-silica fibers. *Optics Letters*, 31(3), pp. 296–298.
- Lee, H.W. Liu, Y. and Chiang, K.S., 2008. Writing of long-period fiber gratings in conventional and photonic-crystal polarization- maintaining fibers by CO<sub>2</sub> laser pulses. *IEEE Photonics Technology Letters*, 20(2), pp. 132–134.
- S. C. Lee, S.C., Yong, Y.T., Yeap, K.H. and Rahman, F.A., 2013. An Asymmetric Tapered Long Period Fiber Grating: Fabrication and Characterization. *2013 IEEE 4<sup>th</sup> international Conference Photonics (ICP)*, pp. 21-24.
- Lee, T.S. et al., 2001. Chemical sensing with microbent optical fiber. *Optics Letters*, 26(20), pp. 1541–1543.
- Li, B., Jiang, L., Wang, S., Tsai, H. and Xiao, H., 2011. Femtosecond laser fabrication of long period gratings and applications in refractive index sensing. *Optics and Laser Technology*, 43, pp. 1420-1423.
- Li, Q. et al., 2009. Actions of sodium nitrite on long period fiber grating with self-assembled polyelectrolyte films. *Optics Communication*, 282, pp. 2446–2450.
- Li~ao, C., Wang, Y., Wang, D.N. and Jin, L., 2010. Femtosecond laser inscribed long-period gratings in all-solid photonic bandgap fibers. *IEEE Photonics Technology Letters*, 22(6), pp. 425–427.

- Lin, Y., Wang, L.A. and Chern, G.W., 2001. Corrugated long-period fiber gratings as strain, torsion, and bending sensors,” *Journal of Lightwave Technology*, 19(8), pp. 1159–1168.
- Lin, Y., Chern, G.W. and Wang, L.A., 2001. Periodical corrugated structure for forming sampled fiber Bragg grating and long-period fiber grating with tunable coupling strength. *Journal of Lightwave Technology*, 19(9), pp. 1212–1220.
- S. Liu, L. Jin, W. Jin, Y. Wang, and D. N. Wang, “Fabrication of long-period gratings by femtosecond laser-induced filling of air-holes in photonic crystal fibers,” *IEEE Photonics Technology Letters*, vol. 22, no. 22, pp. 1635–1637, 2010.
- Loh, M.C., Rahman, F.A., Kuramitz, H. and Yong, Y.T., 2014. Method to sensitize an arc-induced LPFG-based sensor using double-pass configuration. *Microwave and Optical Technology Letters*, 56(12), pp. 2766-2769.
- Loh, M.C., Yong, Y.T., Kuramitz, H., Teh, P.C. and Rahman, F.A., 2015. Double-pass configuration to enhance the sensitivity of a polyelectrolyte-coated arc-induced long-period fiber grating. *Journal of Electromagnetic Waves and Applications*, 29(14).
- Martinez-Rios, A., Monzon-Hernandez, D. and Torres-Gomez, I., 2010. Highly sensitive cladding-etched arc-induced long-period fiber gratings for refractive index sensing. *Optics Communications*, 283, pp. 958–962.
- Martinez-Rios, A., Torres-Gomez, I., Monzon-Hernandez, D., Salceda-Delgado, G., Duran-Ramirez, V.M. and Anzueto-Sanchez, G., 2012. Random period arc-induced long-period fiber gratings. *Optical Laser Technology*, 44, pp. 1176–1179.
- Mysliwiec, M., 2013. Effect of wet etching of arc-induced long-period gratings on their refractive index sensitivity, *Acta Physica Polonica A*, 124, pp. 521–524.
- Nanda, S., Sharma, N. and Roy, S., 2008. Simple and Sensitive Fiber Optic Sensor to Detect Adulteration in Petrol and Diesel. (*PHOTONICS-2008: International Conference on Fiber Optics and Photonics, IIT Delhi, India*).
- O’Regan, J. and Nikogosyan, D.N., 2011. Femtosecond UV long-period fiber grating fabrication with amplitude mask technique. *Optics Communications*, 284(24), pp. 5650–5654.
- Palai, P., Satyanarayan, M.N., Das, M., Thyagarajan, K. and Pal, B.P., 2001. Characterization and simulation of long period gratings fabricated using electric discharge. *Optic Communications*, 193, pp. 181–185.
- Patrick, H.J., Kersey, A.D. and Bucholtz, F., 1998. Analysis of the response of long period fiber gratings to external index of refraction. *Journal of Lightwave Technology*, 16, pp. 1606–1642.

- Petrovic, J.S. et al., 2007. Sensitivity of LPGs in PCFs fabricated by an electric arc to temperature, strain, and external refractive index. *Journal of Lightwave Technology*, 25, pp. 1306–1312.
- Pilla, P. et al., 2011. Transition mode long period grating biosensor with functional multilayer coatings. *Optics Express*, 19, pp. 512-526.
- Poole, C.D., Meester, J.P. and Presby, H.M., 1994. Two-mode fibre spatial-mode converter using periodic core deformation. *Electronics Letters*, 30, pp. 1437–1438.
- Possetti, G.R.C., Kamikawachi, R.C., Prevedello, C.L., Muller, M. and J L Fabris, J.L., 2009. Salinity measurement in water environment with a long period grating based interferometer. *Measurement. Science Technology*, 20, 034003(1-6).
- Possetti, G.R.C., Cocco, L.C., Yamamoto, C.I., de Arruda, L.V.R., Falate, R., Muller, M. and Fabris, J.L., 2009. Application of a long-period fiber grating-based transducer in the fuel industry. *Measurement. Science Technology*, 20, 034012 (1-9).
- Possetti, G.R.C., Muller, M. and Fabris, J.L., 2009. Refractometric optical fiber sensor for measurement of ethanol concentration in Fiber optic sensor for the quality evaluation of ethanol blended petrol 114 ethanol-gasoline blend. (*International Microwave & Optoelectronics Conference (IMOC)*, 2009).
- Quero, G. et al., 2016. Long period fiber grating nano-optrode for cancer biomarker detection. *Biosensors and Bioelectronics*, 80, pp. 590-600.
- Rao, Y.J., Wang, Y.P., Ran, Z.L. and Zhu, T., 2003. Novel fiber-optic sensors based on long-period fiber gratings written by high-frequency CO<sub>2</sub> laser pulses. *Journal of Lightwave Technology*, 21(5), pp. 1320–1327.
- Rao, Y.J. et al., 2004. Novel long-period fiber gratings written by high-frequency CO<sub>2</sub> laser pulses and applications in optical fiber communication. *Optics Communications*, 229(1–6), pp. 209–221.
- Rees, N. D., James, S. W. and Tatam, R. P., 2002. Optical fiber long-period gratings with Langmuir–Blodgett thin-film overlays. *Optics Letters*, 27, pp. 686–688.
- G.Rego, G. et al., 2001. High-Temperature Stability of Long-Period Fiber Gratings Produced Using an Electric Arc. *Journal of Lightwave Technology*, 19(10), pp. 1574–1579.
- Rego, G., Romero, R., Frazão, O., Marques, P.V.S. and Salgado, H.M., 2002. Apodisation of uniform fibre Bragg grating using electric arc discharges. In: *Proceedings of 2002 IEEE/LEOS Workshop on Fibre and Optical Passive Components*; June 5–6 2002, Glasgow, UK.

- Rego, G. et al., 2004. In situ temperature measurement of an optical fiber submitted to electric arc discharges. *IEEE Photonics Technology Letters*, 16, pp. 2111–2113.
- Rego, G., Marques, P.V.S., Salgado, H.M. and Santos, J.L., 2005. Simultaneous measurement of temperature and strain based on arc-induced long-period fibre gratings. *Electronics Letters*, 41.
- Rego, G. et al., 2005a. Simultaneous temperature and strain measurement based on arc-induced long-period fiber gratings. In: *17th International Conference on Optical Fibre Sensors*; Aug 2005, Bellingham, WA, USA.
- Rego, G. et al., 2005b. Arc-induced long-period gratings in aluminosilicate glass fibers. *Optics Letters*, 30, pp. 2065–2067.
- Rego, G. et al., 2005c. Arc-induced Long-Period Gratings. *Fiber and Integrated Optics*, 24, pp. 245-259.
- Rego, G., Santos, J.L. and Salgado, H.M., 2006. Refractive index measurement with long-period gratings arc-induced in pure-silica-core fibres. *Optics Communications*, 259, pp. 598–602.
- Rego, G., 2006. *Arc-induced long-period fibre gratings: fabrication and their applications in optical communications and sensing* [dissertation]. Portugal: University of Porto.
- Rego, G., Durr, F., Marques, P.V.S. and Limberger, H.G., 2006. Strong asymmetric stresses arc-induced in pre-annealed nitrogen-doped fibres. *Electronic Letters*, 42, pp. 1–2.
- Rego, G., Ivanov, O.V. and Marques, P.V.S., 2006. Demonstration of coupling to symmetric and antisymmetric cladding modes in arc-induced long-period fiber gratings. *Optics Express*, 14, pp. 9594–9599.
- Rego, G. and Ivanov, O.V., 2007. Two types of resonances in long-period gratings induced by arc discharges in boron/germanium co-doped fibers. *Optics Letters*, 32(20), pp. 2984–2986.
- Rego, G., 2009. Annealing of arc-induced gratings at high temperatures. *Electronic Letters*, 45, pp. 972–974.
- Rego, G. and Ivanov, O., 2011. Investigation of the mechanisms of formation of long-period gratings arc-induced in pure-silica core fibres. *Optics Communications*, 284(8), pp. 2137– 2140.
- Rego, G., Caldas, P., Ivanov, O. and Santos, J.L., 2011. Investigation of the long-term stability of arc-induced gratings heat treated at high temperatures. *Optics Communications*, 284, pp. 169–171.
- Sakata, H., Yamahata, K. and Wakamiya, K., 2013. magnetic-Force-Induced Tunable Long-Period Fibre Grating and Its Application in Erbium-Doped

Fibre Systems. *Lasers and Electro-Optics Europe (CLEO EUROPE/IQEC), 2013 Conference on and International Quantum Electronics Conference.*

Savin, S., Digonnet, M.J.F., Kino, G.S. and H. J. Shaw, H.J., 2000. Tunable mechanically induced long-period fiber gratings. *Optics Letters*, 25(10), pp. 710–712.

Sevigny, B., Leduc, M., Faucher, M., Godbout, N. and Lacroix, S., 2009. Characterization of the large index modification caused by electrical discharge in optical fibers. In: *Lasers and Electro-Optics. Conference on Quantum Electronics and Laser Science*, June 2–4 2009, Baltimore, MD, USA.

Singh, A., 2015. Study of Modeling Aspects of Long Period Fiber Grating Using Three-Layer Fiber Geometry: *Photonic Sensors*, 5(1), 2015, pp. 32-42.

Shao, Y., Xu, S., Zheng, X., Wang, Y. and Wu, W., 2010. Optical fiber LSPR biosensor prepared by gold nanoparticle assembly on polyelectrolyte multilayer. *Sensors*, 10, pp. 3585–3596.

X. Shu, B. Gwandu, Y. Liu, L. Zhang, and I. Bennion, “Sampled fiber Bragg grating for simultaneous refractive-index and temperature measurement,” *Opt. Lett.*, vol. 26, pp. 774–776, 2001.

Shu, X., Zhang, L. and I. Bennion, I., 2002. Sensitivity characteristics of long-period fiber gratings. *Journal of Lightwave Technology*, 20, pp. 255–266.

Smelser, C.W., Mihailov, S.J. and Grobncic, D., 2005. Formation of type I-IR and type II-IR gratings with an ultrafast IR laser and a phase mask. *Optics Express*, 13(14), pp. 5377–86.

Smietana, M., Korwin-Pawlowski, M.L., Bock, W.J., Pickrell, G.R. and Szmidt, J., 2008. Refractive index sensing of fiber optic long-period grating structures coated with a plasma deposited diamond-like carbon thin film. *Measurement Science Technology*, 19 pp.085301.

Smietana, M., Bock, W.J. and Mikulic, P., 2010. Comparative study of long-period gratings written in a boron co-doped fiber by an electric arc and UV irradiation. *Measurement Science Technology*, 21, pp. 1–8.

Smietana, M., Bock, W.J., Mikulic, P. and Chen, J., 2011. Increasing sensitivity of arc-induced long-period gratings—pushing the fabrication technique toward its limits. *Measurement Science Technology*, 22, pp. 1–6.

Smietana, M., Debowska, A.K., Mikulic, P. and Bock, W.J., 2013. Refractive index sensing with high temperature nano-coated electric arc-induced long-period gratings working at dispersion turning point. In: *Proceedings of 18th Microoptics Conference (MOC'13)*, Oct 27–30 2013, Tokyo, Japan.

Statkiewicz-Barabach, G., Anuszkiewicz, A., Urbanczyk, W. and Wojcik, J., 2008. Sensing characteristics of rocking filter fabricated in microstructured

- birefringent fiber using fusion arc splicer. *Optics Express*, 16, pp. 17249–17259.
- Steinvurzel, P., Moore, E.D., M<sup>o</sup>agi, E.C. Kuhlmeier, B.T. and Eggleton, B.J., 2006. Long period grating resonances in photonic bandgap fiber. *Optics Express*, 14(7), pp. 3007–3014.
- Su, L., Chiang, K.S. and Lu, C., 2005. Microbend-induced mode coupling in a graded-index multimode fiber. *Applied Optics*, 44(34), pp. 7394–7402.
- Tan, S.Y., Yong, Y.T., Lee, S.C., Faidz, A.R., 2015. Review on an arc-induced long-period fiber grating and its sensor applications. *Journal of Electromagnetic Waves and Applications*, 29(6), 703-726.
- Tang, J., Cheng, S., Hsu, W., Chiang, T. and Chau, L., 2006. Fiber-optic biochemical sensing with a colloidal gold-modified long period fiber grating. *Sensors and Actuators B*, 119, pp. 105-109.
- Thyagarajan, K., 2006. Optical fiber grating. *In: Guided Wave Optical Components and Devices*. : Elsevier Inc., pp. 233-242, Chapter 8: Erbium-doped Fiber Amplifiers.
- Mishra, V., Jain, S.C., Singh, N., Poddar, G.C. and Kapur, P., 2008. Fuel adulteration detection using long period fiber grating sensor technology. *Indian Journal of Pure & Applied Physics*, 46, pp. 106-110.
- Vengsarkar, A.M., Lemaire, P.J., Judkins, J.B. Bhatia, V., Erdogan, T. and Sipe, J.E., 1996. Long-period fiber gratings as band-rejection filters. *Journal of Lightwave Technology*, 14(1), pp. 58–64.
- Vengsarkar, M., Pedrazzani, J.R., Judkins, J.B., Lemaire, P.J., Bergano, N.S. and Davidson, C.R., 1996. Long-period fiber-grating-based gain equalizers. *Optics Letters*, 21, pp. 336.
- Villar, I. D., Matias, I. R., Arregui, F. J. and Lalanne, P., 2005. Optimization of sensitivity in Long Period Fiber Gratings with overlay deposition. *Optics Express*, 13, pp. 56-69.
- Villar, I. D., Achaerandio, M., Matías, I.R. and Arregui, F. J., 2005. Deposition of overlays by electrostatic self-assembly in long-period fiber gratings. *Optics Letters*, 30, pp. 720–722.
- von Bibra, M.L., Roberts, A. and Canning, J., 2001. Fabrication of long-period fiber gratings by use of focused ion-beam irradiation. *Optics Letters*, 26(11), pp. 765–767.
- Wang, L.A., Lin, C.Y. and Chern, G.W., 2001. A torsion sensor made of a corrugated long period fibre grating. *Measurement Science and Technology*, 12(7), pp. 793–799.

- Wang, Y., Xiao, L., Wang, D.N. and Jin, W., 2007. In-fiber polarizer based on a long-period fiber grating written on photonic crystal fiber. *Optics Letters*, 32(9), pp. 1035–1037.
- Wang, Y. et al., 2008. Long period gratings in air-core photonic bandgap fibers. *Optics Express*, 16(4), pp. 2784–2790.
- Wang, Y., 2010. Review of long period fiber gratings written by CO<sub>2</sub> laser. *Journal of Applied Physics*, 108(8), pp. 081101-1–081101-18.
- Wang, Y. et al., 2013. Long period fiber gratings written in photonic crystal fibers by use of CO<sub>2</sub> Laser. *Photonic Sensors*, 3(3), pp. 193-201.
- Wang, Y.P., Rao, Y.J., Ran, Z.L., Zhu, T. and Zeng, X.K., 2004. Bend-insensitive long-period fiber grating sensors. *Optics and Lasers in Engineering*, 41(1), pp. 233–239.
- Xuan, H., Jin, W. and Zhang, M., 2009. CO<sub>2</sub> laser induced long period gratings in optical microfibers. *Optics Express*, 17(24), pp. 21882–21890.
- Yin, Z.H., Zhang, X.B., Liu, Y.Q., Pang, F.F. and Wang, T.Y., 2012. Refractive index sensitivity characteristics of fiber taper long-period grating. *In: Asia Communications and Photonics Conference (ACP 2012)*, Nov 7–10 2012, Guangzhou, China.
- Yin, G.L. et al., 2014. Improved arc discharge technique for inscribing compact long period fiber gratings. *In: Proceedings of SPIE. International Conference on Optical Fibre Sensor*,; Santander, Spain.
- Yong, Y.T., Lee, S.C. and Rahman, F.A., 2015. Sensitization of hybrid LPFG-FBG refractometer using double-pass configuration. *Optics Communications*, 338, pp. 590–595.
- Zheng, Z.Z., Li, C.M., Lee, C.L. and Horng, J.S., 2013. Arc-induced long period fiber gratings based on flat-clad fibers. *In: Progress in Electromagnetics Research Symposium Proceeding*; March 25–28 2013, Taipei.
- Y. Zhu, Y., Shum, P., Chong, J.H., Rao, M.K. and Lu, C., 2003. Deepnotch, ultracompact long-period grating in a large-mode-area photonic crystal fiber. *Optics Letters*, 28(24), pp. 2467–2469.
- T. Zhu, T., Shi. L., Liu M. and Huang, W., 2012. Sensing and Demodulation of Special Long-Period Fiber Gratings Induced by Scanning CO<sub>2</sub> Laser Pulses. *Journal of Sensors*, 2012, 539095.
- Zulkifly, M.Z.R.M., Rahman, F.A. and Wong, H.Y., 2010. Arc-induced long period fiber gratings (LPFG) characterization: comparison between cladding etched and non-etched LPFG. *In: Photonics (ICP), 2010 International Conference on. IEEE*, July 5–7 2010, Langkawi, Malaysia.